Geophys. J. Int. (1998) **134,** 102–144

Sea-level change, glacial rebound and mantle viscosity for northern Europe

Kurt Lambeck, Catherine Smither and Paul Johnston

Research School of Earth Sciences, The Australian National University, Canberra, ACT 0200 *Australia. E-mail: Kurt.Lambeck@anu.edu.au*

Accepted 1998 January 5. Received 1997 December 4; in original form 1997 August 13

SUMMARY

Northwestern Europe remains a key region for testing models of glacial isostasy because of the good geological record of crustal response to the glacial unloading since the time of the Last Glacial Maximum. Models for this rebound and associated sea-level change require a detailed knowledge of the ice-sheet geometry, including the ice thickness through time. Existing ice-sheet reconstructions are strongly model-dependent, and inversions of sea-level data for the mantle response may be a function of the model assumptions. Thus inverse solutions for the sea-level data are sought that include both ice- and earth-model parameters as unknowns. Sea-level data from Fennoscandia, the North Sea, the British Isles and the Atlantic and English Channel coasts have been evaluated and incorporated into the solutions. The starting ice sheet for Fennoscandia is based on a reconstruction of a model by Denton & Hughes (1981) that is characterized by quasi-parabolic cross-sections and symmetry about the load centre. Both global (northwestern Europe as a whole) and regional (subsets of the data) solutions have been made for earth-model parameters and ice-height scaling parameters. The key results are as follows. (1) The response of the upper mantle to the changing ice and water loads is spatially relatively homogenous across Scandinavia, the North Sea and the British Isles. (2) This response can be adequately modelled by an effective elastic lithosphere of thickness 65–85 km and by an effective upper-mantle viscosity (from the base of the lithosphere to the 670 km depth seismic discontinuity) of about $3–4 \times 10^{20}$ Pa s. The effective lower-mantle viscosity is at least an order of magnitude greater. (3) The ice thickness over Scandinavia at the time of maximum glaciation was only about 2000 m, much less than the 3400 m assumed in the Denton & Hughes model. (4) The ice profiles are asymmetric about the centre of the ice sheet with those over the western part being consistent with quasi-parabolic functions whereas the ice heights over the eastern and southern regions increase much more slowly with distance inwards from the ice margin.

Key words: glacial rebound, mantle viscosity, sea level, Scandinavia.

1 INTRODUCTION

Scandinavia remains the key test region for the study of glacial isostasy and mantle viscosity because of the exceptionally good geological record of crustal rebound since Late-glacial time and a comprehensive knowledge of the history of ice retreat across the region. Yet definitive models for the isostatic rebound of the region do not yet exist, despite the fact that there has been much progress in understanding the underlying models since the first quantitative models were proposed by Haskell (1935, 1937), Niskanen (1939, 1948), Vening Meinesz (1937) and Gutenberg (1941). The reasons for this are several, some of which are still valid and prevent attainment of definitive answers about the viscosity of the mantle beneath Fennoscandia. One reason concerns the observational evidence for the crustal rebound. Many observations exist today that are securely dated using radiocarbon methods or varve chronologies for the late-glacial and postglacial stages, but little information exists for the early period of deglaciation or for the time of maximum glaciation. Also, reliable data are scarce for some areas such as along the southern margin of the Baltic Sea, or along the western Siberian Arctic coast. Another reason is that knowledge of the past ice sheet over Scandinavia remains incomplete. Ice limits at the time of maximum glaciation on the coastal shelf area of western Norway and the shallow Barents–Kara Seas remain uncertain, as do the ice limits over western Russia. Ice heights at and subsequent to the time of maximum glaciation remain largely unconstrained

by other than theoretical considerations of ice-sheet growth. The growth part of the Last Glacial cycle is also poorly constrained by observational evidence. A third reason, valid for much of the past work, is that high-resolution models of the rebound problem were not possible. But with the computer and numerical developments of the past decade or so, this is no longer the case and the highest resolution and mathematically complete models can now be efficiently achieved. There is, however, one major caveat to this last comment, namely that the models are largely restricted to radially symmetric earth models, with little scope for introducing realistic lateral variation in mantle viscosity or lithospheric thickness. Models with lateral variation in these properties have sometimes been attempted, but mostly at the expense of dropping a number of other important aspects of the already complex radially symmetric models.

Despite the limitations of the observational database, both for the crustal rebound and for the ice-sheet models, yet another revisit of the problem is worthwhile if only because of the rather diverse interpretations of these rebound data that have been reached in recent years. Thus Lambeck *et al.* (1990) inferred effective viscosities of about 4×10^{20} and $\gtrsim 5 \times 10^{21}$ Pa s for the average mantle above and below the 670 km seismic discontinuity, and Mitrovica (1996) noted a similar contrast. Mitrovica & Peltier (1993) had, however, previously ruled out such a contrast. Furthermore, Fjeldskaar (1994), following van Bemmelen & Berlage (1935), Lliboutry (1971) and others, introduced a low-viscosity layer beneath the lithosphere. These differences are attributable to a number of factors. All of these studies rest on only a subset of the available data. Others assume that the ice sheet is perfectly known. None has examined the entire range of possible earth-model parameters that may describe the rebound. Because of trade-offs that may occur between these parameters and with some ice-sheet parameters this limitation may be particularly severe, as is the case for the rebound analysis of the British Isles (Lambeck *et al.* 1996).

Thus this paper returns to the Scandinavian rebound problem once more and attempts to address some of the perceived limitations of earlier work. First, a comprehensive observational database for crustal rebound and relative sea-level change is compiled for northern Europe as a whole and Fenno-Scandinavia in particular. Second, a high-resolution ice-sheet model is developed, based largely on the ice limits and ice retreat proposed by Andersen (1981) and Pedersen (1995) and on the relative ice heights proposed by Denton & Hughes (1981). A scaling factor β^{F} for the ice height is included as an unknown in the solution. Simple three-layer viscosity models, comprising only a lithosphere, an upper mantle (base of lithosphere to a depth of 670 km) and a lower mantle are considered, although realistic density and elastic moduli gradients, inferred from seismic data, are used within these layers. The observations for sea-level change are inverted for the three unknown parameters describing this earth model (effective lithospheric thickness H_{l}, the effective viscosities of the upper (η_{um}) and lower (η_{lm}) mantle) and for the ice parameter β^{F}. The Scandinavian region is then divided into subregions, partly along tectonic lines, partly guided by aspects of the ice model, to determine whether there is evidence for lateral variation in the response of the Earth to the ice loading, and/or evidence for major departures in the relative ice heights from that initially proposed. The latter turns out to be the major requirement in modelling the observed values of sea-level change, with proportionally less ice over the eastern region than over the western part. In contrast, major lateral variation in the Earth response does not appear to be an essential requirement. In the second part of the paper a new ice model is constructed both from the recent observational evidence that points to a need to make further adjustments to the starting model and from loose constraints inferred from the preliminary analysis.

2 SEA-LEVEL OBSERVATIONS

2.1 Nature of the observational evidence for sea-level change in Scandinavia and surrounding region

The nature of evidence for sea-level change within and near formerly glaciated regions is very much dictated by geological factors, the nature of the ice sheet, and whether the sea level was falling or rising. Within the formerly glaciated regions of Scandinavia, the sea-level signal during the latest Pleistocene (Late Weichselian) and Holocene has been primarily one of a falling level, and much of the evidence for past shorelines is now above present sea level. However, at sites near the former ice margins, the signal may also exhibit a period of a rising relative sea level during the early part of the Holocene. Beyond the former ice limits the signal is primarily one of a rising sea level. As sea levels fall relative to the land, low-altitude topographic depressions or basins are isolated from the main body of water, leaving behind sediments that reflect the changing depositional environments. The majority of the sea-level evidence for Scandinavia consists of these isolation events, and well-developed methods exist for identifying and dating the transitions (e.g. Eronen 1974; Hafsten 1983; Svensson 1989). Despite the intrinsic simplicity of the method, the observations are beset with a number of generally well-understood difficulties. In certain circumstances the isolation threshold is defined by the high-tide level of the former sea, and the observation needs to be reduced to mean sea level if the tidal range is significant. Depending on the particular pollen or diatom concentrations used to define the transition, the timing of the isolation of the basin, or of the marine incursion in a rising sea-level environment, may refer to different parts of the tidal range. Tidal ranges at the time of isolation therefore need to be known. In most instances little can be done other than to assume that the tidal regime has not changed with time. Another problem concerns the possibility that a hiatus in the sediments may develop between the brackish and lacustrine sequences as tidal currents across the sill erode soft lacustrine sediments. Thus the timing of the transition may be systematically too old if the age is inferred from underlying sediments or it may be too young if inferred from overlying sediments. In some instances, the threshold itself may have been eroded subsequent to the isolation so that its present height is not a true measure of the sea-level change. In other instances the sill heights have been artificially lowered in the course of early land drainage projects. In yet other situations the sill heights may have been increased by beach deposits or by organic growth. A different set of problems is associated with the radiocarbon dating of the transition. Has there been an influx of water containing old carbon into the lake such that the radiocarbon of the acquatic vegetation may not have been in equilibrium with the atmosphere? Are the transition ages contaminated by younger plant roots that penetrate the sediment

layer? Most of these issues are well understood and methods have been developed to test for the occurrence of some of these potential difficulties. Also, the methodologies have been largely standardized such that the database is generally both reliable and consistent for much of Scandinavia.

An important element of the sea-level observation is the geographical position of the isolation basin. In some instances the age–height observations for a number of basins have been combined to form a sea-level curve for the area in question, but, because of the very considerable spatial variability in the sea-level signature observed across much of the Scandinavian region, this is only valid if the sites are very close to each other. In other publications the heights have been 'corrected' for this spatial variability, or reduced to a common geographical location, by using the gradients of the slopes of some of the principal shorelines observed in the area (see below). In the subsequent analyses, the original heights and site coordinates are used in the analyses rather than the composite curves unless the latter are based on very tightly clustered basins (within 1 km of each other).

Table 1 summarizes the data sources used for the various regions. In most instances the original data sources have been consulted, and age, heights, and coordinates have been checked against a range of other sources including the summaries of ages in Radiocarbon (e.g. the ages from the Trondheim, Lund, Helsinki and Groningen radiocarbon-dating laboratories), and appropriate large-scale maps for the regions. Where possible the radiocarbon ages have been checked against the regional pollen stratigraphy. Heights have been reduced to mean sea level in all instances, using the questionable but unavoidable assumption that tidal ranges have remained unchanged with time. Most of the sill heights have been levelled relative to the local datums with accuracies of typically a few tens of centimetres. The actual height errors considered are, however, considerably greater, including the effect $|d\zeta/dt|_t \sigma_t$ of any uncertainty σ_t in the age t of the isolation event, where $|d\zeta/dt|_t$ is the rate of sea-level change at time t at the locality in question. In all subsequent estimates of the height accuracy $2\sigma_t$ estimates are used. The adopted minimum height errors range from 1 to 2 m for the more recent observations, and the maximum height errors range up to 15 m for some of the higher basin thresholds where both the age uncertainties and sea-level rates are large. Overall, the adopted observational accuracies are at least a factor of two larger than the formal error estimates often quoted. All ages are referred to the conventional radiocarbon timescale (with a half-life of 5568 or 5570 years), with reservoir and fractionation corrections applied where necessary. Provided that this timescale is used consistently to describe the observational sea-level data and the ice-sheet history, the viscosities are defined in terms of C^{14} s, and the adopted standard deviations σ_t reflect the irregularities in this timescale, then this choice of the C^{14} timescale is sufficient (Lambeck 1998a).

An important data set for northern Sweden is based on the varve records contained within deltaic sediments, particularly from the Ångermanland and Västerbotten regions. Several potential uncertainties do exist with this database, namely the relation between the varve and radiocarbon timescales and the level at which the varves are deposited, but both issues appear to be adequately controlled by comparisons of this record with isolation events (Renberg & Segerström 1981; Wallin 1993). Radiocarbon AMS dating of varves (Wohlfarth *et al.* 1993) will further contribute to this resolution. For present purposes the varve data from Ångermanland and Västerbotten have been reduced to the radiocarbon timescale (Cato 1992). Varve data from southern Sweden have not been used because many of these data correspond to the isolated lake stages of the Baltic and do not relate directly to the position of mean sea level.

While many of the Scandinavian data are in the form of these basin isolation events, other evidence, in the form of well-developed shorelines of distinct ages that can be correlated over long distances, is also important. Well-developed examples are the Main Line and the Tapes Shoreline of the western coast of Norway. The former, the Main Line, is of Younger Dryas age; its age of formation has been constrained in several localities by studies of isolation basins whose thresholds occur at heights to either side of the shoreline. Such studies also confirm that the Main Line is primarily a synchronous feature that formed at 10 500–10 300 BP during an interval of a few hundred years when relative sea levels at these localities were relatively constant. Exposure age dating of this feature, as done for the analogous Scottish shoreline (Stone *et al.* 1996), remains to be done. The Tapes Shoreline is of a younger age, about 6500–6000 yr BP, and generally lies below the Main Line. An important feature of both shorelines is that their heights exhibit a strong spatial gradient, in a direction approximately orthogonal to the former ice fronts, across the region. This evidence is not used in the subsequent solutions for earth- and ice-model parameters but will be used in a subsequent paper for comparison purposes once optimum models have been derived.

For sites in Denmark and farther away from the former ice margin, the evidence for past sea levels is mostly below present sea level and the data are correspondingly more difficult to interpret. The source of information is primarily from now-submerged peat deposits or from the present depths of shell beds. Difficulties in the interpretation of both records are well known. Most of the peat information provides an upper-limit sea level: sea levels must have been below the peat by an amount that will depend on the primary species making up the peat colony and on the past tidal range and whether or not the peats formed behind barriers such that the growth levels were controlled by lagoon or groundwater levels rather than by sea level. Subsequent compaction of the peats also presents potentially important error sources unless the samples are selected from the base of peat units or the layers are very thin. The shell information is also ambiguous, since in most instances it is not known whether the samples were *in situ*, in which case they provide lower limits to sea level, or whether they were deposited by wave and wind action, in which case they provide upper limits only. The primary source of data used in this paper from sites beyond the former ice margin is based on submerged peats and therefore represents upper limits to past sea level.

2.2 The Baltic Lakes

As the ice sheet retreated over southern Sweden and the Baltic region, the sea now called the Baltic Sea experienced a complex history of alternating freshwater and marine stages depending on whether or not the water body was in open contact with the Atlantic Ocean or, possibly, the Arctic Sea. Several lake stages have been identified, the principal ones being (Björck 1995):

Table 1. Summary of sea-level observation data sources for Northwestern Europe.

Finland	Southern, central and northern Finland	See references to original sources in Eronen *et al.* (1995) Eronen (1974)
	S.W. Finland	Glückert (1976, 1978)
	Northern Finland	Saarnisto (1981)
	Helsinki	Hyvärinen (1980, 1987)
Sweden	Hunneberg	Björck & Digerfeldt (1982)
	Billingen	Björck & Digerfeldt (1986)
	Kroppefjäll	Björck & Digerfeldt (1991)
	Risveden	Svedhage (1985)
	Sandsjöbacka	Påsse (1987)
	Blekinge	Berglund (1964, 1971)
	Småland	Svensson (1989, 1991)
	Stockholm-Uppsula	Åse & Bergstrom (1982)
	Ångermanälven	Lidén (1938) Cato (1992)
	Västerbotten	Renberg & Segerstrom (1981) Broadbent (1978)
Norway	Oslofjord (Inner)	Hafsten (1956)
	Ski	Sørensen (1979)
	Ostfold	Danielsen (1970)
	Telemark	Stabell (1980)
	Vestfold	Henningsmoen (1979)
	Jæren	Bird & Klemsdal (1986) Thomsen (1982)
	Yrkjeforden	Anundsen (1978, 1985)
	Bømlo & Austrheim	Kaland (1984)
	Sotra	Kryzwinski & Stabell (1984) Kaland *et al.* (1984)
	Sunnmöre	Svendsen & Mangerud (1987) Lie *et al.* (1983)
	Nordmöre	Johansen *et al.* (1985)
	Sör Tröndelag	Kjemperud (1981, 1982, 1986)
	Andøya	Vorren *et al.* (1988) Møller (1986)
	Nord Trondelag	Ramfjord (1982)
	Lofoten	Møller (1984) Vorren & Moe (1986)
	Trömso	Hald & Vorren (1983)
	Varanger	Donner *et al.* (1977)
Denmark	Fakse Bugt	Krog (1979)
	Store Bælt	Krog (1979)
	Limfjord	Petersen (1975, 1994)
	Tude Ålven	Petersen (1977)
North Sea	German Bight	Linke (1979, 1982)
	Netherlands	van de Plassche (1982) Jelgersma (1961) Kiden (1989)
	Belgium	Kiden (1989) Baeteman (1981) Denys (1993) Denys & Baeteman (1995)
	North Sea floor	Beets *et al.* (1981) Jelgersma (1961)
British Isles	Scotland, England & Wales	Data sources summarized in Lambeck (1993)

(1) the freshwater Baltic Ice Lake from before 12 300 to 10 300 BP (C^{14} years before present);

(2) the Yoldia Sea with marine influence from about 10 300 to 9500 BP;

(3) the predominantly fresh-water Ancylus Lake isolated from marine influence until after about 8500 BP;

(4) the Mastagloia stage and the Litorina Sea, both subjected to marine influence, from after 8500 BP to the present.

The Baltic Ice Lake stage is defined by the onset of deglaciation of the Baltic and this occurred at about 12 300 BP in the Oskarshamn area of Småland, southern Sweden (Svensson

1991). It appears to have been isolated from the Atlantic Ocean at this time by a combination of topographic and ice barriers through central Sweden and by the fact that the eustatic sea level was at this time some 70–80 m lower than today. The elevation of the lake was regulated by several factors, including (1) differential glacio-hydro-isostatic uplift; (2) changing threshold locations because of glacier withdrawal and damming and erosion in the outlet areas; and (3) changes in global sea level. Thus observations of shore-line elevations for this period cannot be assumed to refer to the same reference level, and all Baltic observations for this interval are excluded from the initial comparisons with model predictions.

At about 10 300 BP the Baltic Ice Lake barrier was breached for the last time and very rapid lake drainage took place. A marine incursion into the Baltic, identified by marine fauna, occurred briefly, from about 10 300 to before about 9500 BP, forming the Yoldia Sea. The earliest marine incursions occurred in the Närke region of south–central Sweden, but the penetration of salt water farther into the Baltic was not immediate. For example, the marine influence reached the Stockholm region only about 200 years later and southern Finland about 300 years later. Observations during the Yoldia stage could be used in the comparisons with model predictions of mean sea level, but because the timing and duration of this period is uncertain and the age constraints on sea-level indicators may not be particularly precise, the few observations corresponding to the Yoldia stage are also excluded in the first instance.

The Ancylus stage formed when the Närke region was isostatically uplifted above the prevailing sea level and the Baltic basin was isolated to form a lake free of marine influence. Radiocarbon dates from peats and lake sediments suggest that the Ancylus stage had begun after about 9500 BP. A clear transgression is associated with the Ancylus stage, reaching its maximum before 9000 BP, and well-defined shorelines formed at this time. The maximum limit was followed by a pronounced regression in all parts of the Baltic Basin and a renewed salinity increase occurred in the Late Ancylus stage, or Mastogloia phase, after about 8500 BP. This was followed by the clearly brackish Litorina Sea. The Mastogloia phase, represented by a slightly increasing salinity with a sparse occurrence of weakly brackish taxa, is usually interpreted as reflecting a gradual spread of salinity into the Baltic Basin after the formation of an open ocean connection. Thus the actual lowering of the lake level to mean sea level predates the oldest occurrence of the brackish fauna and while younger sediments may not yet exhibit such taxa, the lake levels at that time should refer to sea level. There remains, however, considerable uncertainty about the exact timing of the first post-Ancylus opening of the Baltic Sea to marine influence, and in this paper only Baltic levels after 8100 BP are assumed to refer to mean sea level.

The beginning of the Litorina stage before about 7500 BP is one of the most clearly marked horizons in the sediments of the Baltic, being characterized by the gastropod *Litorina littorea* and by brackish diatom flora. The highest Litorina shoreline is clearly defined although it does not appear to be a synchronous event, its age ranging from around 7300–7400 in the south and southwest of Finland to about 7000 bp in the north of the Gulf of Bothnia. (It correlates with the Tapes Shoreline of western Norway.) Few observational data exist for northern Sweden, north of Västerbotten, and the contours of sea-level change for this part of the Gulf of Bothnia remain poorly constrained.

2.3 The database

2.3.1 Finland

A very considerable amount of information on the changing relationship between the Baltic Sea and the land has been published. The primary contributors to the database have been Eronen (1974), Glückert (1976, 1978), Hyvärinen (1980, 1987), Saarnisto (1981) and Salomaa (1982). Recently much of this information has been collected together by Eronen *et al.* (1995) and this compilation has been used here as the basis for discussing the relative sea-level change in Finland. The data extend from about 10 500 BP to the present and cover much of Finland, although the majority of the information is from the southern part of the country, in the vicinity of the Salpaussalkä Moraines (Fig. 1a), and the first part of Finland to become ice-free after the last glaciation. The observational evidence used is based on the age–height relations inferred from isolation basins, and the methodologies used by the various authors cited above are very similar. All reported ages refer to the conventional radiocarbon timescale and many of them have been checked with the pollen evidence for consistency. Most of the data points in the Eronen *et al.* (1995) compilation have been checked against the original publications and some observations have been rejected: some because the ages were identified by the authors as being either too young or too old to be consistent with the pollen evidence; others because they were associated with a Baltic Lake stage that was inconsistent with the radiocarbon age; others because the observations refer to fresh-water sediments that post-date the isolation event and which therefore only place an upper limit on sea level; and yet others because a hiatus has been identified in the sediment sequence at the time of the basin isolation. Only original observations are used and composite sea-level curves, based on observations from different localities in a region, are excluded. Inferences of water-level change from the deltaic sequences in the Salpaussalkä region have not been used either.

Fig. 1(b) illustrates the age–height distribution of all the Finnish data that appear to provide reliable indicators of sea-level change since the area became ice-free. The considerable spread of height values within any time interval reflects the spatial variability in the rebound, one mainly of increasing rebound from the southeast to the north of Finland with a lesser east–west variability. The reference for the water levels has changed with time because of the isolation of the Baltic from the open sea during both the Baltic Ice Lake stage and the Ancylus stage (see above). Thus in the initial comparisons of rebound-model predictions with the observations, only the observations referenced to the Yoldia, Mastagloia and Litorina lake levels should be used. However, the timings of the various openings and closings of the Baltic Sea remain uncertain. In particular, a substantial number of observations with ages as young as 8000 years are referred to the Ancylus Lake stage despite evidence elsewhere that the Baltic at this time may already have been open to marine influence. The height–age plots (Fig. 1b) also point to some changes occurring until about 8000 BP that, if correct, appear to be too rapid to be attributable to crustal rebound alone. Thus in the preliminary

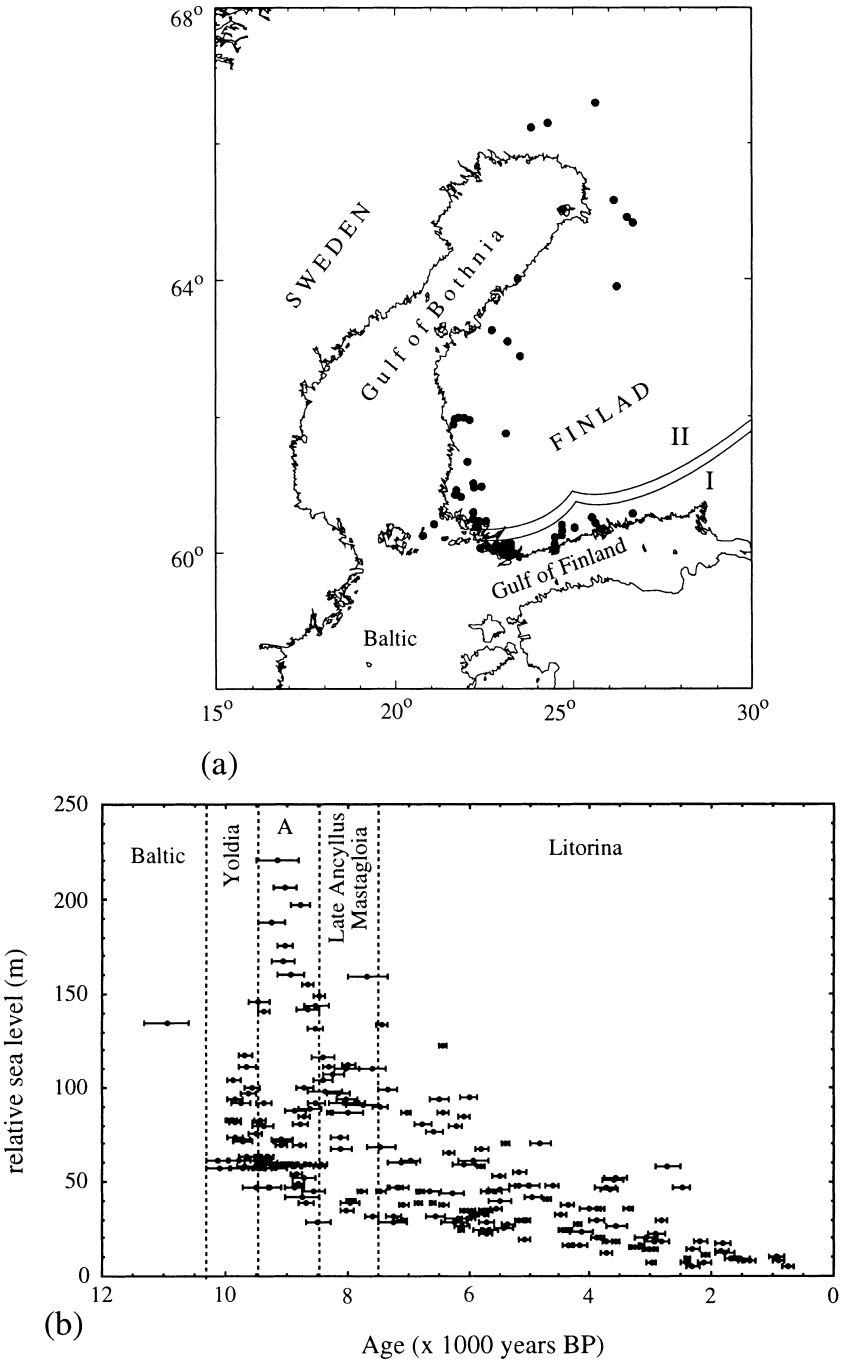

Figure 1. (a) Geographic and (b) temporal distribution of sea-level indicators in Finland. I and II in (a) denote the location of the Salpaussalkä I and II Moraines. A in (b) refers to the Ancylus Lake stage.

analyses discussed below only the data post-dating 8100 BP are considered and the earlier data will be examined in a later paper to establish the timing of the rapid falls in lake level.

2.3.2 Sweden

The Swedish evidence for changes in the land and water levels is also extensive and the data used here have come from a variety of sources (Table 1; Fig. 2). A considerable part of the data is based on lake isolation events, and the methods used are consistent with each other and with those used in Finland and Norway. Published ages refer either to the conventional radiocarbon scale or to the varve timescale in the case of the data from the Gulf of Bothnia (Ångermanland, Västerbotten). Heights are with respect to the Swedish height datum, which is close to mean sea level throughout the region.

Data from several localities in the southwest of Sweden describe the relative changes with respect to the sea. These are from Hunneberg (Björck & Digerfeldt 1982), Billingen (Björck & Digerfeldt 1986), Kroppefjäll (Björck & Digerfeldt 1991), Risveden (Svedhage 1985) and Sandsjöbacka (Påsse 1987) (Fig. 2a). These data cover the important period from about

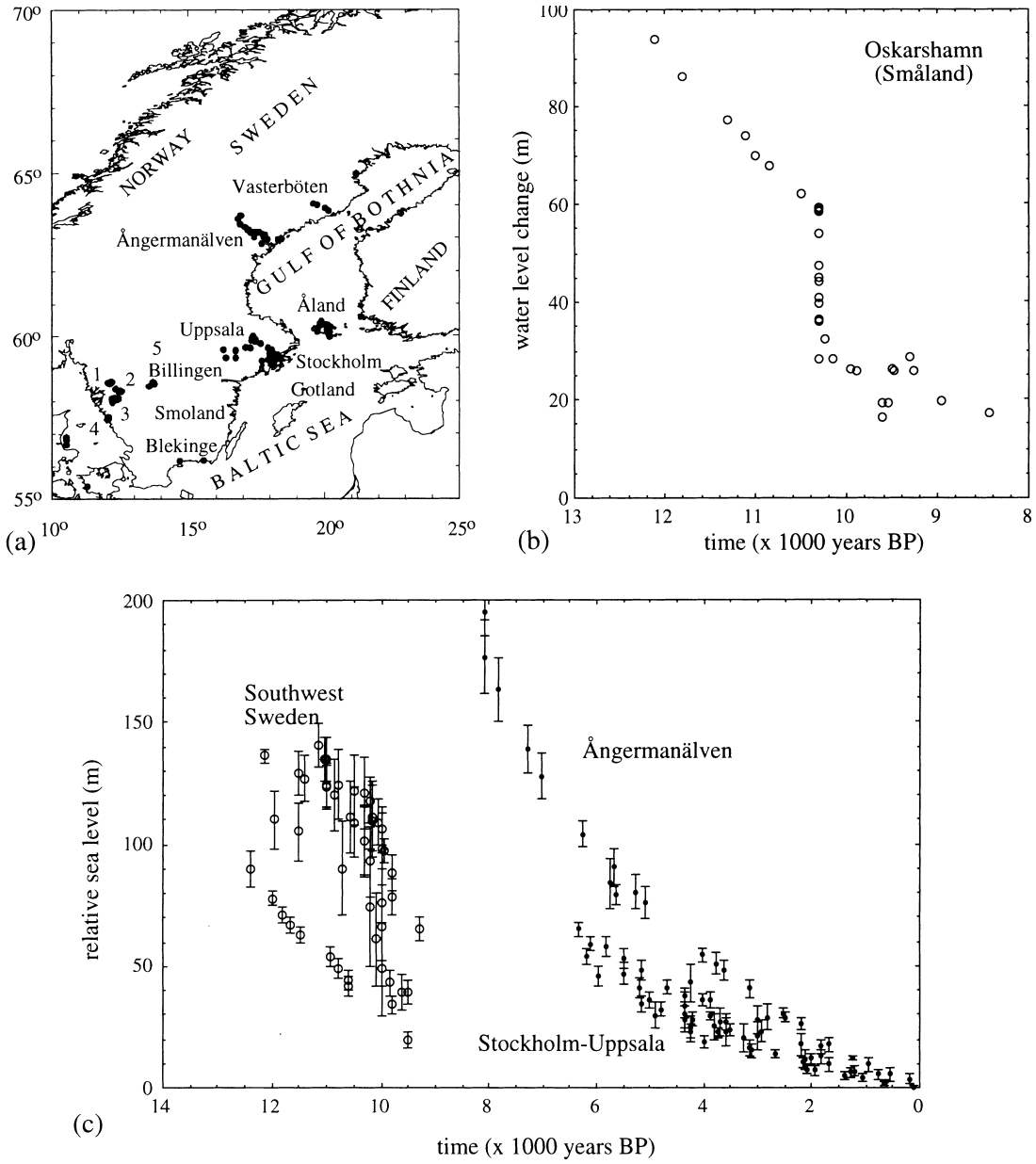

Figure 2. (a) Geographic distribution of sea-level indicators for Sweden. 1: Kroppefjäll; 2: Hunneberg; 3: Risveden; 4: Sandsjöbacka; 5 denotes the location of the Närke region. (b) The time–height relationships of shorelines in the Blekinge area of southern Sweden. (c) The time–height relationships of all shoreline information, reduced to mean sea levels for Sweden.

12 500 BP, when the region began to emerge from under the ice cover, to about 9000 BP, after which the hitherto rapid fall in sea level was replaced by an apparently oscillating shoreline. The observations from Billingen are from the locality where the Baltic Ice Lake was believed to have been dammed by ice and the observations are subsequent to the disappearance of this barrier. Most ages of the isolation events have been dated by radiocarbon and checked for consistency with pollen information. For the oldest data points from Sandsjöbacka, however, it was not possible to measure reliable radiocarbon ages and biostratigraphical correlations have been used instead (Påsse 1987). Age uncertainties ($2\sigma_t$) of these points have been correspondingly increased to typically about 300 years. The original geographical locations have been used for all points rather than using the results of the composite curves for any region, although in most instances the data points for each locality are geographically closely clustered.

The evidence from Blekinge, Småland, and Gotland in southern Sweden is from Berglund (1964, 1971), Björck (1979) and Svensson (1989), again using the standard Swedish methods for identifying and dating the isolation events. The older data here, prior to about 8500 BP, refer to either the Baltic Ice Lake or the Ancylus Lake levels and not to mean sea level. The data from the Oskarshamn area of Småland (Fig. 2b) illustrate the very rapid fall in the relative land–sea relationship, which has been interpreted as a nearly instantaneous fall in the Baltic Ice Lake level by as much as 30 m by drainage through the Mount Billingen area to the north. Another significant data set is from the region of Stockholm and Uppsala, where Åse & Bergstrom (1982) have established

a number of lake isolation events. The majority of these data correspond to the Litorina stage of the Baltic, but the oldest points, at about 9000 BP, may be with respect to the Ancylus Lake level.

The Ångermanälven data are originally from Lidén (1938) and are based on the height–age relationship of varve sequences that extend from the Gulf of Bothnia to about 150 km inland. The original sites examined by Lidén have been identified in the field and the coordinates taken from 1 : 50 000 maps for the region. The age data are based on the revised varve chronology of Cato (1992). For consistency with the rest of the database, these ages have been reduced to conventional radiocarbon ages. Several lake isolation events in the Ångermanland area have also been examined by Cato (1992) and they are consistent with the varve-based data, once allowance for the different timescales is made. With the possible exception of the oldest data point, all levels are from epochs when the Gulf of Bothnia was open to the sea. The evidence from Västerbotten, to the north of Ångermanland, is from Renberg & Segerström 1981). This is also varve-based, and the ages have been converted to conventional radiocarbon ages. Farther north again, Broadbent (1978) has provided some age–height relations that are based on archaeological and historical data as well as on the height and age of the marine limit.

Fig. 2(c) illustrates the age–height distribution of the Swedish data set, with the spread in height data for any time interval being indicative mainly of the spatial variability in the crustal rebound from south to north and from east to west.

2.3.3 *Norway*

A major part of the Norwegian data is based on evidence from isolation basins using standard and well-tested methods described by Hafsten (1983), Kjemperud (1981) and others. The age determinations are almost entirely based on radiocarbon ages, controlled in most cases by pollen analyses. Fig. 3 illustrates the spatial and temporal distribution of the Norwegian database used.

Evidence from the Oslofjord region (Fig. 3a) comes from several adjacent localities: Inner Oslofjord (Hafsten 1956), Ski (Sørensen 1979) and Ostfold (Danielsen 1970) to the east of the fjord and Telemark (Stabell 1980) and Vestfold (Henningsmoen 1979) to the west of the fjord (Fig. 3a). For the first and third of these regions, only age determinations based on pollen chronologies are available and these have been converted to radiocarbon ages using the calibrations appropriate for this region. The age errors ($2\sigma_t$) have been correspondingly increased for these sites, to typically 300 years at about 10 000 BP. Fig. 3(b) includes the height–age relationship for sites in this region, the highest points corresponding to the most northerly sites in the Oslofjorden.

Evidence from the southwestern area of Norway (Fig. 3a), mainly Rogaland and Hordaland, is given for Jæren by Bird & Klemsdal (1986) and Thomsen (1982), for Yrkjefjorden by Anundsen (1978, 1985), Bømlo and Austrheim by Kaland (1984), and the Sotra area by Krzywinski & Stabell (1984) and Kaland *et al.* (1984). All data, with the exception of that by Bird & Klemsdal, are for isolation events, with the exception being based on a variety of sources, and different observations, including evidence from dune and lagoon development. Despite these data being less robust than the basin isolation observations, they are potentially important because the sea-level trend here appears to be distinctly different from that for sites only a few tens of kilometres to the north [the Yrkjefjorden data of Thomsen (1982) and Anundsen (1985)]. Of the older isolation-basin data, of approximately Younger Dryas age, the radiocarbon ages are sometimes inconsistent with the pollen information.

Data for central western Norway include the regions of Sunnmöre (Svendsen & Mangerud 1987; Lie *et al.* 1983), Nordmöre (Johansen *et al.* 1985), Sör Tröndelag (Kjemperud 1981, 1982, 1986), and Nord Tröndelag (Ramfjord 1982) (Fig. 3a). All information is from basin isolation events, with a dating problem similar to that for some of the Younger Dryas and older ages for the southwestern sites.

Isolation basins in northwestern Norway have been examined for the Lofoten area by Møller (1984) and Vorren & Moe (1986), near Tromsö by Hald & Vorren (1983), and for Andøya by Vorren *et al.* (1988). The relative sea-level data from the Varanger Peninsula of Finnmark are from Donner *et al.* (1977). Some of this evidence is from isolation basins, other from beach deposits.

2.3.4 *Denmark*

Compared with the data from Finland, Sweden and Norway, the published data for Denmark are relatively few in number (Fig. 4a) and unsatisfactory in nature—a result of a more complex and subtle change in sea level across the region and of past levels having been near or below the present levels for prolonged periods of time. A shoreline corresponding to the Tapes Shoreline in Norway and referred to as the Maximum Littorina Shoreline in Denmark[1], has been identified across Jylland (Jutland) and Sjælland (Zealand) and has been dated at about 6000 BP. Likewise a shoreline with an attributed Younger Dryas age has been identified (Krog 1979) and correlated with the Main Shoreline of Norway. Near Præstø, in Fakse Bugt a sea-level curve has been established from the age–depth relationship of submerged peats and a similar result has been obtained for locations within the Store Bælt. The data from these two localities are consistent with each other and indicate that sea levels about 8500 years ago were some 25 m lower than today and that the present sea level was approached or exceeded only about 6000 years ago, at the time of the formation of the Littorina shoreline. Despite the agreement, both curves are considered to be tentative only (Krog 1979). Because the early part of this record may refer to the Ancylus Lake levels rather than sea level, data older than 8000 years are not used in the preliminary analysis. A number of sea-level indicators have also been examined for the Limfjord region (Petersen 1975, 1994). These suggest that sea levels may have risen very quickly from about −25 m or deeper at 9000 BP to be near present sea level about 1000 years later.

2.3.5 *North Sea*

The evidence for sea-level change in the North Sea comes from a variety of sources and is all inferred from the depths of now-submerged peats. Thus the majority of the estimates represent upper limits to past levels. Where possible only basal peats are used so as to reduce the effect of the subsequent compaction

[1] In Denmark the spelling Littorina is used for the same stage of the Baltic Sea as the Litorina of Finland and Sweden.

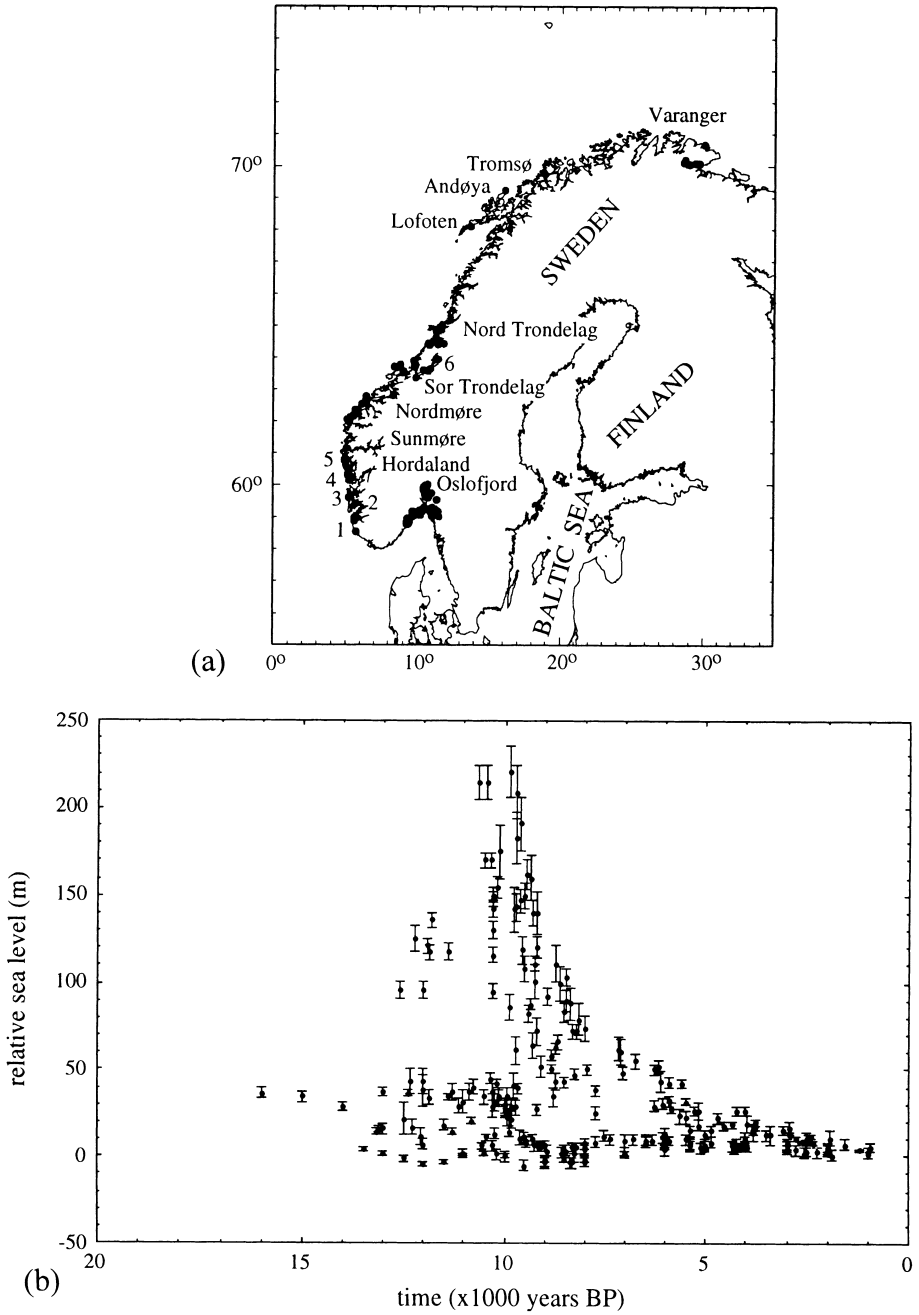

Figure 3. (a) Geographic distribution of sea-level indicators for Norway. 1: Jæren; 2: Yrkefjorden; 3: Bømlo; 4: Sotra; 5: Austrheim; 6: Trondheimsfjorden. (b) The time–height relationships of all Norwegian shoreline information reduced to mean sea level.

of the peat beds under an increasing sediment and water load. Tide corrections are based on the present tidal range for the locality and, since these corrections can be substantial, this must represent a major source of uncertainty in the inferred sea levels. Fig. 4(a) illustrates the data distribution in space and Fig. 5 that in time. The principal source of information used for the German North Sea sector is from Linke (1979, 1982) for the German Bight. The Netherlands coastal data have been selected from van de Plassche (1982), which covers mainly the province of Zuid Holland, as well as additional sources (Table 1). Data for Belgium are mainly from Kiden (1989), Baeteman (1981), Denys (1993) and Denys & Baeteman (1995). Potentially important data come from the North Sea floor itself, as the region gradually flooded over the past 10 000 years. However, much of this evidence is poorly constrained in terms of the original formation height of the peats, and tide-correction uncertainties are large. The data included in the present analysis are mainly from Beets *et al.* (1981), Ludwig *et al.* (1979) and Jelgersma (1961). The sea-level evidence from the British Isles up to about 1992 has been discussed in Lambeck (1993), and this same database is used below in aspects of the present solution.

2.3.6 *Barents and Kara seas, northwestern Russia*

The evidence from the arctic islands of Svalbard, Franz Josef Land and Novaya Zemlya has been discussed previously and

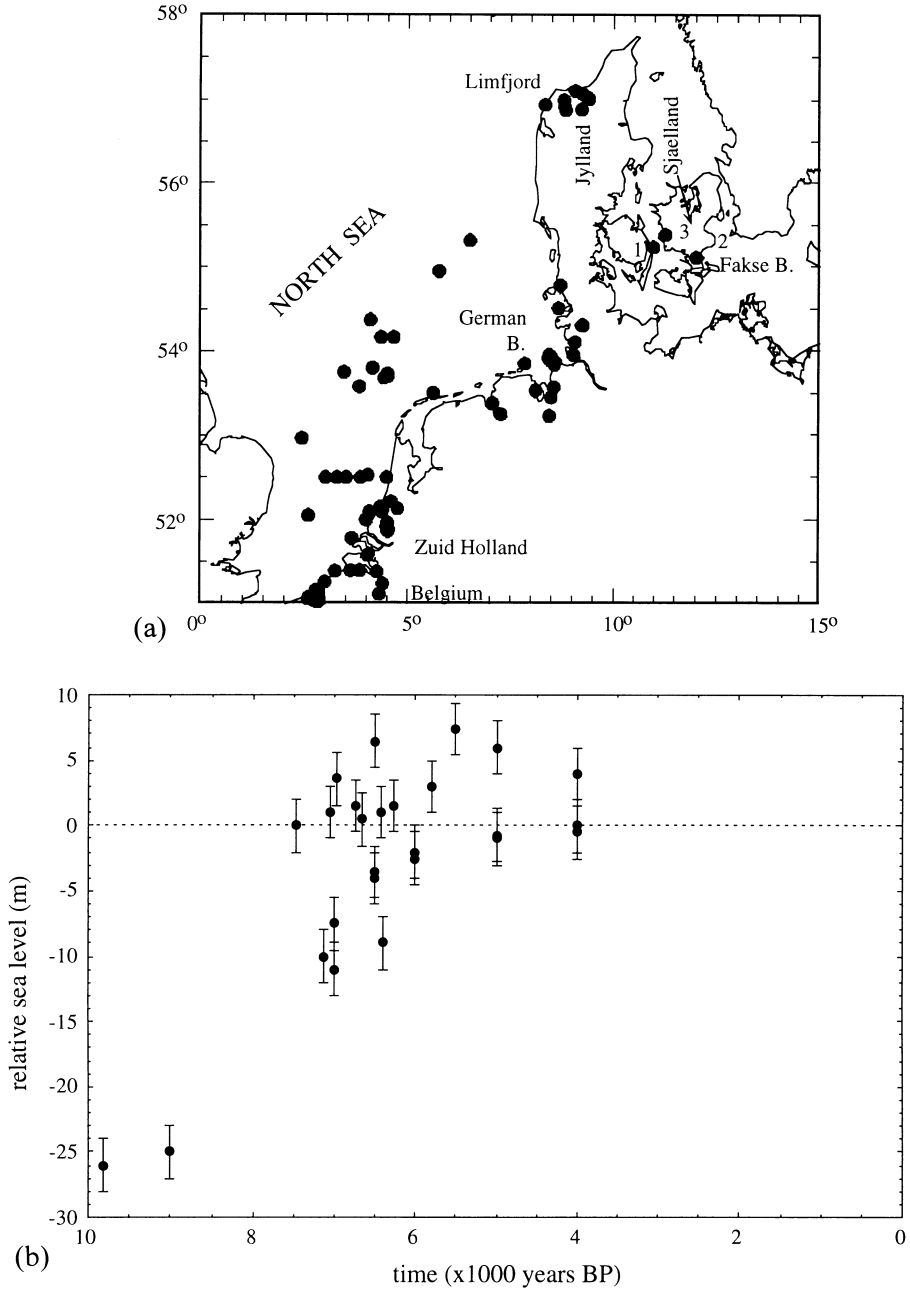

Figure 4. (a) Geographic distribution of sea-level indicators for Denmark and the North Sea. The Store Bælt is denoted by 1, the Öresund by 2 and the Tude Ålven by 3. (b) The time–height relationships of the shoreline information for Denmark, reduced to mean sea level.

has been used to constrain the ice model over this region (Lambeck 1995c, 1996). Hence these data will not be considered further in the present analysis. Important new information is becoming available for western Siberia, mainly in the form of an absence of raised shorelines in Late Weichselian and Holocene time, east of Novaya Zemlya, confirming that thick ice sheets, rivalling that of Scandinavia, did not exist in Arctic Russia in Late Weichselian time. One exception to the absence of raised shorelines occurs for the Kola Peninsula, where well-developed shorelines have been identified (Snyder *et al.* 1996).

2.3.7 *Summary*

Fig. 6 illustrates some typical time series for sea-level change in areas where the individual sites are grouped closely together. No corrections for the spatial variability of the rebound within these localities have been made in these figures. Thus the height–age relations are only approximate, but they do represent the main characteristics of sea-level change observed across the region. The results for the Ångermanälven area are characteristic of the areas near the centre of the ice load, with sea levels falling in an approximately exponential way from the time that the region first became ice-free. No other region in central Scandinavia exhibits such a complete record from a relatively small area. The data (not illustrated) from the Stockholm area exhibit a similar fall in sea level but only for about the last 6000 years and at a much reduced rate. Before this, the few available observations suggest that sea levels may have been relatively constant between about 8000 and

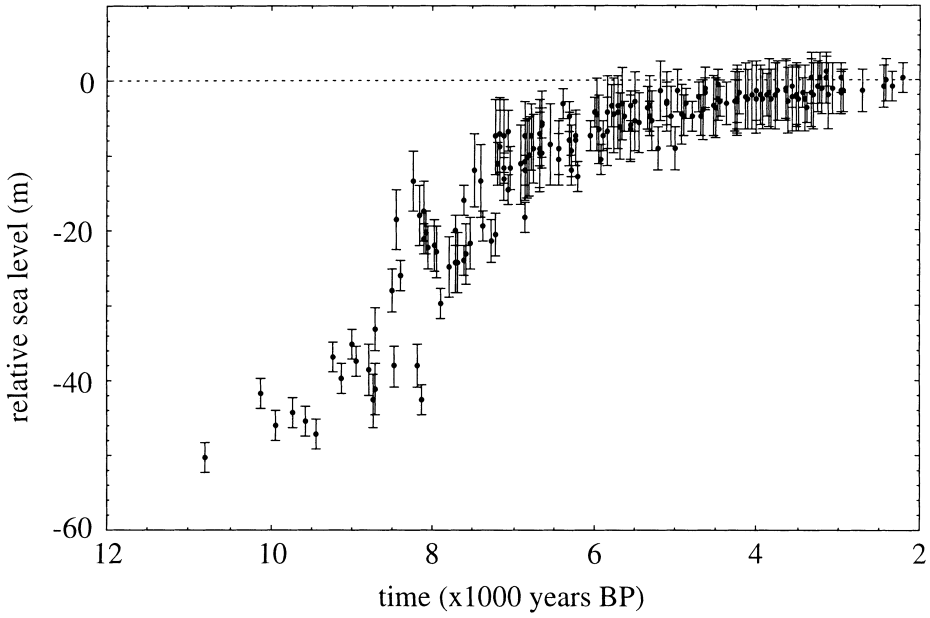

Figure 5. The temporal distribution of sea-level indicators for North Sea and English Channel localities. Nearly all observations are based on the position of fresh-water peats and therefore represent upper limits to means sea level.

6000 years BP. A similar pattern occurs for southern Finland, when, for example, the observations from the Turku, Salo, Pernio and Karjalohja regions are combined into a single sea-level curve, here carried out for illustrative purposes only.

The sea-level change for the Oslofjord region is characterized by a rapid fall once the region became ice-free, followed by a more gradual fall for the past 9000 years. The sea-level curves along the west coast of Norway exhibit a more complex pattern, with a rapidly falling sea level in Lateglacial time until about $\approx$9000 BP (e.g. for the Trondheimsfjorden sites), followed by a short period of nearly constant sea level, a period of rising relative sea level until about 7000–6000 BP and then again a gradually falling sea level until the present. This is well illustrated by the observations from Andøya, for example. In southern Norway the high shorelines of Lateglacial age vanish, and sea-level changes since the region became ice-free are considerably less than for the more northerly regions. For southwestern Sweden the sea-level trends are generally indicative of a period of relatively little change from the time the area became ice-free to about 10 300 BP (see Fig. 2a) followed by a rapid fall in early Holocene time. The amplitudes and pattern here change quite rapidly, and in northern Jylland and the Store Bælt (Denmark) the Lateglacial sea levels were well below present level.

3 A PRELIMINARY ICE MODEL

The initial rebound predictions and comparisons with observations are based on an ice model over Scandinavia and Arctic Europe discussed in Lambeck (1996). This model over Scandinavia is defined by the isochrons for ice retreat by Andersen (1981) and Pedersen (1995) (see Fig. 7) and by the ice thickness estimates at the time of maximum glaciation given by Denton & Hughes (1981), with the maximum ice thickness attaining 3400 m over northern Finland and the Gulf of Bothnia. The Arctic ice cover is restricted mainly to the Barents Sea, with the Kara Sea and western Siberia being free from substantial ice cover. This part of the ice sheet yields predictions for relative sea level that are consistent with observations from Svalbard and Franz Josefland as well as with the observation of an absence of significantly raised shorelines along the coast of Arctic Russia east of Novaya Zemlya (Lambeck 1996).

In the ice model proposed by Denton & Hughes (1981), the ice thickness h_{max} at the centre of the ice load at the time t_{max} of maximum glaciation h_{max} (t_{max}) can be approximated by

$$h_{max}(t_{max}) = \alpha S_{max}^{1/2}, \tag{1}$$

where S_{max} is the distance of the ice margin from the centre at t_{max}. The coefficient α is a function, *inter alia*, of the basal shear stress along the section from the ice margin to the centre of the load. Thus from their model of the ice sheet at the time of the Last Glacial Maximum, effective α parameters can be estimated from h_{max} and S_{max} for profiles radiating from the centre of the load. Then, as the ice sheet retreats, the maximum ice thickness at time t, $h_{max}(t)$, follows from (1) with the corresponding α and S for each profile. Once $h_{max}(t)$ is established for the epoch (the average of the estimates for the individual sections selected), the ice thickness along the profile follows from the relation (Paterson 1969)

$$h(S,t) = h_{max}(t)\left[1 - \left(\frac{S(t)}{S_{max}(t)}\right)^{1.5}\right]^{0.4}, \tag{2}$$

which approximates well the ice profiles for the Denton & Hughes ice sheet. Thus the underlying assumption is that the basal shear parameter adopted for the maximum glaciation model remains unchanged along any profile, although the parameter itself may vary from profile to profile, and that, implied by (2), the ice is frozen to its base. Fig. 34 (below) illustrates two profiles across this ice-sheet model.

Previous modelling of the Fennoscandian uplift, based on the Denton & Hughes (1981) ice model, indicated that the ice thickness at the time of maximum glaciation may be excessively large (Lambeck *et al.* 1990) and for this reason all ice heights

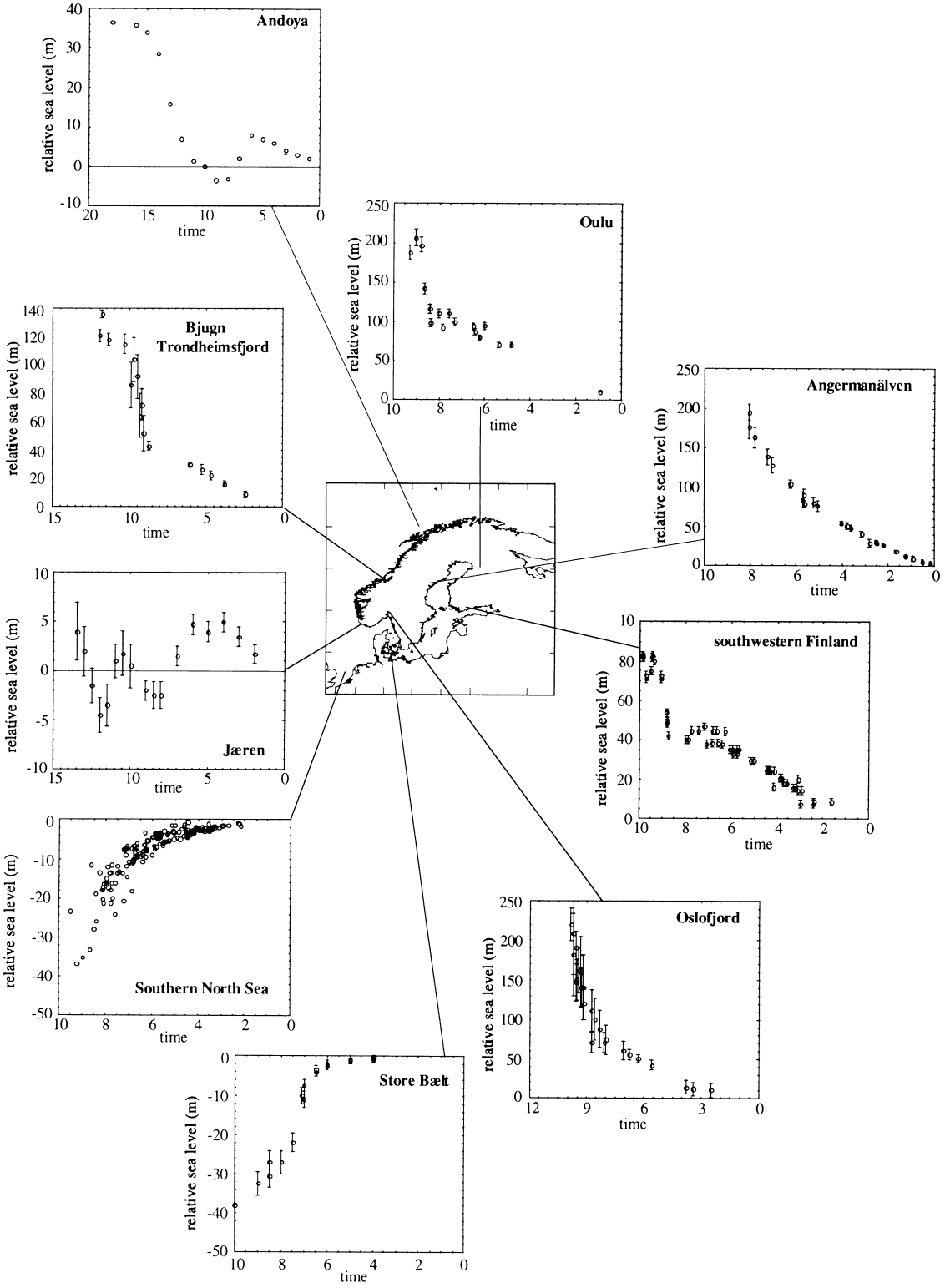

Figure 6. Sea-level observations at a number of localities in Scandinavia. All observations have been reduced to present mean sea level. Within each locality no corrections to the observations have been made for any spatial gradients in sea levels. Note the different scales used in the various age–height plots. Time units are 1000 years.

are scaled by a single parameter that is treated as an additional unknown in the inversion of the sea-level data (*cf.* Lambeck 1993).

A significant element in the ice model is the loading cycle before 18 000 BP going back to the Last Interglacial period. For this an approximate model has been adopted in which the ice-volume changes over Scandinavia are in phase with the global sea-level changes inferred by Shackleton (1987) from

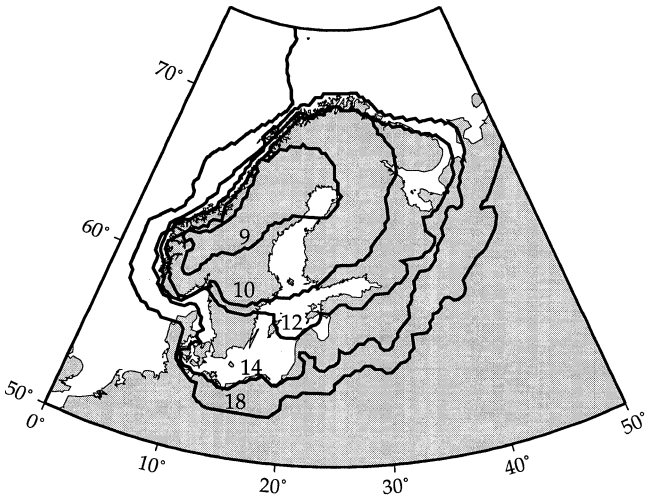

Figure 7. The starting ice-model limits at maximum glaciation (18 000 BP) and at selected times during the ice retreat (14 000, 12 000, 10 000 and 9000 BP).

the oxygen isotope record, with the ratio of Fennoscandian ice volume to total ice volume remaining the same as for the past 18 000 years. Fig. 8 illustrates that part of the eustatic sea-level functions used back to 30 ka BP.

The ice sheet over Great Britain is the same as that discussed in Lambeck (1993) but with the ice heights modified as discussed in Lambeck (1995a). The choice of this model is important only for predictions in the North Sea region. The more distant ice-sheet models over North America and Antarctica are the same as those used in Lambeck (1993) and extend back to the Last Interglacial period. The total ice volumes of the combined ice sheets are consistent with the eustatic sea-level curve proposed by Shackleton (1987) for the past 120 000 years.

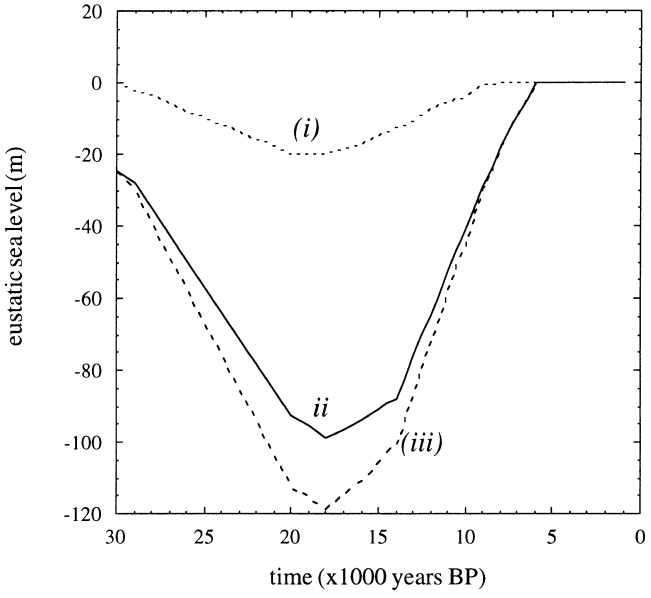

Figure 8. Eustatic sea-level function for the last 30 000 years from (i) the ice sheet over northern Europe according to the initial model and including the Barents ice sheet, (ii) the far-field ice sheets, and (iii) the total.

4 SOME FORWARD MODELLING EXPERIMENTS

4.1 The sea-level equation

The equation relating sea-level change to time-dependent changes in the surface load as ice sheets wax and wane has been discussed in considerable detail (Farrell & Clark 1976; Nakada & Lambeck 1987; Johnston 1993; Mitrovica & Peltier 1991) and its derivation needs no further discussion. Schematically, the relationship can be written as

$$\Delta\zeta(\varphi,t) = \Delta\zeta_e(t) + \Delta\zeta_I(\varphi,t) + \Delta\zeta_T(\varphi,t), \quad (3)$$

where $\Delta\zeta(\varphi,t)$ is the mean sea level at location φ and time t, measured with respect to present sea level. On the continents, $\Delta\zeta(\varphi,t)$ represents the change in separation between the geoid and the land surface. $\Delta\zeta_e(t)$ is the eustatic sea-level change defined as

$$\Delta\zeta_e(t) = \text{change in ocean volume/ocean surface area}. \quad (4)$$

$\Delta\zeta_I(\varphi,t)$ is the additional change that results from the isostatic adjustment of the crust to the changing ice-water surface load: from the deformation of the Earth under the changing ice and water loads and from the changing gravitational potential as the Earth deforms and the surface load is redistributed. This is the glacio-hydro-isostatic term. The third term in (3) is any additional tectonic contribution resulting from geophysical factors other than the glacio-hydro-isostatic effects that may alter the relationship between the land and sea surfaces. This tectonic term is ignored for the present and the emphasis is on the isostatic term which can be written schematically as the sum of three contributions:

$$\Delta\zeta_I(\varphi,t) = \Delta\zeta_r(\varphi,t) + \Delta\zeta_i(\varphi,t) + \Delta\zeta_w(\varphi,\Delta\zeta,t). \quad (5)$$

The first of these allows for the changing gravitational potential of the surface load as mass is redistributed between the land-based ice sheets and the oceans when ice sheets melt or expand. During times of ice-sheet growth, the mass concentration increases the gravitational potential in the vicinity of the ice and the sea surface is pulled up. This is in addition to the eustatic fall resulting from the decreasing ocean volume. The second term allows for the crustal deformation under the changing ice load and for the further change in gravitational potential resulting from the new shape and mass distribution within the Earth. This is the glacio-isostatic term. The third term allows for the crustal deformation under the changing water load and includes the additional modification of the gravity field. The rigid-body term $\Delta\zeta_r$ is a function of the ice-sheet geometry and, to a lesser extent, of the geometry of the ocean basins. The glacio-isostatic term is a function of the ice-sheet geometry through time, whereas the hydro-isostatic term is a function of the shape of the ocean basins. Both isostatic terms are also functions of the Earth rheology and their formulation establishes the link between the sea-level change and the mantle parameters describing the elastic and viscous response of the Earth. In addition, the hydro-isostatic term is a function of the sea-level change itself, and eq. (3) is an integral equation in $\Delta\zeta$.

The various isostatic terms can be further separated into the contributions from each of the individual ice sheets making

up the total water–ice exchange. Thus for N ice sheets

$$\Delta\zeta_{\mathrm{I}} = \sum_{n=1}^{N} \Delta\zeta_{\mathrm{I}}^{n},$$

but for local studies this will usually be split into two parts: the local ice sheet, in this case the ice over Fennoscandinavia $\Delta\zeta_{\mathrm{I}}^{\mathrm{F}}$ and the more distant ice sheets (Laurentia, Greenland, British Isles, Antarctica) making up the far-field term $\Delta\zeta_{\mathrm{I}}^{\mathrm{FF}}$. Thus, ignoring the tectonic term $\Delta\zeta_{\mathrm{T}}$, the relative sea-level change is expressed as

$$\Delta\zeta(\varphi,t) = \Delta\zeta_{\mathrm{e}}(t) + (\Delta\zeta_{\mathrm{r}} + \Delta\zeta_{\mathrm{i}} + \Delta\zeta_{\mathrm{w}})^{\mathrm{F}} + (\Delta\zeta_{\mathrm{r}} + \Delta\zeta_{\mathrm{i}} + \Delta\zeta_{\mathrm{w}})^{\mathrm{FF}}. \quad (6)$$

In quantifying $\Delta\zeta(\varphi,t)$, expressions relating the ice sheet, Earth rheology and ocean–land configuration are required. Inputs include an ice model which is defined on a high-resolution (25 km × 25 km) grid for the northern European and British ice sheets and on a coarser ($1^\circ \times 1^\circ$) grid for the distant ice sheets. Both these ice models and the ocean–land configuration are expanded into spherical harmonic series to very high degrees (256 in the cases discussed below), and the ocean–land–ice boundary is time-dependent. In formulating the latter, the case where the ice is grounded below coeval sea level needs special attention. The Earth's rheology is assumed to be spherically symmetric, compressible and with realistic elastic moduli and density parameters established from seismology (the PREM model of Dziewonski & Anderson 1981). The lithosphere is assumed to be elastic, with an effective thickness of H_{l}, the sublithospheric mantle is assumed to be viscoelastic and the core is inviscid. The anelastic response is described by a linear Maxwell rheology with uniform viscosity within concentric mantle shells. In all models considered here only two mantle shells are included: an upper mantle, with average viscosity η_{um} extending from the base of the lithosphere to the 670 km seismic discontinuity, and a lower mantle of average viscosity η_{lm}. Thus in all the preliminary models the mantle response is defined by known elastic parameters and three unknowns H_{l}, η_{um}, η_{lm}. In these preliminary models the 670 km seismic discontinuity is assumed to be a material boundary which moves with the mantle material as deformation occurs (Johnston *et al.* 1997). Other phase boundaries, such as that at about 400 km depth, are also treated as material boundaries in these models. Similar analyses for other areas indicate that these three-layered models provide a satisfactory first-order description of the rebound if the parameters are considered as effective parameters only (Lambeck 1993; Lambeck *et al.* 1996).

Once the relative sea-level change is evaluated, the topography $h(t)$ at any epoch is given by

$$h(t) = h(t_{\mathrm{o}}) - \Delta\zeta(t) \quad (7)$$

where $h(t_{\mathrm{o}})$ is the present topography (positive when above sea level). This does assume that other processes shaping landforms on these timescales are unimportant.

4.2 Contributions to sea-level change in the Fennoscandian region

The preliminary ice model discussed in Section 3 is used here to illustrate the magnitudes and spatial patterns of sea-level change and to evaluate the magnitudes of the various contributions, as defined by eq. (6), to the total change. Fig. 8 illustrates the eustatic sea-level term for both the northern European ice sheet and the combined distant ice sheets for the last 30 000 years. The total eustatic change at the time of the Last Glacial Maximum is 120 m in these models: 99 m from the western and southern hemispheres and 21 m from northern Europe including the Barents Sea area.

Four principal test sites have been selected (Fig. 9a) which are representative of many of the locations for which sea-level data exist. These are Prästmon, in the Ångermanälven valley of central Sweden and near the centre of maximum rebound; Oslofjord (Norway), within the maximum ice limits and becoming ice-free during the Younger Dryas; Limfjord, Jylland (Denmark) just outside the margin of the ice at the time of the Last Glacial Maximum; Zuid Holland, The Netherlands, well outside the former ice margin but where the sea-level change may still be strongly influenced by the removal of the Fennoscandian ice. The predictions are based on the complete model summarized by eq. (6), including the effect of moving shorelines as the ocean volumes change. The ice over the Barents Sea region is included as part of the Fennoscandian ice model. For reasons of computational expediency the British Isles ice has been included here as part of the far-field terms rather than as a part of the northern European ice. All models include earlier cycles of glaciation and deglaciation. Only the three-mantle-layer models summarized in Table 2 are considered in these preliminary predictions.

4.2.1 *The rigid-body solution*

For a rigid earth model, the sea levels exhibit spatial variability because of the changing gravitational attraction between the ice and water as the ice sheets decay and the meltwater is redistributed into the oceans. These effects, the $\Delta\zeta_{\mathrm{r}}$ in eq. (6), are illustrated in Fig. 9(a) for the far-field contributions $\Delta\zeta_{\mathrm{r}}^{\mathrm{FF}}$ at 18 000 BP. The spatial pattern through time remains similar for as long as ice remains over North America, and at 10 000 BP the amplitude of the term varies between about 7 and 4 m over the region. The primary contribution is from the Laurentide ice sheet, and across northwestern Europe, at a distance of 40° to 55° from the centre of this ice load, the effect remains positive: that is, sea level at these distances is raised by the attraction of this ice sheet. The contours of relative sea-level change form an approximately concentric pattern around the Laurentide ice load with the minor perturbations seen in the Baltic, North and Barents seas resulting from the changing gravitational attraction of the water load in these bodies of water.

The gravitational attraction of the Scandinavian ice is more important and approaches 80 m near the centre of the Gulf of Bothnia at the time of the Last Glacial Maximum (Fig. 9b). The term remains positive out to distances of about 60° from the centre of the ice load (see, for example, Johnston 1993; Lambeck 1995b) and its spatial variation in amplitude across northern Europe is significant. Consider, for example, the prediction for the Younger Dryas at about 10 000 years ago (Fig. 9c). Across the Baltic Sea the gradient of the sea surface, relative to the present, is about 15 m from the island of Åland to the southern shore of the Baltic Sea, and this may be of importance in discussions of the changing levels of the Baltic Lakes before the final disappearance of the ice: an instantaneous disappearance of the ice at this time could result in a substantial differential fall in level across the Baltic Sea.

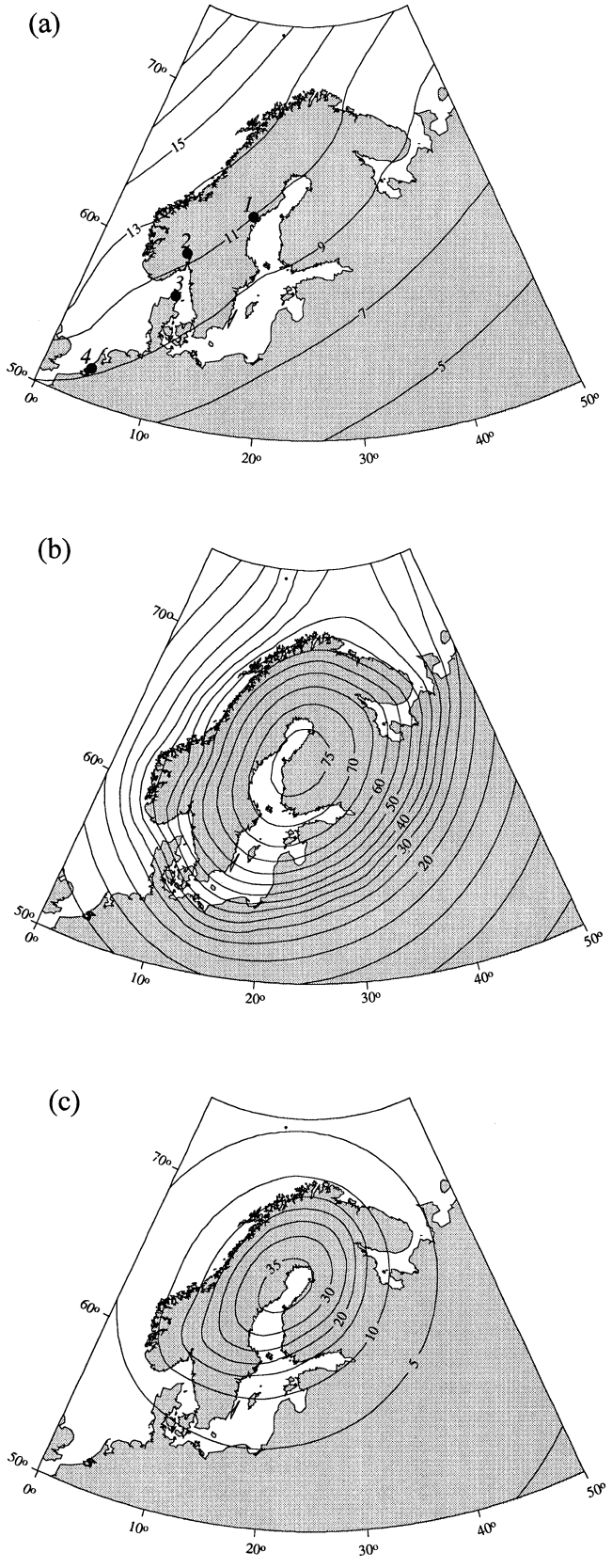

Figure 9. Spatial variability in predicted sea level on a rigid Earth due to (a) the far-field contributions at 18 000 BP, (b) the northern European contributions at 18 000 BP and (c) the latter at 10 000 BP. The following site locations are shown in (a). *1:* Prästmon, Ångermanälven; *2*: Oslofjord; *3*: Limfjord; *4*: Zuid Holland. All predictions are based on the nominal ice model and the earth model 1 from Table 2.

Table 2. Summary of earth-model parameters for three-layer models. The upper–lower-mantle boundary is at 670 km depth. H_1: effective lithospheric thickness, η_{um}: effective upper-mantle viscosity, η_{lm}: effective lower-mantle viscosity.

Earth model	H_1	η_{um}	η_{lm}
1	65	4×10^{20}	10^{22}
2	30	4×10^{20}	10^{22}
3	150	4×10^{20}	10^{22}
4	65	10^{20}	10^{22}
5	65	10^{21}	10^{22}
6	65	4×10^{20}	10^{21}
7	65	4×10^{20}	10^{23}

4.2.2 *The far-field glacio-hydro-isostatic contributions*

Fig. 10(a) illustrates the total far-field glacio-hydro-isostatic contributions to the sea-level change over northern Europe for the nominal earth model 1 (Table 2). This includes the glacio-isostatic effects of the North American, Greenland, Antarctic, and British Isles ice sheets according to the ice models discussed in Section 3, as well as the hydro-isostatic contribution from the combined meltwater of these ice sheets. Ignoring the southwest corner of the figure, where the sea-level change is dominated by the response to the deglaciation of the British Isles, the dominant pattern of the far-field contribution is established by the outline of the present land mass. This illustrates the dominance of the water-load term to the far-field contribution, with a movement of mantle material from beneath the water-loaded oceanic lithosphere to beneath the continent. Thus, 18 000 years ago sea levels in central Scandinavia, in the absence of the Fennoscandian contributions, are predicted to have been some 15 m higher than the eustatic change for this epoch. Over the Gulf of Bothnia and the Baltic Sea this magnitude is reduced because of the water-loading contributions in this area by the late-stage flooding. Offshore, the far-field contribution leads to a subsidence of the seafloor such that the predicted changes are greater than the corresponding eustatic changes. The magnitudes of the far-field contribution are of the order of 10–15 per cent of the eustatic change, and the overall pattern persists into Younger Dryas and middle Holocene times. Fig. 11(a) illustrates the time dependence of the far-field contributions separated into the glacio- and hydro-isostatic parts at the four sites in Fig. 9(a). (Because these parts include the changes in gravitational attraction between the ice and water and because the evolution of the ice model at any location is represented by a series of linear functions, the isostatic rebound functions have discontinuities in their first derivative.) These predictions confirm that the water-load term dominates the far-field contributions at these continental margin sites for the Lateglacial stage but that subsequently, in Late Holocene time, the glacio-isostatic contributions are relatively more important for most locations.

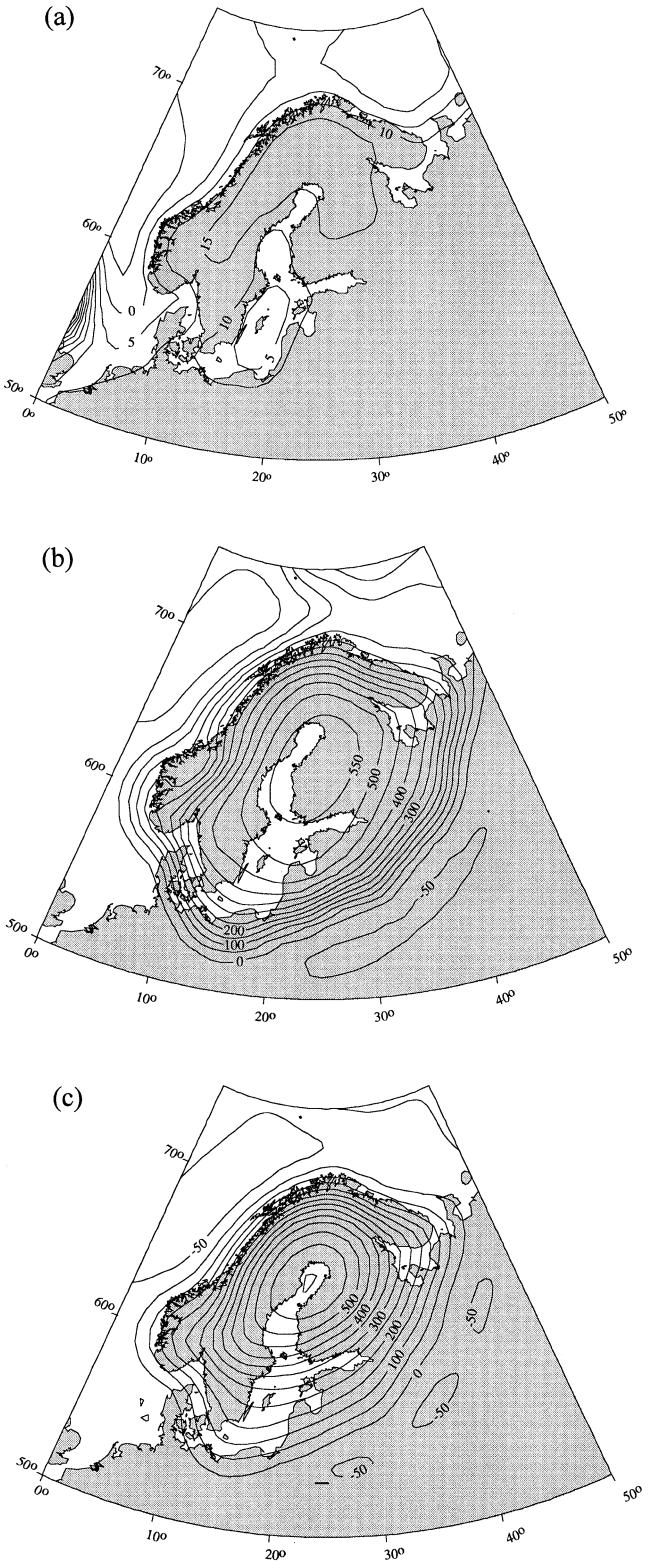

Figure 10. Far-field (a) and Scandinavian glacio-hydro-isostatic contributions to sea-level change at 18 000 BP (b), and at 10 000 BP (c). Predictions are for earth model 1.

The predicted far-field hydro-isostatic contribution $\Delta\zeta_w^{FF}$ is relatively insensitive to the choice of mantle parameters, as is illustrated in Figs 12 and 13. The dependence on lithospheric thickness is illustrated in Fig. 12(a) for the earth models 2 and 3 at the Ångermanälven and Zuid Holland locations. At both sites this variability does not exceed about 3 m for $30 < H_1 < 150$ km throughout the entire lateglacial and postglacial period for which most of the observational data are available. Elsewhere, with the exception of the North Sea area, the H_1 dependence of this term is also small (Fig. 13a). Within the North Sea area itself the dependence of the relative sea-level change on lithospheric thickness is more important, reaching 14 m in the example illustrated, in part because of the lithospheric thickness dependence of the glacio-isostatic rebound over the British Isles (Lambeck *et al.* 1996).

Fig. 12(b) illustrates the dependence of the far-field predictions on upper-mantle viscosity η_{um} for two models, both with $H_1 = 65$ km and $\eta_{lm} = 10^{22}$ Pa s, but which differ in their upper-mantle viscosity by one order of magnitude (models 4 and 5 in Table 2). This dependence on η_{um} is also relatively small but not insignificant when compared with the stated accuracies of about 1 m or better for much of the observational data. The differences are greatest for the sites near and immediately outside the ice margins (Limfjord and Zuid Holland) where the combined far-field effect of the hydro- and glacio-isostatic parts can exceed 10 m in lateglacial times. The spatial variation of the difference between the two model predictions is illustrated in Fig. 13(b). The pattern is similar to that for the difference between the two lithospheric thickness models—the model with higher upper-mantle viscosity ($\eta_{um} = 10^{21}$ Pa s) damping the departures from eustasy compared with the lower-viscosity model ($\eta_{um} = 10^{20}$ Pa s) in a similar way to the effect of increasing lithospheric thickness.

The lower-mantle viscosity dependence of the far-field contributions to the sea-level change is of similar magnitude to that for the upper-mantle viscosity variations, with the low viscosity value, $\eta_{lm} = 10^{21}$ Pa s, leading to greater departures from eustasy than the high-viscosity model with $\eta_{lm} = 10^{23}$ Pa s (Fig. 12c). The spatial variability of the difference between the predictions for the two cases (Fig. 13c) does exhibit a quite different spatial pattern from that of the other mantle dependencies, suggesting that the far-field contributions provide the basis for the separability of upper- and lower-mantle viscosities, provided that a good spatial distribution of high-accuracy relative sea-level data exists for lateglacial times.

In summary, the far-field contributions to sea-level change across northern Europe are not insignificant, varying between about 10 and 15 per cent of the eustatic sea level in the lateglacial period and attaining between -6 and $+2$ m 6000 years ago, the actual amount depending on geographical position and earth rheology. Quoted accuracies of the observational data are often better than this, particularly for the last 9000–8000 years, so that these far-field contributions need to be included in any detailed solutions for mantle- and ice-model parameters. Earth-rheology dependence of these far-field contributions is not insignificant either, particularly during the postglacial phase, and contributes to the separation of the two viscosity parameters.

4.2.3 The Fennoscandian glacio-hydro-isostatic contributions to sea-level change

Fig. 10(b) illustrates the total glacio-hydro-isostatic contribution to sea-level change from the Fennoscandian ice sheet only and for earth model 1. The principal part is the glacio-isostatic

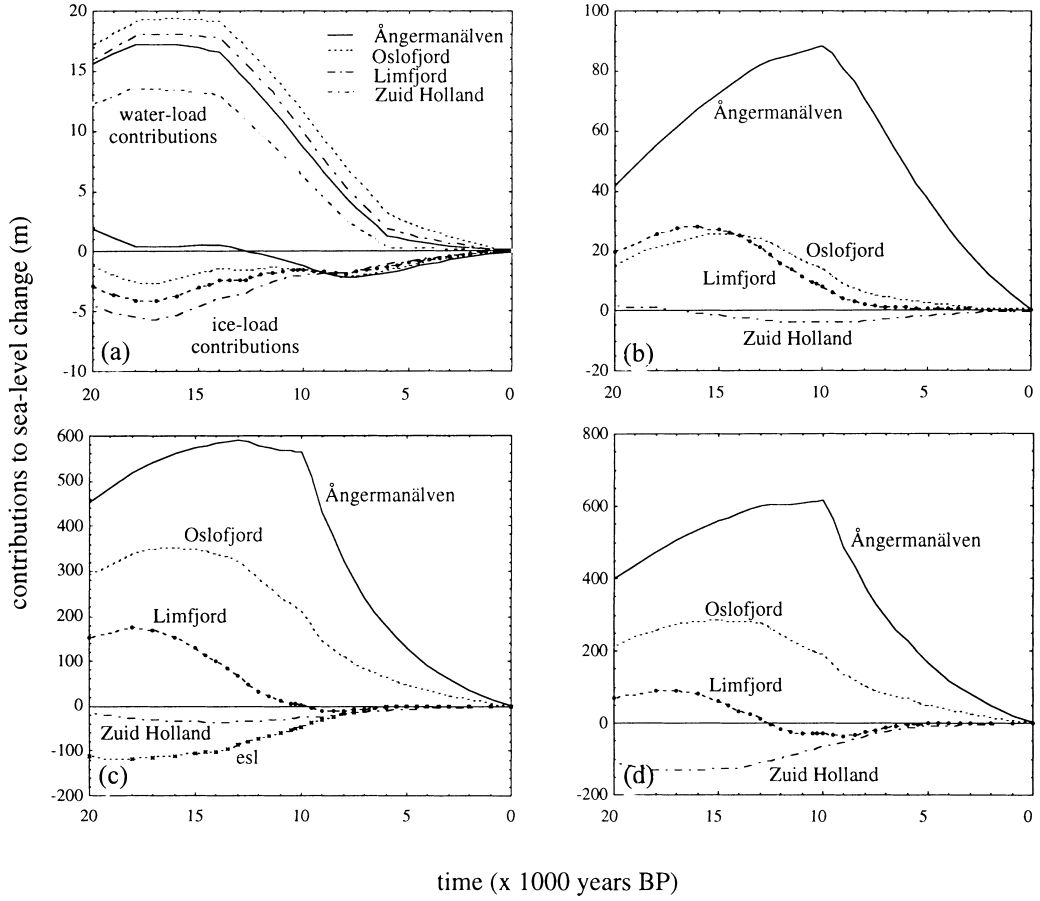

Figure 11. Time dependence of sea-level contributions at four sites (*cf.* Fig. 9a) for earth model 1: (a) the hydro- and glacio-isostatic components from the distant ice sheets, (b) the hydro-isostatic contributions from the north European ice sheet, (c) the glacio-isostatic contributions from the north European ice sheet and the eustatic (esl) curve for the total ice model, and (d) the total predicted sea level. Note the different sea-level scales used in the four figures.

term but the hydro-isostatic contribution is non-negligible, as is illustrated in Fig. 11(b). This latter part, the hydro-isostatic contribution, consists of several elements. The first is that the Fennoscandian meltwater is distributed over the oceans and contributes to the global sea-floor loading. For the adopted ice models the Fennoscandian contribution to eustatic sea-level is about 15 per cent of the total, so this part of the hydro-isostatic term will generally be small (*cf.* the hydro-isostatic contribution in Fig. 11a from the far-field ice sheets). A second element is caused by the gravitational attraction of the ice upon the adjacent ocean waters, raising sea levels in the neighbourhood of the ice margins and increasing the water load and crustal response accordingly. The third and most important element for sites near the ice margin results from the more localized water loading produced by the filling-in of the time-dependent depression of the sea floor during, and subsequent to, the existence of the ice sheet. Within the limits of the ice margin, these hydro-isostatic factors are included only once the area is ice-free, and then only if the land surface is below the contemporaneous sea level. These various elements combine to produce the contributions illustrated in Fig. 11(b) for the Ångermanland and Zuid Holland sites. At the former site the contribution exceeds about 80 m and clearly it cannot be ignored. Notable is that its maximum effect occurs well after the peak glaciation, a consequence of the delayed response of the crustal deformation to the changing ice load and of the time dependence of the position of the ice margin with respect to the site. The dependence of the hydro-isostatic Fennoscandian contributions on the mantle parameters is illustrated in Fig. 14 by the curves labelled -*w*; for different lithospheric thicknesses (earth models 2 and 3) in Fig. 14(a), for different upper-mantle viscosities (earth models 4 and 5) in Fig. 14(b), and for different lower-mantle viscosities (earth models 6 and 7) in Fig. 14(c). In all cases the dependence on these parameters is substantial when compared with the observational accuracies for some of the sea-level data, even though it is significantly less than for the glacio-isostatic factors (curves labelled -*i*).

The glacio-isostatic contributions due to the Fennoscandian ice and earth model 1 are illustrated in Fig. 11(c) for the four sites, and form the dominant contributions at the Ångermanland and Oslofjord regions. The dependence of this contribution on the mantle parameters is illustrated in Fig. 14 for two of the sites (curves labelled -*i*). Lithospheric thickness dependence of the rebound beneath the ice sheet is quite significant for the extreme values adopted ($H_1 = 30$ km and $H_1 = 150$ km), as is illustrated in Fig. 15(a) in terms of the spatial variability, at 10 000 years BP, of the difference in the predictions for the two models. This difference reflects the high-spatial frequency content of the sea-level predictions for

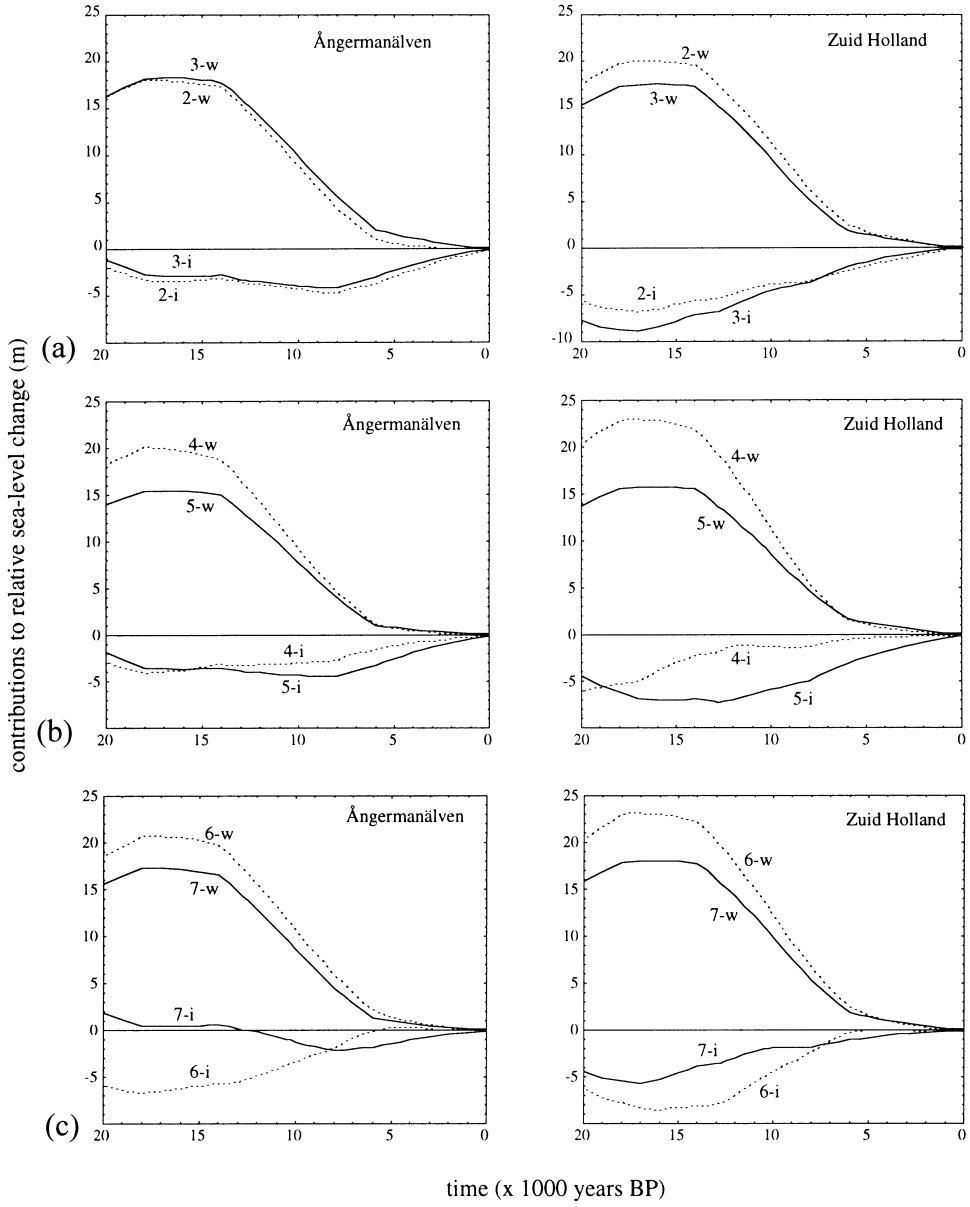

Figure 12. Predicted far-field glacio- and hydro-isostatic contributions to sea-level change at the Ångermanälven and Zuid Holland sites. (a) For earth models with different lithospheric thicknesses (earth models 2 and 3, Table 2). The curves labelled -*w* refer to the hydro-isostatic term and those labelled -*i* refer to the glacio-isostatic contributions. (b) For earth models with different upper-mantle viscosities (earth models 4 and 5). (c) For earth models with different lower-mantle viscosities (earth models 6 and 7).

the thin-lithosphere model. In particular, these differences illustrate the greater gradients predicted for isochronous shorelines, in directions orthogonal to the ice margin, for the thin-lithosphere models. Observations of such gradients along the major fjords of Norway may therefore have the potential to distinguish between the thick- and thin-lithosphere models.

The predicted dependence of the sea level on the upper-mantle viscosity is illustrated in Figs 14(b) and 15(b). Increasing the upper-mantle viscosity reduces the maximum sea-level change at sites well within the ice margins, a trend that can also be partly achieved by increasing the lithospheric thickness (see the Ångermanland results in Fig. 14a). However, in the postglacial stage, after about 9500 years BP at this locality, the curvature of the age–height plots is distinctly different for the two cases, raising the possibility that a separation of lithospheric thickness and upper-mantle viscosity parameters may be achievable. Such separability is further enhanced by sites near and beyond the former ice margins, as is illustrated for Zuid Holland in Fig. 14 where the H_1 and η_{um} dependences are distinctly different.

The dependence of the sea-level change on lower-mantle viscosity is illustrated in Figs 14(c) and 15(c) for two models (earth models 6 and 7) that differ in their lower-mantle viscosity by two orders of magnitude. The dependence is similar to that on the upper-mantle viscosity except for the different degrees of curvature in the postglacial stage. This is more clearly illustrated in Fig. 15(c), where the difference plot generally exhibits longer-wavelength spatial variability than does the difference plot for the upper-mantle viscosity models (Fig. 15b).

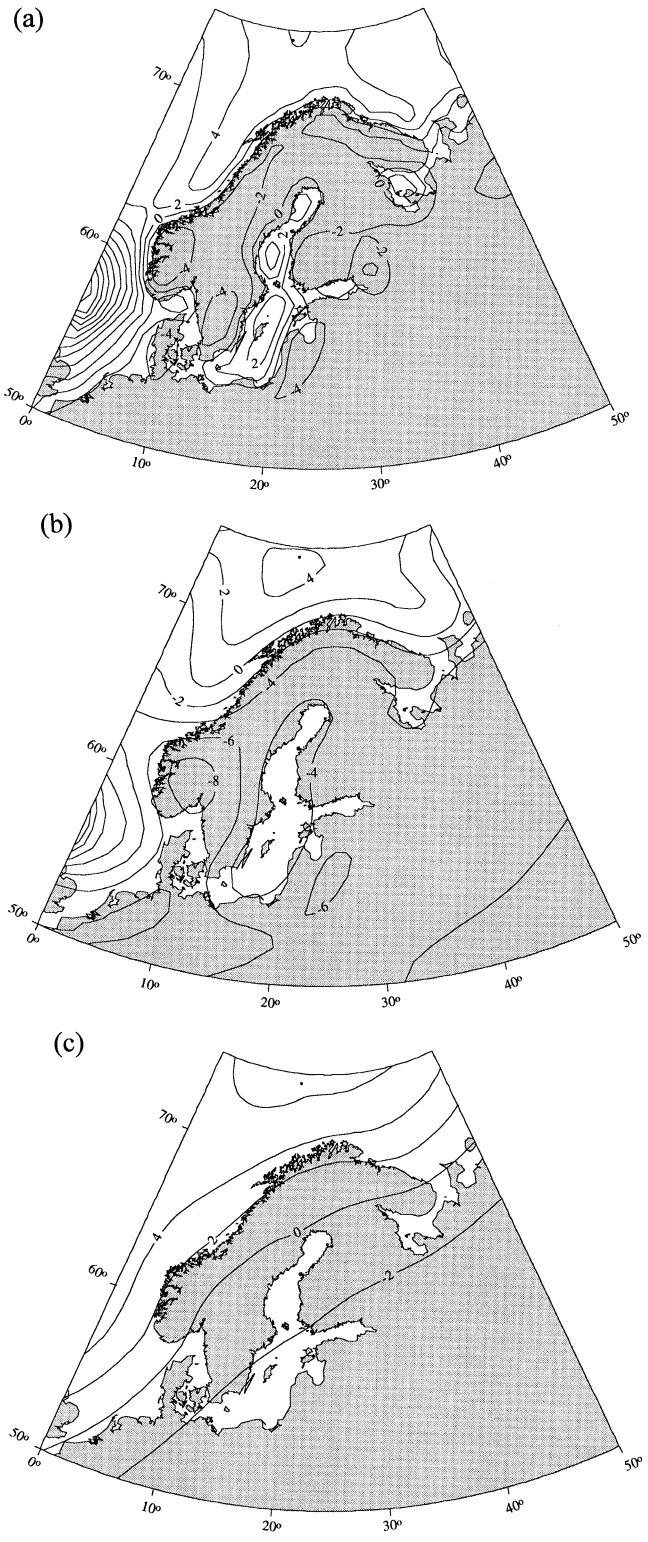

Figure 13. Spatial variability in the predicted total differences in the far-field contributions (glacio- and hydro-isostatic terms) at 10 000 BP for two earth models differing only in (a) lithospheric thickness (earth model 3 less earth model 2), (b) upper-mantle viscosity (earth model 5 less earth model 4), and (c) lower-mantle viscosity (earth model 7 less earth model 6).

5 PRELIMINARY SOLUTIONS FOR EARTH-MODEL PARAMETERS

5.1 A Scandinavia-wide solution

In these preliminary model predictions, the ice limits are assumed known and the profiles of the ice sheet follow the simple relations (1) and (2) given above. That is, the basal friction is assumed constant along any one radial profile but it may vary from profile to profile. The ice heights at maximum glaciation are based on the model by Denton & Hughes (1981), but heights can be scaled by a single parameter β. The adopted far-field ice sheets have been discussed in Section 3 and any limitations in them are assumed to result in a correction to eustatic sea level that is spatially uniform over the region in question.

The observation equation, relating the sea-level observations to the model parameters, is written as

$$\Delta\zeta_o(\varphi,t)+\varepsilon_o(\varphi,t)=\Delta\zeta_e(t)+\delta\zeta_e(t)+\beta^F\Delta\zeta^F(E_k,\varphi,t)+\Delta\zeta^{FF}(E_k,\varphi,t)$$
$$=\Delta\zeta_p(E_k,\varphi,t,\beta^F), \quad (8)$$

where $\Delta\zeta_o$ is the observed sea level at location φ and time t, with a standard deviation σ_ζ.

$\Delta\zeta_p$ is the predicted sea level at (φ,t) as a function of the earth models E_k and the ice scale factor β. ε_o is the observational error including the uncertainty in relating the observed heights to mean sea level. $\Delta\zeta_e$ is the nominal eustatic sea-level function corresponding to the totality of the ice sheets. $\delta\zeta_e$ is a correction to $\Delta\zeta_e$ due to uncertainties in the far-field ice models and may include other factors that result in a time dependence only in the sea level over the area. $\Delta\zeta^F$ is the predicted Fennoscandian glacio-hydro-isostatic contribution to sea-level change for an earth model E_k at the location φ and time t. β^F is the scaling parameter for the Fennoscandian ice sheet. $\Delta\zeta^{FF}$ is the predicted far-field glacio-hydro-isostatic contribution to sea-level change for an earth model E_k.

The unknown parameters are $\delta\zeta_e(t)$, β^F, and the earth-model parameters $E_k(H_l, \eta_{um}, \eta_{lm})$. In the preliminary models the eustatic function is assumed known and $\delta\zeta_e(t)$ is set to zero. The solution is therefore restricted initially to the four parameters $(H_l, \eta_{um}, \eta_{lm}, \beta^F)$.

The solution of eq. (8) follows procedures used previously for the British ice-sheet solutions (Lambeck 1993; Lambeck *et al.* 1996). That is, for any earth model E_k in a defined model space, parameters β^F, H_l, η_{um}, η_{lm} are sought that minimize the quantity

$$\Psi_k^2=\frac{1}{M}\sum_{m=1}^{M}\left[\frac{\Delta\zeta_o^m-\Delta\zeta_p^m(E_k)}{\sigma^m}\right]^2, \quad (9)$$

where M is the total number of observations, each with a standard deviation σ^m, and $\Delta\zeta_p^m$ are the corresponding predicted sea levels for location φ and time t.

The statistic Ψ_k^2 defined by (9) identifies the model E_{k*} that, within the adopted model space limits, best satisfies the observational data. If the models are complete and the observational errors are normally distributed with known standard deviations and uncorrelated, then the expected value of Ψ_{k*}^2 is unity. This statistic does not, however, indicate the range of earth models that will also satisfy the observations within their

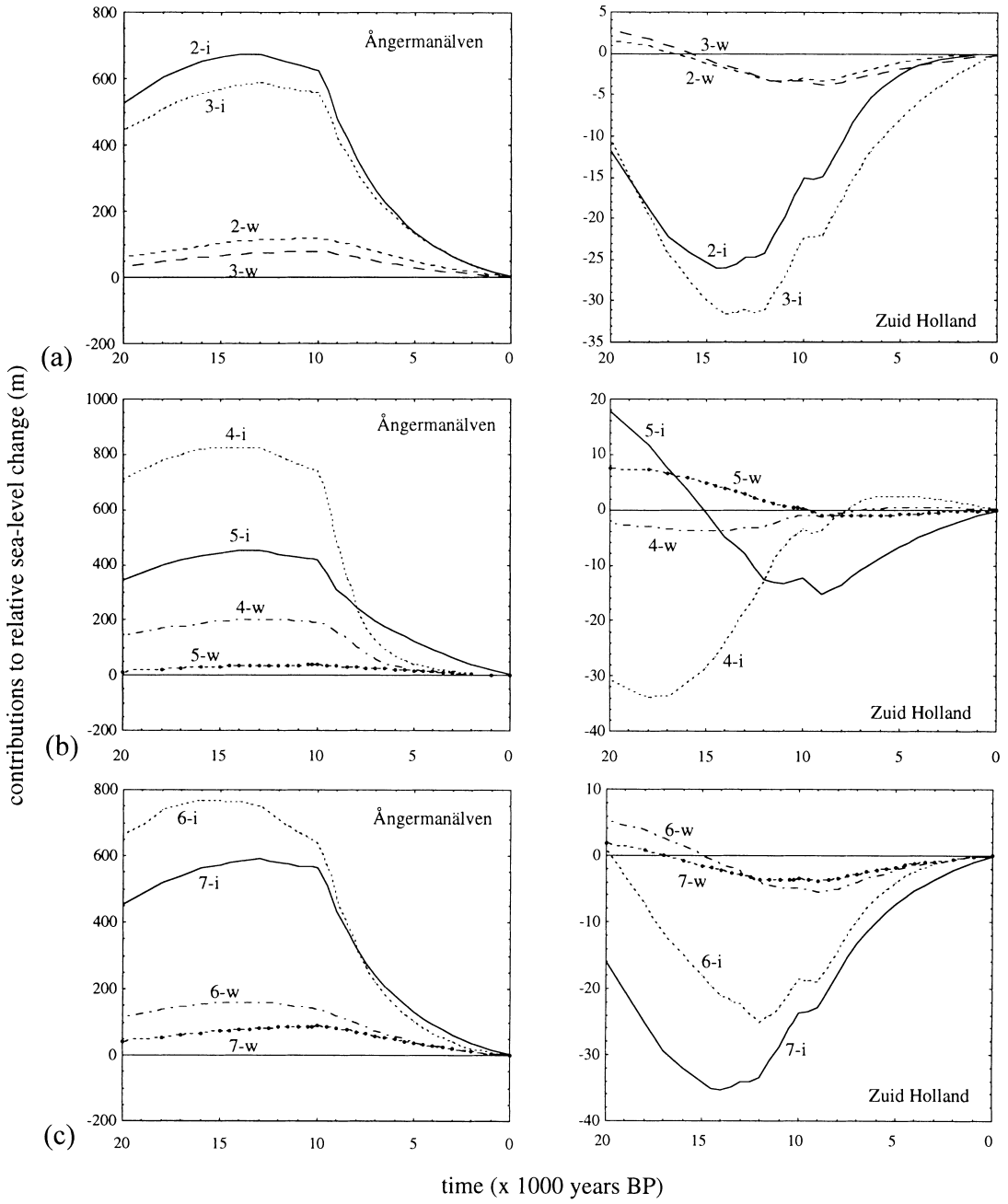

Figure 14. Predicted hydro-isostatic (curves labelled -*w*) and glacio-isostatic (curves labelled -*i*) contributions to sea-level change from the northern European ice sheets. (a) Models with different lithospheric thicknesses (earth models 2 and 3, Table 2), (b) models with different upper-mantle viscosities (earth models 4 and 5), and (c) models with different lower-mantle viscosities (earth models 6 and 7).

standard deviations. Such a statistic is defined by the quantity

$$\Phi_{\mathrm{k}}^{\mathrm{s}} = \frac{1}{M} \sum_{m=1}^{M} \left\{ \left| \frac{\Delta\zeta^{\mathrm{m}}_{\mathrm{p,k}} - \Delta\zeta^{\mathrm{m}}_{\mathrm{p,k*}}}{\sigma^{m}} \right| \right\}^{\mathrm{s}}, \tag{10}$$

where the exponent s will be set to 2 in the following examples. $\Delta\zeta^{\mathrm{m}}_{\mathrm{p,k*}}$ are the predicted relative sea levels for each observation m for the model $E_{\mathrm{k*}}$ that lead to the least variance defined by (9). The statistic $M\Phi_{\mathrm{k}}^2$ will have a χ^2 distribution with $M-4$ degrees of freedom and models for which $M\Phi_k^2 \leq \chi^2|_{M-4,\gamma}$ satisfy the data at the γ confidence limit. Models for which $\Phi_k^2 \leq 1$ differ on average from the best-fitting models by an amount less than or equal to the observational accuracy of the data.

Because of a certain clustering of the data in both geographical location and time, the observations have been grouped into space–time bins with each observation within such a bin being weighted according to the total number of observations n that fall into that bin. Thus the effective standard deviation of each observation is

$$\sigma_{\zeta}^{\mathrm{m}} \mathrm{n}^{-1/2}. \tag{11}$$

Experiments with different dimensions for the space–time bins indicate that the solutions for the minimum-variance models are only weakly dependent on this choice, although

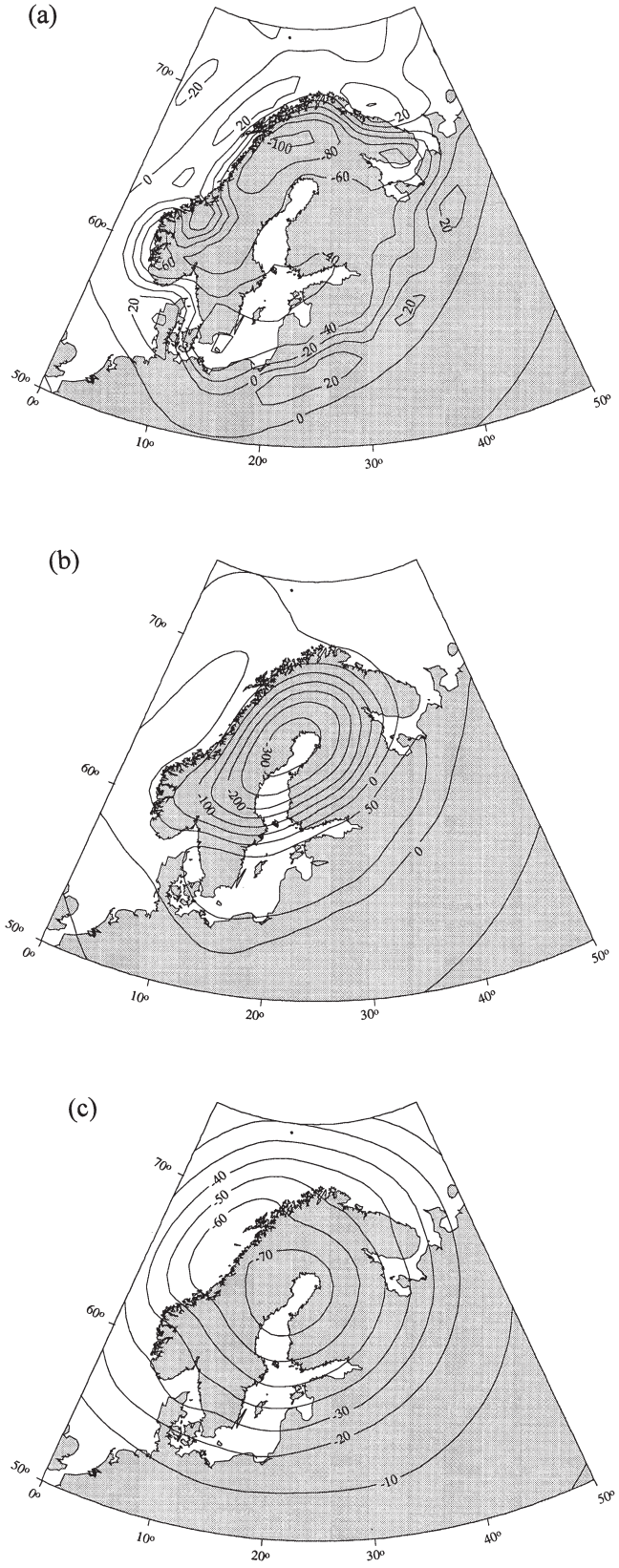

Figure 15. Spatial variability of the predicted differences in the glacio- and hydro-isostatic contributions to sea-level change from the northern European ice sheet for earth models that differ in (a) lithospheric thickness (earth model 3 less earth model 2), (b) upper-mantle viscosity (earth model 5 less earth model 4), (c) lower-mantle viscosity (earth model 7 less earth model 6).

the resulting Ψ_k^2 is a function of this choice. The adopted bin size is 0.5° in latitude, by 1.0° in longitude and 500 years in time.

The search through the model space has been conducted through the following range:

$$30 < H_1 < 150 \text{ km}$$
$$5 \times 10^{19} < \eta_{um} < 10^{21} \text{ Pa s} \quad (12)$$
$$10^{21} < \eta_{lm} < 10^{23} \text{ Pa s}$$

Fig. 16(a) illustrates the function Ψ_k^2 as a function of η_{um}, η_{lm} for $H_1 = 80$ km and for the case where the ice-sheet scaling parameter β^F is set to unity throughout. The minimum occurs for low values of both η_{um} and η_{lm} but the actual value of Ψ_k^2 is excessively high. Nor do satisfactory solutions occur within the explored viscosity parameter space for other values for H_1 within the range specified by (12) (Table 3). In all cases, the variance factor is more than an order of magnitude greater than the expected value of unity, and, if the models are appropriate, would imply that the observational variances have to be increased by about 30–50. More plausible is that the predictions grossly overestimate the relative sea levels because the assumed ice thickness is excessive. Fig. 17, for example, compares the predicted and observed levels for sites in Finland for the earth model 1 of Table 2 with different values β^F for the scaling parameter. Only when $\beta^F \simeq 0.4$ does the correlation coefficient approach unity, suggesting that the ice height is significantly overestimated if this particular choice of earth model is appropriate. However, earth models throughout the parameter space (12) give equally unsatisfactory results for this as well as for other regions.

Fig. 16(b) illustrates the variance function Ψ_k^2 for solutions in which the scale factor β^F is considered unknown, $H_1 =$ 80 km, and with the observational accuracies as defined by (11) (see Lambeck 1993 for details). Solutions for other discrete values of H_1 within the range (12) are summarized in Table 3. The minimum-variance solution now corresponds to mantle parameters of about $\eta_{um} \sim (1\text{–}2) \times 10^{20}$ Pa s and $\eta_{lm} \sim (2\text{–}10) \times 10^{21}$ Pa s, although all solutions remain unsatisfactory because of the large magnitudes of the minimum-variance factors. If the models are correct in all respects, these variance factors would imply that the original standard deviations of the observations have been underestimated by at least $\sqrt{14}$ or that the typical observational accuracy at 10 000 BP would approach and sometimes exceed 50 m, which in most instances would be unacceptably large. Alternatively, the large values for the least variance are indicative of model limitations: of lateral variation in the ice parameter or earth-model parameters, or an inadequate parametrization of the depth dependence of the mantle viscosity.

Fig. 16(b) also illustrates the corresponding scale factor β^F within the defined model space. These estimates point to a need to reduce the ice heights at and subsequent to the maximum glaciation by as much as 60 per cent of the heights originally assumed. Similar conclusions are reached for models with different values for lithospheric thickness in the range defined by (12), as is summarized in Table 3. The initial value for the maximum ice thickness following Denton & Hughes (1981) is 3500 m and the 'corrected' value is now about 2000 m, much lower than often assumed in models of the Scandinavian ice sheet for the time of maximum glaciation. The limitation of the assumed ice model also becomes readily apparent when past shorelines are computed for the region in that for the

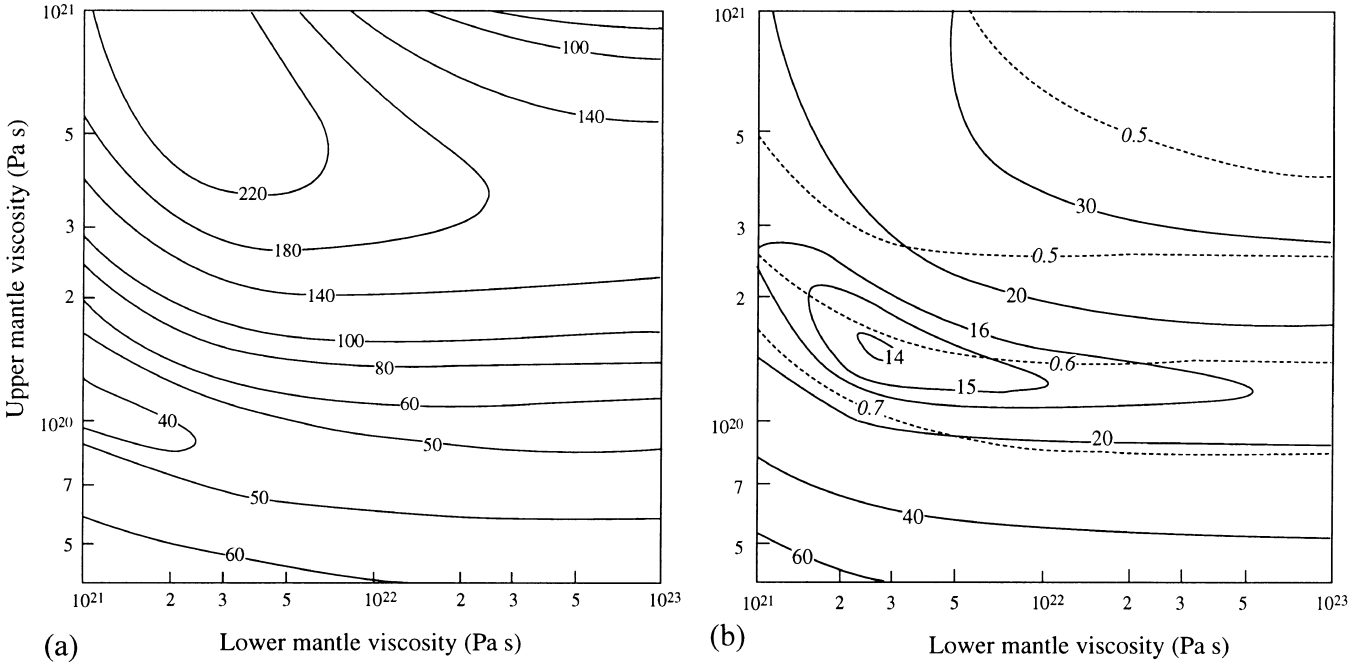

Figure 16. (a) Variance factor Ψ_k^2 as a function of upper- and lower-mantle viscosity for $H_1 = 80$ km and $\beta^F = 1.0$ with the observational standard deviations defined by (11). (b) Same as (a) but for solutions in which β^F is an unknown. Contours of constant β^F are shown by dashed lines and italic numbers.

Table 3. Summary of earth-model parameters for the Scandinavian region for two cases: (i) in which the ice model is assumed known ($\beta^F = 1$) and (ii) in which the ice-height scale factor β^F is included as a single unknown for the entire region. Solutions for selected values of lithospheric thickness, H_1, are included in both instances. The least-variance solution occurs for $H_1 = 80$ km.

	H_1 (km)	η_{um} $\times 10^{20}$ Pa s	η_{lm} $\times 10^{21}$ Pa s	Ψ_k^2	β
(i)	β set to unity				
	30	0.7–1	1–100	40–63	1
	50	0.7–1	1–100	33–43	1
	80	0.7–1	1–100	38–48	1
	100	0.7–1	1–100	43–63	1
	150	2.2	1	66	1
		2–10	20–100	43–55	1
(ii)	β included as unknown				
	30	5	1	15.9	0.48
	50	1.7	3	14.9	0.63
	80	1.5	3	13.9	0.61
	100	2	3	14.9	0.59
	150	3	1	15.6	0.58

entire range (12) of models much of Finland and Sweden is predicted to be below sea level in early Holocene time once the ice sheet has retreated to the mountain region. This is illustrated in Fig. 18 for two cases in which the shoreline position is predicted from (7). In the first, with $\beta = 1$ and the earth model E_{k*} corresponding to the least-variance solution in Fig. 16(a), the central Scandinavian region 9000 years ago is well below the then sea level and the Baltic Sea is open to marine influence, from the north through the White Sea. The same pattern results from a wide range of plausible earth models and the region remains below sea level for both earlier and later periods, including times when the Baltic region is understood to have been free from marine influence, as during the Baltic Ice Lake and Ancylus stages. The second example corresponds to the minimum-variance solution illustrated in Fig. 16(b) with $\beta = 0.62$. Now at 9000 BP a tenuous barrier between the Baltic and the White Sea is predicted and the Baltic is closed to marine influence for the first time. Other earth models in the vicinity of the minimum-variance solution given above yield similar conclusions.

A more detailed comparison of predictions with observations based on the above minimum-variance solution indicate some distinct regional patterns. In southern Finland, for example, the predictions for the post-Ancylus Lake stage lie systematically above the observations between about 5000 and 8000 BP (Fig. 19a) and similar patterns are seen for central Finland, the southern parts of Sweden and Denmark. Here, a further reduction in the predicted sea levels is required, particularly for the earlier part of the record. In contrast, the predictions for the Oslofjord area lie systematically below the observed values (Fig. 19b), a trend that is also seen for southwestern Sweden and the coastal areas of southwest and central

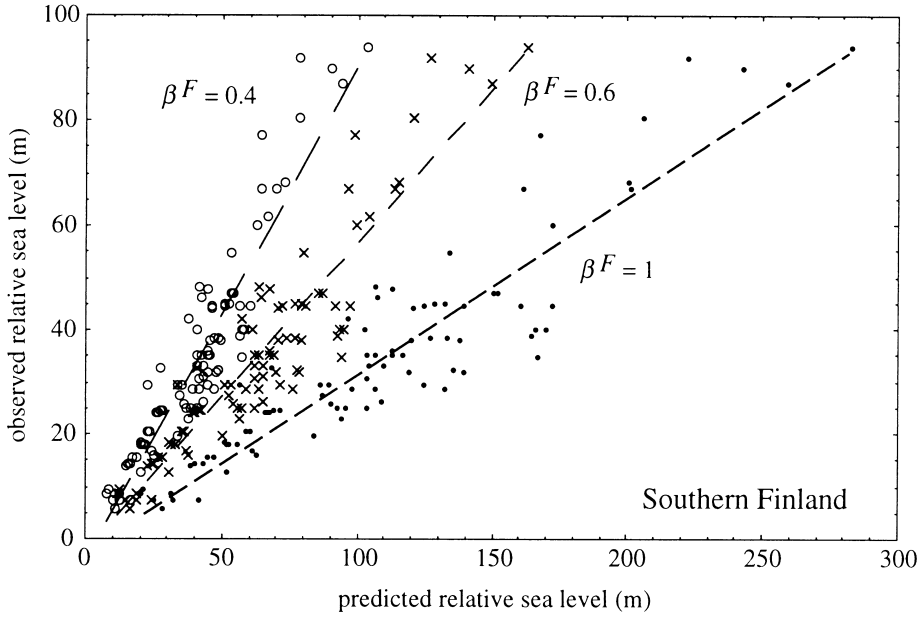

Figure 17. Observed versus predicted sea levels for sites in southern Finland with the latter based on the earth model 1 in Table 2 and on three different values for the ice-height scale parameter β^F (• corresponds to $\beta^F=1$, x to $\beta^F=0.6$, o to $\beta^F=0.4$). The least-squares regression lines for the three cases are illustrated by dashed lines, and the corresponding regression coefficients are 0.33 for $\beta^F=1$, 0.59 for $\beta^F=0.6$, and 0.95 for $\beta^F=0.4$.

western Norway. These trends point to a need to introduce either spatial variability in the earth's response function, or a regionally variable ice-scale parameter. The Finland predictions in Fig. 19(a), for example, could be brought into better agreement with observations by either decreasing the ice thickness over the region by more than the Scandinavian averaged β^F factor, or by reducing the Earth's response to the load by modifying the earth-model parameters. Likewise, the Oslofjord predictions imply a need to increase the ice height, that the β^F factor is too small for this region, or that the mantle viscosity here is less than the average values found.

5.2 Regional solutions

To examine the regional character of the discrepancies between observations and predictions further, the Fenno-Scandinavian region has been divided initially into 10 regions as illustrated in Fig. 20. For each region a search is then made through the model parameter space defined by (12) for the optimum earth-model parameters (H_1, η_{um}, η_{lm}) and ice-scale parameter β. Because the data sets for each zone are now much reduced in number, these regional solutions are based on the original standard deviations of the observations without any attempt to group the data into space–time bins. The discrepancies $|\Delta\zeta_o^m - \Delta\zeta_p^m|$ for each model are evaluated, and if for any observation m this difference exceeds $3\times\sigma_\zeta^m$ for all earth models in the range specified then the observation is re-examined as to whether it provides a reliable indicator of past sea level. If no observation-related reasons can be identified for rejecting the observation, or for increasing the assumed standard deviation, the observation is retained in the database. The range of acceptable models for each zone is then evaluated according to (10). Because the observational standard errors have already been scaled upwards when compared with the original estimates, usually by a factor of 2 or more, a 1-sigma confidence limit is adopted and models E_k for which $\Phi_k^2\le 1$ are consistent with the observational accuracies. Results for the different zones are then compared to determine whether they are consistent with the hypothesis that the earth- and ice-model parameters are uniform between zones. If the earth-model parameters are consistent across several zones then a weighted mean solution is established for the subgroups of zones, with the weights inversely proportional to Ψ_{k*}^2. Finally, a new ice sheet, scaled by the regional β parameters, is constructed and the computational cycle is repeated to check for convergence.

5.2.1 *Finland and central and northern Sweden*

This region is covered by the three zones of southern Finland (1), central and northern Finland (2) and central and northern Sweden (3). All three zones lie well within the ice margins corresponding to the time of maximum glaciation. Geologically, the zones also lie well within the boundaries of the Fennoscandian Shield. The first zone corresponds to sites close to and outside the major southern Finland moraines formed in Younger Dryas time when the northward retreat of the ice from the European plain momentarily halted. The division between southern and central Finland is, however, somewhat arbitrary and introduced primarily to establish whether lateral variations in model parameters, particularly in β, can be detected while retaining a sufficient number of observations to yield satisfactory regional solutions.

Fig. 21(a) illustrates the minimum variance Ψ_k^2 for the zone of southern Finland as a function of η_{um} and η_{lm} with $H_1=$ 65 km, together with the corresponding β parameter and the $\Psi_k^2\le 1$ statistic. Plots for other values of H_1 within the range (12) yield similar results and good separation of earth-model parameters is generally not achieved with these spatially limited data sets. In particular, the resolution for H_1 and η_{lm} is not high in this example, consistent with rebound near the centre of large-sized ice sheets being relatively insensitive to these parameters (e.g. Fig. 14). The insensitivity of Ψ_k^2 to H_1 is also

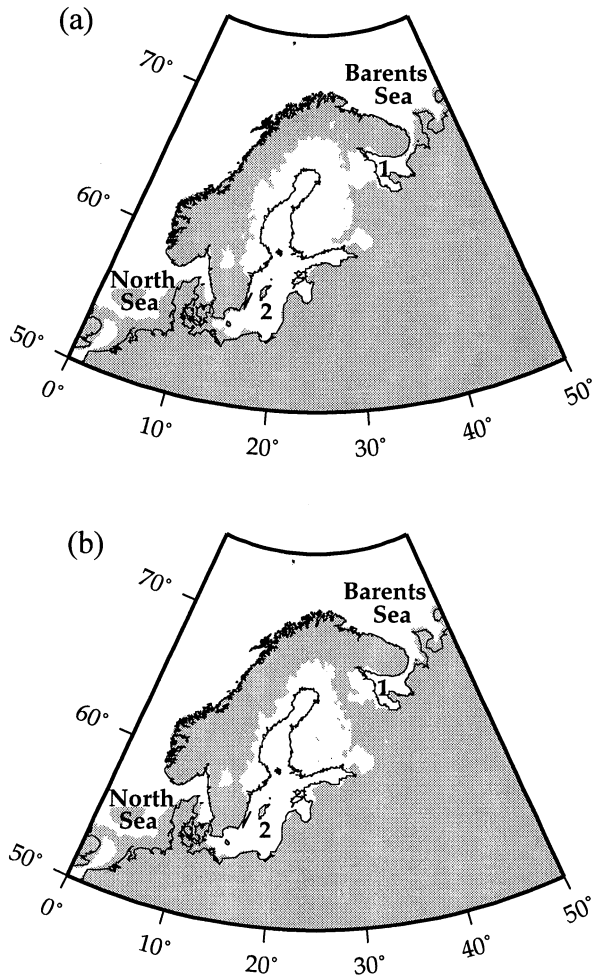

Figure 18. Predicted palaeoshorelines at 9000 BP (based on eq. 7) for (a) the least-variance earth model from Fig. 16(a) with $\beta^F = 1$ and (b) the least-variance earth model corresponding to the case illustrated in Fig. 16(b) with the corresponding value $\beta^F = 0.62$. 1: White Sea; 2: Baltic Sea.

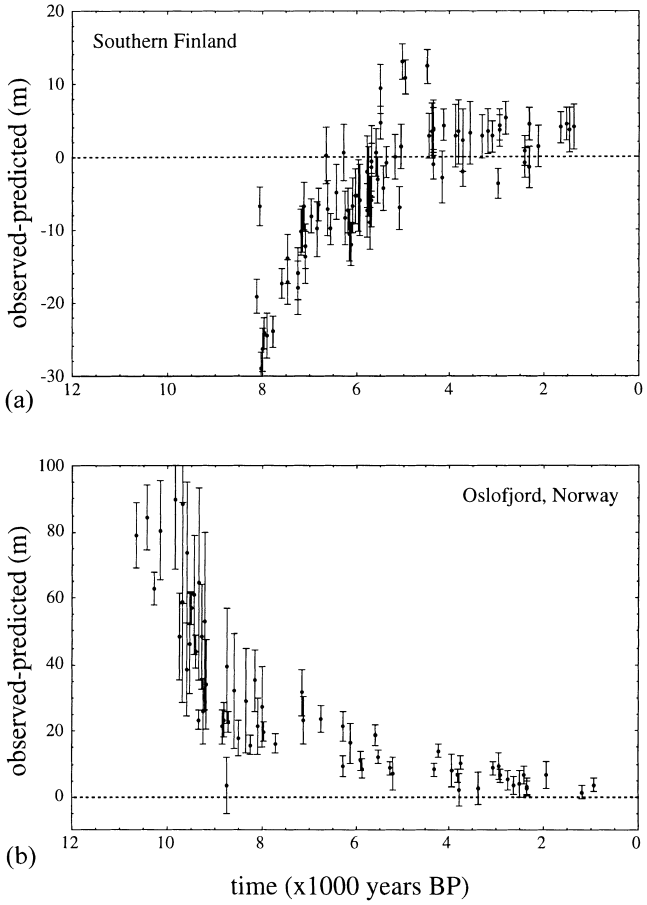

Figure 19. Plots of the residual, observed less predicted, sea levels for the earth model and β^F corresponding to the least-variance solution identified in Fig. 16(b): (a) for southern Finland, (b) for the Oslofjord region of Norway.

illustrated in Fig. 21(a), where it is plotted as a function of η_{um} and H_1 for $\eta_{lm} \simeq 2 \times 10^{22}$ Pa s, indicating further the poor resolution achieved for the lithospheric thickness. The overall least variance Ψ_k^2 for this zone, within the parameter limits defined by (12), is given in Table 4 and the Φ_k^2 function in Fig. 21(a) follows from (10) with the $\Delta\zeta^m_{p,k*}$ based on these values. The region, $\Phi_k^2 \leq 1$, defines quite a broad zone of the parameter space within which the model predictions are consistent with the observational accuracy estimates. Models with low upper-mantle viscosity, however, are excluded. The β estimates (dashed-line contours) vary substantially across the entire model space explored, from about 2 for the lowest-viscosity models to about 0.30, but within the subspace defined by the condition $\Phi_k^2 \leq 1$, the variation in β is much reduced, ranging from about 0.3 to 0.5. Thus, while the resolution for the earth-model parameters is not high for this zone, the β estimate is nearly independent of these parameters and an effective separation of the earth and ice parameters appears to be feasible.

Similar results are illustrated in Fig. 21(b) and Table 4 for central and northern Sweden (zone 3), including the Finnish islands of Ålund. As for the first zone, the resolution for the earth-model parameters is, with the exception of η_{um}, relatively low. The observations for the central and northern areas of Finland (Table 4) lead to a similar solution and the acceptable earth-model parameter space overlaps with that of the other two zones. In particular, the solutions are consistent with the hypothesis of laterally uniform earth-model parameters for the region covered by these three zones. As for the first zone, the β parameters for the other two zones remain nearly constant within the corresponding $\Phi_k^2 = 1$ contours. The individual estimates of the β parameters for the three regions are, however, different and less than the values found for the Scandinavian-wide solutions, confirming that major modifications of the ice model are required. In particular, the β parameter over southern Finland is consistently lower than that for the other regions and implies that the maximum ice thicknesses for this region must be substantially less than assumed in the starting model.

The minimum-variance factors obtained for the three regions are all much smaller than that found for the Scandinavia-wide solution (*cf.* Fig. 16b), although they are still larger than the expected value of unity. Possibly the observational standard deviations should be increased by a factor of 1.5 to 2.2, or there is scope for further model improvement, such as variation

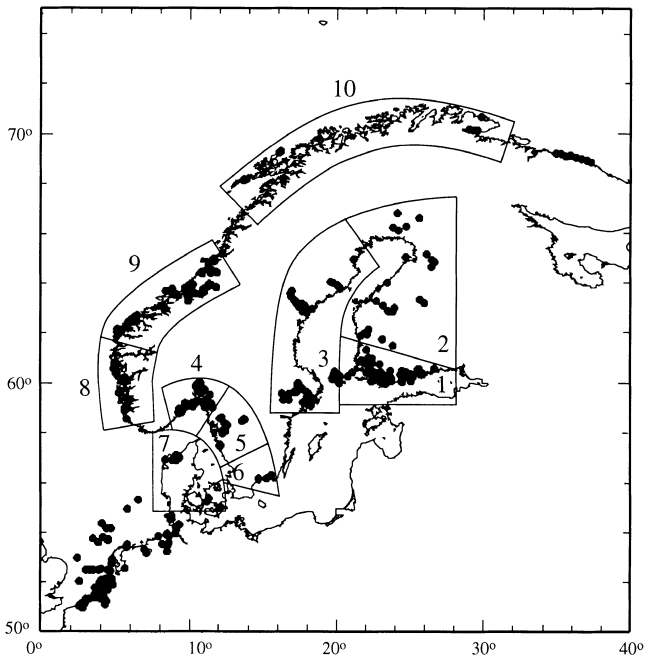

Figure 20. Division of the observational database into 10 zones. (1) Southern Finland, (2) central and northern Finland, (3) central and northern Sweden, (4) Oslofjord, (5) southwest Sweden, (6) southern Sweden (Blekinge), (7) Denmark, (8) southwestern Norway, (9) central western Norway, (10) northern Norway.

in the β parameter within a region or for a greater layering of the viscosity model (Lambeck *et al.* 1996). For example, an examination of the discrepancies between the observed and predicted values for southern Finland shows that they tend to be mostly positive in the west and negative in the east (Fig. 22), consistent with a need to increase ice heights, relative to the average scaling for this zone, for the western area and with a relative decrease in ice height to the east. This is also consistent with a westward increase in the β seen in the solutions for the three zones (Table 4). Within the northern Sweden zone, some latitudinal dependence of the residuals is also suggested, with a slightly higher β-value for the Stockholm region than for the zone as a whole.

5.2.2 *Southwestern Scandinavia*

The four zones making up this region (Fig. 20) cover the southwest and south of Sweden, the Oslofjord of Norway, and Denmark. The southwest Sweden and Oslofjord zones lie well within the Glacial Maximum ice-sheet limits, although they are close to the Younger Dryas limits. In contrast, the Danish sites lie close to the maximum ice-limit margin, both within it and outside it, and the results for this zone can be expected to be sensitive to details of the ice distribution. In particular, the ice-height scaling model with a single parameter is expected to be inadequate here and considerable trade-off between earth- and ice-model parameters may occur.

The Oslofjord region (4) yields satisfactory results (Fig. 23, Table 4) that are characterized by lower values for the upper-mantle viscosity than found for the eastern zones. Solutions with lithospheric thicknesses near the limits (30 and 150 km) of the explored model space are unsatisfactory, as are lower-mantle viscosities less than about 3×10^{21} Pa s. As for the previous zones, constraints on this last parameter are, however, poor. Of note is that the optimum ice-scaling parameter is considerably greater than for the previously examined regions. The southwest Sweden zone includes data from a number of sites that lie within about 50 km of the coast as well as from the more inland sites near Mt Billingen, about midway between the lakes Vänern and Vättern. Solutions based on all data in this zone are less satisfactory than for the previously discussed zones in that the least-variance estimate is relatively large (Table 4). This is largely a consequence of the predictions for Mt Billingen lying systematically and substantially above the observed values (Fig. 24) and the solution which excludes the Billingen data is more satisfactory (Table 4). Adopting this solution, and solving for β only, yields $\beta \simeq 0.65$ for the local ice thickness over the Billingen region, suggesting that the gradient of the ice profile across central Sweden may be less than assumed in the starting model. The southern Sweden data from Blekinge yield a solution for earth-model parameters that is similar to that found for the other two zones, but the β parameter is now much reduced (Table 4), indicating that the maximum ice heights over southern Sweden and the western Baltic Sea are only about 30 per cent of the initially adopted values.

Table 4. Solutions for earth-model parameters and ice-height scale factor β for the individual zones. The first column for β corresponds to the solutions for local earth-model and β parameters. The second β column corresponds to the solutions for β based only on the earth model defined by the solution (13).

Zone	H_1	η_{um} ($\times 10^{20}$)	η_{lm} ($\times 10^{22}$)	Ψ_k^2	β (1)	β (2)
1. Southern Finland	30	5	5	2.42	0.32	0.35
2. Central–northern Finland	80	4	10	1.95	0.43	0.42
3. Central–northern Sweden	50	3	10	2.75	0.49	0.47
4. Oslofjord	80	1.5	3	2.08	0.88	0.79
5. Southwest Sweden	80	1.0	1	4.02	0.84	—
5a. Southwest Sweden without Billingen data	50	2.5	3	0.96	0.75	0.75
6. Southern Sweden	80	2.5	10	3.37	0.30	0.26
7. Denmark	150	4	3	3.68	0.40	0.27
8. Southwestern Norway	50	5	0.5	6.69	0.61	0.87
9. Central–western Norway	80	2	0.3	3.30	0.80	1.03
10. Northern Norway	50	2	10	1.51	0.83	0.90
11. North Sea	50–120	<3	>0.5			

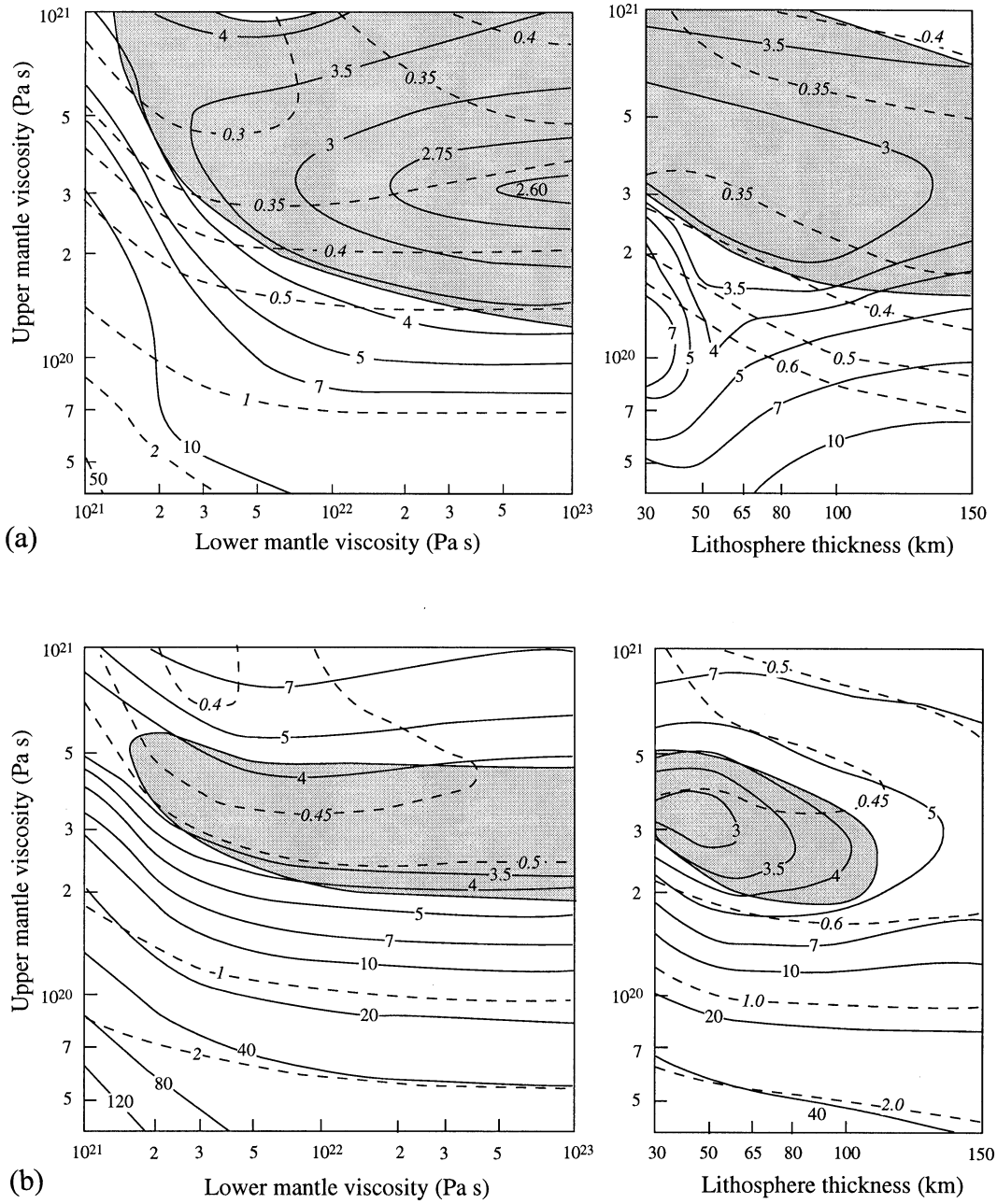

Figure 21. (a) Variance factor Ψ_k^2 (solid lines) and the β estimate (dashed lines) for southern Finland in (left) $\eta_{\rm um}$–$\eta_{\rm lm}$ space for $H_1 = 65$ km and (right) $\eta_{\rm um}$–H_1 space for $\eta_{\rm lm} = 2 \times 10^{22}$ Pa s. The region of the model space for which $\Phi_k^2 \leq 1$ is shaded. (This statistic is based on the earth-model parameters corresponding to the least variance Ψ_k^2 found in the $\eta_{\rm um}$–$\eta_{\rm lm}$–H_1 space.) (b) Same as (a) but for the data from central and northern Sweden.

The solutions for the Denmark zone are generally unsatisfactory in that: (i) the least-variance estimates are large; (ii) the least variance occurs for models with $H_1 \geq 150$ km, the only region examined so far that gives such large values; and (iii) the residuals for the best-fitting models exhibit systematic patterns that point to inadequacies in either the models or the data. At Præstø in Fakse Bugt, and for sites within the Store Bælt, the predictions for the best-fitting model lie significantly above the observed values, whereas at Limfjord the reverse is noted (Fig. 25). With the assumed ice model, models with thin lithospheric thickness are rejected because they lead to predictions of significant mid-Holocene highstands at these localities, whereas this is not recorded in the observational evidence from either Præstø or the Store Bælt. Because of the approximate nature of the ice model in representing the rather complex movements of ice over this region in Late Weichselian time (e.g. Houmark-Nielsen 1989), the likely first-order explanation for the anomalous results is that the ice model for the region is inadequate. For example, in the initial model the ice over Jylland and over the western Baltic is comparable in terms of thickness and profile shape, and agreement between observed and predicted sea levels for the two areas can be achieved by reducing the ice thickness of the western Baltic ice stream relative to the northern ice stream, as is indeed suggested by the substantially different ice scale-height parameters estimated for southern Sweden and the Oslofjord regions. Thus a more

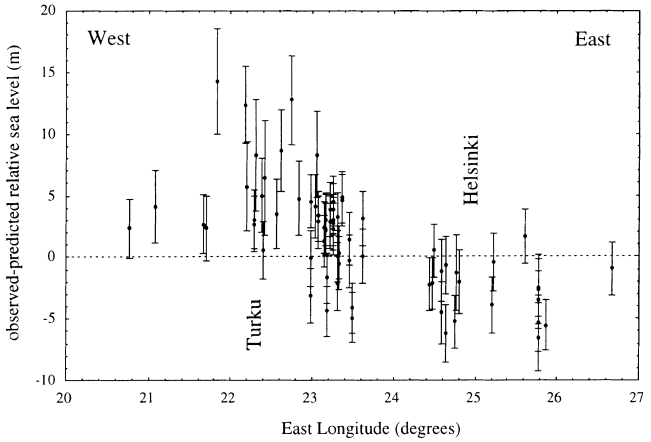

Figure 22. Residuals, observed less predicted, for the southern Finland data corresponding to the post-Ancylus Lake stage. The predictions are based on the least-variance solution for this zone (Table 4).

satisfactory approach may be to adopt the earth-model solution for the Swedish regions and to use the observational evidence to estimate necessary modifications of the ice model. Adopting the earth-model parameters for southern Sweden yields an average ice-height scale factor of about 0.25–0.30 for the region, but the discrepancies with the observed values are now much larger at the Præstø and Store Bælt sites (Fig. 25). Solutions in which the ice limitation of the starting model is described by a single local parameter remain unsatisfactory for these locations near the former ice margin.

5.2.3 *Western and northern Norway*

The regional solutions discussed so far are, with the exception of the Denmark zone, characterized by the zones occurring within the maximum ice limits such that the rebound predictions are not strongly dependent on small changes in the shifts of the ice margins. Also, the ice margins immediately beyond these zones lie on land and their locations and times of occurrence and subsequent retreat are reasonably well known. However, the situation along the western margin of Norway is more complex because the limits of the ice on the continental shelf and shallow parts of the North Sea are generally not well constrained by observational data. Predictions of crustal rebound and relative sea-level change are therefore likely to be sensitive not only to the uncertainties in ice thickness over the region but also to the location of the ice limits. The situation is similar to that encountered for Spitsbergen, where it was not possible to constrain all unknowns from relative sea-level data alone but where some constraint, which was not strongly dependent on the assumed earth-model parameters, could nevertheless be placed on the ice models (Lambeck 1995c, 1996).

The observational data for the western and northern coastal region of Norway have been divided into three zones (Fig. 20). The first, the southwestern zone, extends from Jæren in the south to latitude 60.5°N (Fonnes, north of Bergen) and includes data from Brusand, Yrkjefjorden, Bømlo, Sotra and Fonnes. The second zone, central western Norway, covers latitudes from 62° to 65°N and corresponds to the coastal region between Nordfjorden and Nærøy. The third region, northern Norway, extends from Lofoten in the west to the Varanger peninsula in the east. The geology of the three zones is characterized by the Permo-Carboniferous Caledonian Orogeny, possibly by Neogene uplift, and by a nearby continental margin. Hence not only may the response parameters for these zones differ from those for the eastern region, but lateral variation within the zones could also be anticipated. Furthermore, these zones are characterized by uncertainty about the location of the offshore ice limits at the time of the Last Glacial Maximum, and some trade-off between earth- and ice-model parameters can be expected. One example of this trade-off is illustrated in Fig. 26(a) for the Sotra locality (west of Bergen). Here, two earth models that differ only in lower-mantle viscosity (10^{22} and 10^{23} Pa s, respectively) yield virtually indistinguishable predictions for crustal rebound when

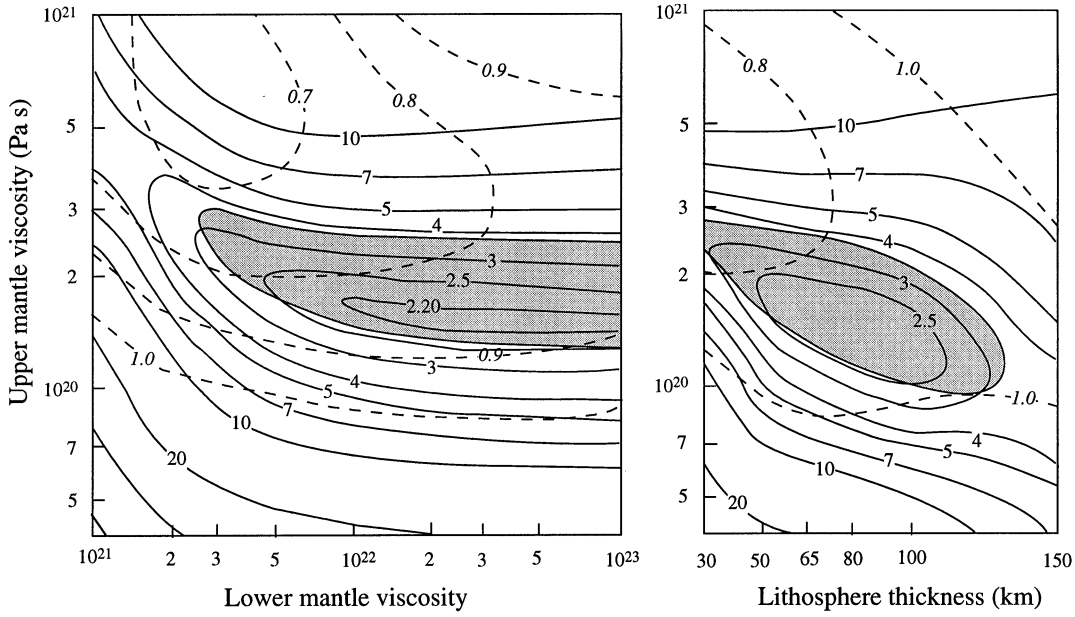

Figure 23. As Fig. 21, but for the Oslofjord area of Norway.

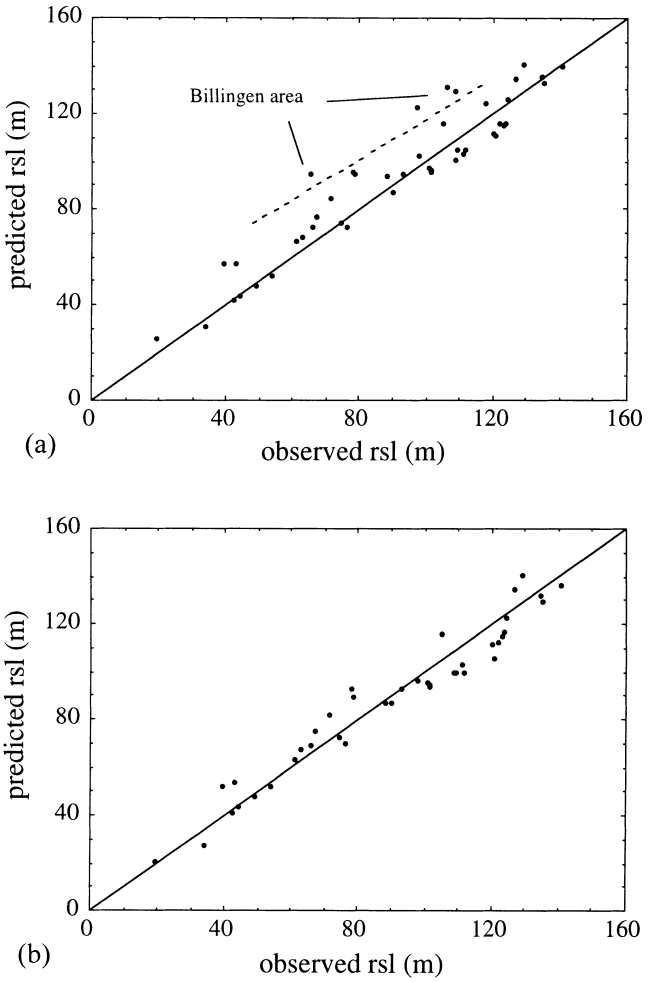

Figure 24. Observed versus predicted relative sea levels for southwest Sweden corresponding to the solutions (a) zone 5 and (b) zone 5a in Table 4. The first solution (zone 5) contains the Mt Billingen data points for which the predicted values are systematically greater than the observed values.

the ice-sheet margin for the higher-viscosity models is expanded offshore by about 20–30 km. The effect of increasing η_{lm} is to reduce the predicted late-glacial rebound at these near-marginal sites, and this is compensated for by expanding the ice outwards. A second example of the earth–ice parameter trade-off is illustrated in Fig. 26(b), where the variable parameter is the lithospheric thickness. If H_1 is decreased, the rebound immediately within the ice margin is increased but this can be negated by reducing the ice load. Thus models with a thin lithosphere with limited offshore ice expansion lead to similar predictions of rebound to models with thicker lithospheres in which the ice sheet is expanded outwards. These trade-offs can be partly resolved when observational data are available from geographically well-distributed sites, but only in a few instances is the information available from deeply penetrating fjords that would permit such a separation.

The offshore ice limits for southern Norway (zone 8) are particularly uncertain, with some models extending the Last Glacial Maximum ice cover across the Norwegian Trench and into the North Sea to join up with the British ice sheet (e.g. Denton & Hughes 1981), and others in which the southwestern corner of Norway was ice-free (e.g. Larsen & Sejrup 1990).

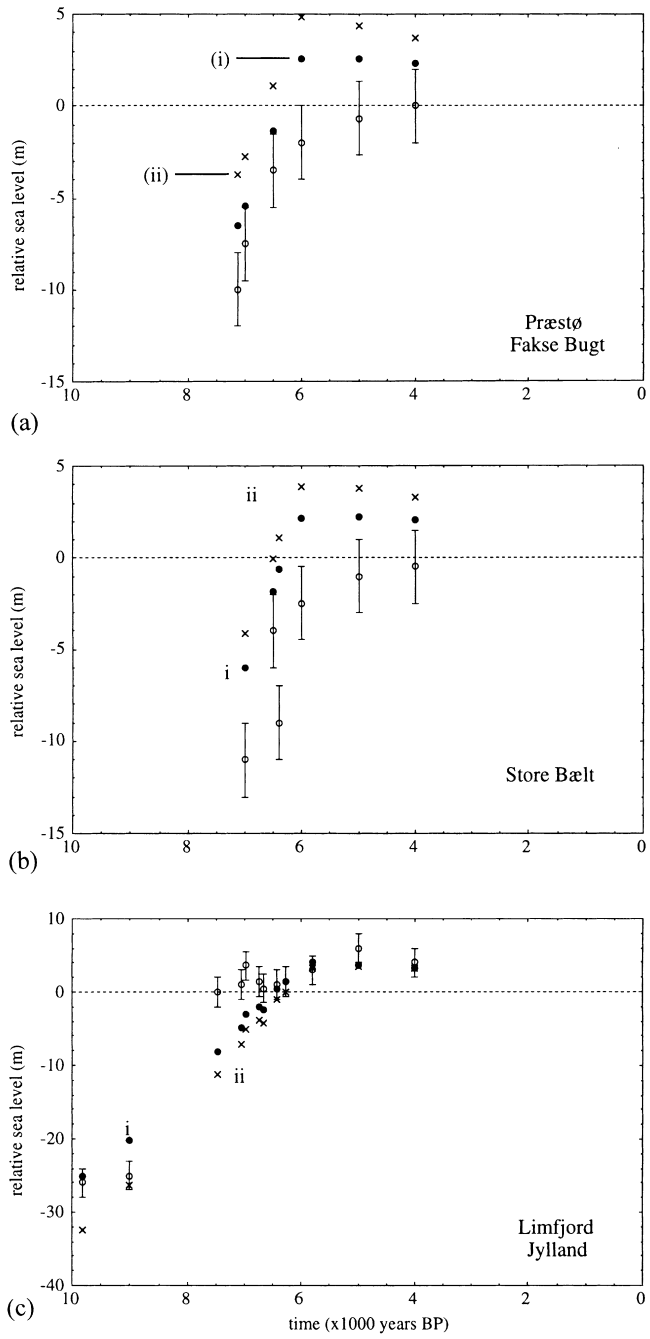

Figure 25. Observed (with error bars) and predicted estimates of relative sea level at three sites in Denmark: (a) Præstø, Fakse Bugt, (b) Store Bælt, and (c) Limfjord (Jylland). The predicted values are based on (i) the best-fitting earth-model parameters for Denmark (Table 4) (•) and (ii) the earth-model parameters for the southern and southwestern Sweden solutions and the corresponding β estimate based on the data from the Danish zone (x). The observed values are identified by the error bars.

The adopted ice model is an intermediate one in which the ice extended up to 150 km offshore with the maximum limit in the southwest corresponding to the 16 000 year isochron of Andersen (1981). If the actual ice margin departs from this, the characterization of the ice model limitations by a single height-scaling parameter is unsatisfactory for these ice-margin zones. Indeed, the solution for this zone yields large values for

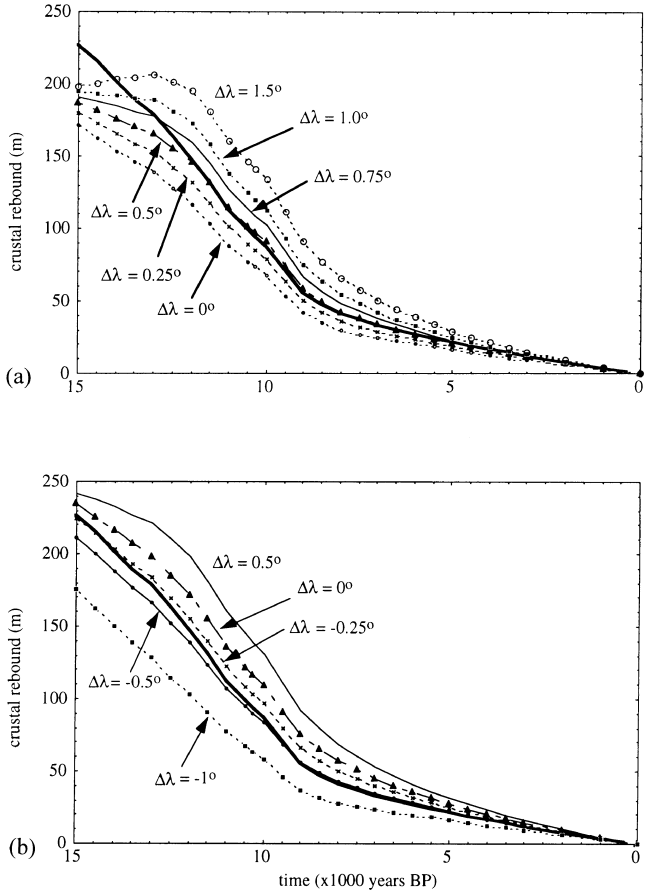

Figure 26. (a) Predicted sea levels for a site on Sotra, west of Bergen, based on an earth model with a lower-mantle viscosity of 10^{22} Pa s (thick continuous line) compared with predictions for a model with $\eta_{lm} = 10^{23}$ Pa s but in which the ice margin has been displaced westwards by an amount $\Delta\lambda$. For both models $H_1 = 65$ km and $\eta_{um} = 3 \times 10^{20}$ Pa s. When the ice margin is shifted westwards by about 0.5° the predictions for the second model are very similar to those of the first model with zero shift in the ice limit for the interval in which there is observational evidence of sea-level change ($t \lesssim 12\,000$ years). (b) Same as (a), but for models that differ only in lithospheric thickness. The thick line corresponds to a model with $H_1 = 65$ km ($\eta_{um} = 3 \times 10^{20}$, $\eta_{lm} = 10^{22}$ Pa s), and the other predictions are for a model with a thin lithosphere (30 km) and with the ice sheet shifted westwards (positive $\Delta\lambda$) or eastwards (negative $\Delta\lambda$). In this case the thin-lithosphere model leads to comparable predictions to the $H_1 = 65$ km model for the interval $t \lesssim 12\,000$ years if the ice margin in the former case is moved eastwards by about 0.5°.

the least minimum-variance function Ψ_k^2 (Table 4) with the 'best' results occurring for $H_1 = 30$–65 km. If the scaled ice model is correct, then models with $H_1 \gtrsim 80$ are excluded, as are models with $\eta_{um} \lesssim 3 \times 10^{20}$ Pa s (Fig. 27a). The estimate for the lower-mantle viscosity is distinctly less than any value found for the other zones examined so far, although values of 10^{22} Pa s fall within the $\Phi_k^2 = 1$ contour if $H_1 \lesssim 50$ km. In view of the trade-off between the earth-model parameter and the position of the ice margin (Fig. 26), and the uncertainty in the precise location of the latter, it is inappropriate to attach great importance to any differences between the parameters for this zone and those of the previously discussed zones where the dependence on details of the ice sheet is less critical. Because the lower-mantle viscosity is likely to exhibit less spatial variability than the upper-mantle parameters (seismic evidence for dispersion), one approach to constraining the solution parameters is to fix η_{lm} to the value determined from the other regions and solve for H_1 and η_{um}. Such a solution leads to $H_1 < 65$ km and $(3 \times 10^{20} < \eta_{um} < 7 \times 10^{20})$, consistent with the solutions for the other regions. In many instances this model results in reasonable agreement with the observations, such as for Bømlo and Fonnes (Fig. 28a,b) where the predictions for the past 10 000 years give the same temporal pattern of relative sea-level change as is observed. For Sotra (Fig. 28c), however, where the observational evidence covers the lateglacial period before about 10 000 BP, the agreement is less satisfactory, with the predictions being consistently too low.

The central-western Norway zone 9 leads to a better but still not wholly satisfactory solution (Table 4; Fig. 27b), with the least-variance solution occurring for $H_1 = 80$ km, and models with $H_1 \lesssim 65$ km are excluded. Here the inversion of sea-level data, without examining possible limitations of the ice models, leads to the inference of a relatively thick lithosphere when compared with the inference from the data for southwestern Norway. Again, however, the explanation is likely to rest with the ice-model limitations, particularly as the discrepancies between observed and predicted values exhibit significant patterns. For example, the residuals for the northern part of the zone are consistently negative whereas they tend to be positive in the south (Fig. 29a), suggesting that the ice-scaling parameter may vary from north to south across the zone. Furthermore, the residuals tend to exhibit a dependence on distance from the coast, as is illustrated for the Trondheim area where the observational record extends a considerable distance inland (Fig. 29b). Here, for a wide range of plausible earth models, the predictions for the near-coastal localities of Frøya and Hitra, in the Trondheimsfjorden west of Trondheim, lie systematically below the observations, whereas some 90 km inland, at Frosta and Inderoy, the pattern is reversed. At the coastal localities the predictions mirror well both the spatial and temporal pattern of change but not the magnitudes of the rebound, and at the intermediate locality of Bjugn the agreement is good (Fig. 30). For the area as a whole, an improved agreement between observations and prediction can be reached by extending the ice margin further onto the shelf by about 40 km and by reducing the inland ice thickness.

The northern Norway zone leads to more consistent results for the solution of earth-model parameters, in the sense of smaller values for Ψ_k^2, of earth-model parameters that are more consistent with those obtained for the better-constrained zones (Table 4), and of residuals that show little regional pattern. In part this agreement may be a consequence of the ice model over the Barents Sea having been previously constrained by sea-level information from the Varanger Peninsula areas as well as from Svalbard and Frans Josef Land (Lambeck 1995c, 1996).

5.2.4 *Discussion of regional solutions*

Table 4 summarizes the results for earth-model parameters for the individual zones comprising the Fennoscandian region. The most satisfactory solutions, in terms of low values for the variance estimate Ψ_k^2, occur for the zones that lie well within the ice-sheet margins where the sea-level predictions are least affected by any uncertainties in the ice model and where, because the spatial gradients of the ice sheets are relatively

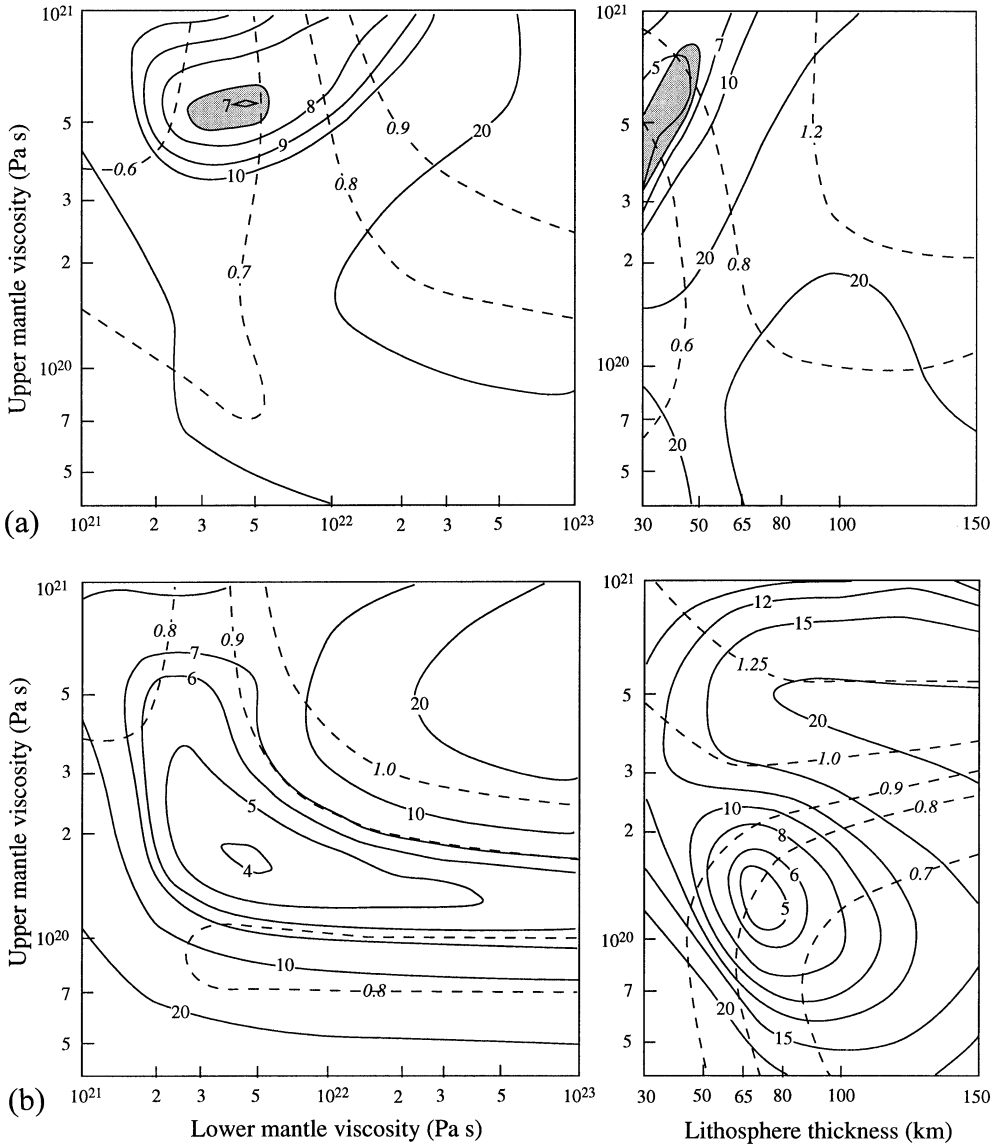

Figure 27. (a) As Fig. 21, but for southwestern Norway (zone 8). (b) As Fig. 21, but for central western Norway (zone 9). In this second example the $\Phi_k^2 \leq 1$ region does not intersect the H_l–η_{um} plane when $\eta_{lm} = 2 \times 10^{22}$ Pa s, and is tangential to the η_{um}–η_{lm} plane when $H_l = 65$ km at about $\eta_{um} = 2 \times 10^{20}$, $\eta_{lm} = 5 \times 10^{21}$ Pa s.

small, the characterization of the ice-model limitations by the single β parameter is reasonable. However, sea-level data from these zones do not provide a good resolution for all earth-model parameters, particularly for the lithospheric thickness and lower-mantle viscosity. As previously noted, the three eastern zones covering Finland and northern Sweden yield comparable results for the mantle parameters, and a weighted mean of the three yields $H_l = 55$ km, $\eta_{um} = 4 \times 10^{20}$ Pa s and $\eta_{lm} > 10^{22}$ Pa s, although a wide range of models about these values, indicated by the associated accuracy estimates in Table 5, yield predictions that are consistent with the observational accuracies of the relative sea-level data. Upper-mantle viscosity estimates less than 2×10^{20} Pa s are excluded, as are values greater than about 7×10^{20} Pa s. Models with a lower-mantle viscosity less than 2×10^{21} are also inconsistent with the combined observational data for the three zones. To obtain better constraints on these parameters will require improved accuracy for the observational evidence, particularly for the periods of earliest deglaciation, improved observational constraints on the ice sheet that are independent of the rebound modelling, and an expansion of the region to include observational data from areas near and beyond the ice margins at the time of the Last Glacial Maximum so as to give improved resolution for the lower-mantle viscosity. This last requirement has the proviso that these areas have had similar tectonic histories so that the mantle parameters can be expected to be reasonably uniform over the region as a whole.

The three individual zones covering southwestern and southern Sweden and the Oslofjord (zones 4, 5a, b in Table 4) area also yield consistent parameters and relatively small values for the least-variance Ψ_k^2 statistic. The weighted mean for these zones yields $H_l = 66$ km, $\eta_{um} = 2.8 \times 10^{20}$, and $\eta_{lm} > 10^{22}$ Pa s. Upper-mantle viscosities greater than about 4×10^{20} Pa s and less than about 2×10^{20} Pa s are excluded, as are lithospheric thicknesses less than 30 km or greater than about 120 km and lower-mantle viscosities less than about

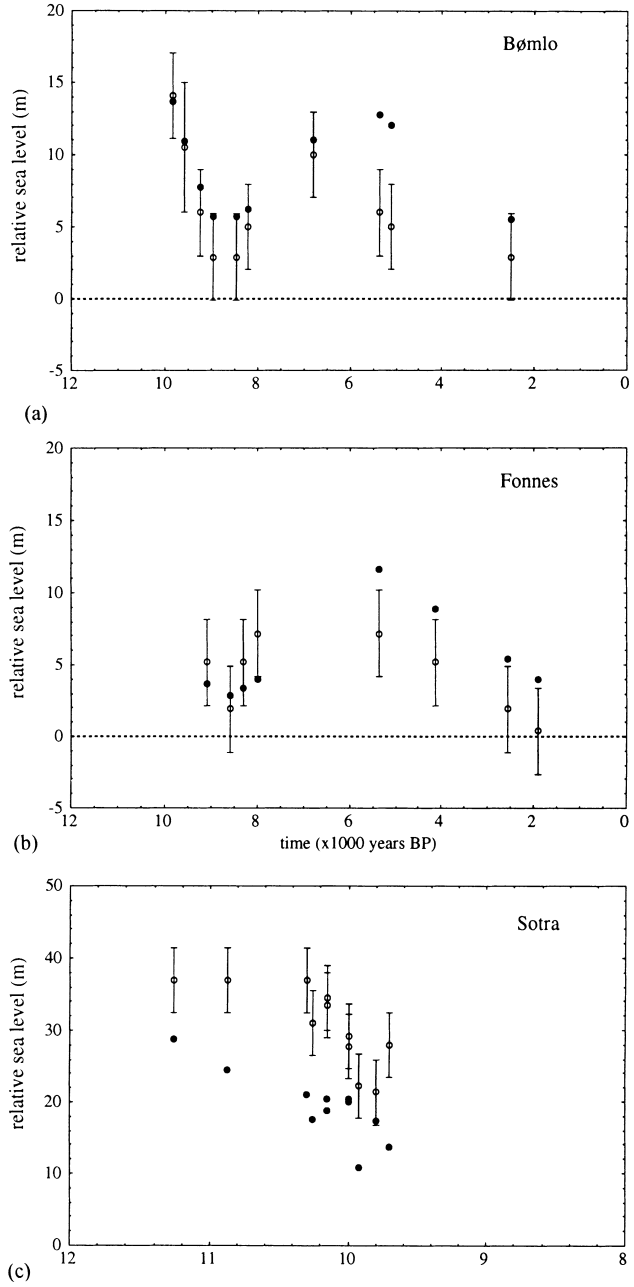

Figure 28. Predicted and observed (with error bars) relative sea-level estimates for three localities in southwest Norway: (a) Bømlo (midway between Bergen and Stavanger), (b) Fonnes, about 50 km north of Bergen, and (c) Sotra, west of Bergen. The predicted values are based on an earth model with $H_1 = 65$ km, $\eta_{um} = 3 \times 10^{20}$ Pa s and $\eta_{lm} = 2 \times 10^{22}$ Pa s. Note the different scales used for the axes.

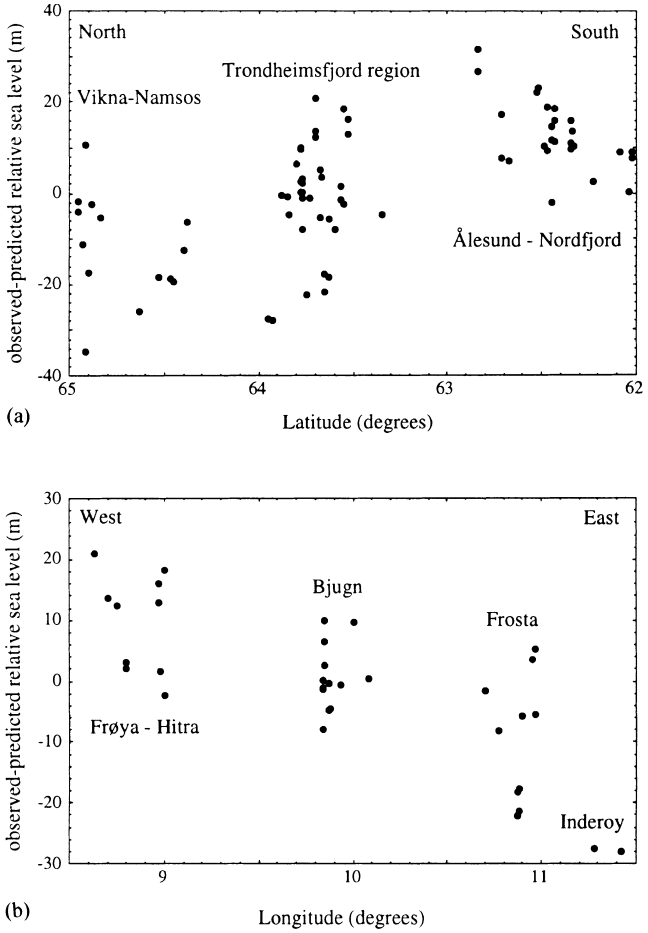

Figure 29. Residuals, observed less predicted, for the observational data in central western Norway (zone 9). The observations tend to group into three localities. Within each locality the discrepancies tend to increase with increasing time. (a) Data for the entire zone plotted as a function of latitude, and (b) data from the Trondheimsfjorden region only, plotted as a function of longitude.

3×10^{21} Pa s. The two Swedish localities (zones 5a and 6), corresponding to pre-Cambrian terrains, yield results that are consistent with those for the three eastern zones and whose upper-mantle viscosities are greater than that for the Oslofjord zone. However, this latter difference, while suggestive, is not statistically significant within the limitations of these preliminary solutions.

The three coastal areas of Norway (zones 8, 9, 10) yield a combined solution of $H_1 = 58$ km, $\eta_{um} = 2.3 \times 10^{20}$ Pa s and $\eta_{lm} = 2 \times 10^{22}$ Pa s (Table 5), results that also are consistent with those for the other regions and with the hypothesis that the upper-mantle response is laterally uniform across the region within the resolution of the data and the assumptions about the ice-sheet and the earth rheological description. With the exception of the Danish and southwestern and central-western zones of Norway, the $\Phi_k^2 \leq 1$ regions for each of the 10 zones have a common intersection in the earth-model parameter space, and the individual solutions are consistent with lateral uniformity of the mantle response across the region as a whole. A combination of data from all zones leads to the first iteration solution:

$$H_1 = 61 \pm 7 \text{ km}$$
$$\eta_{um} = (3 \pm 0.5) \times 10^{20} \text{ Pa s}, \quad (13)$$
$$\eta_{lm} = 4 \times 10^{22} \text{ Pa s}.$$

The lower limit on the last parameter is about 5×10^{21} Pa s, but the upper limit is not established.

While the evidence suggests that for these first iteration solutions the mantle parameters can be considered to be laterally uniform, the same cannot be said for the β parameters, with estimates ranging from as low as 0.3 for southern Sweden

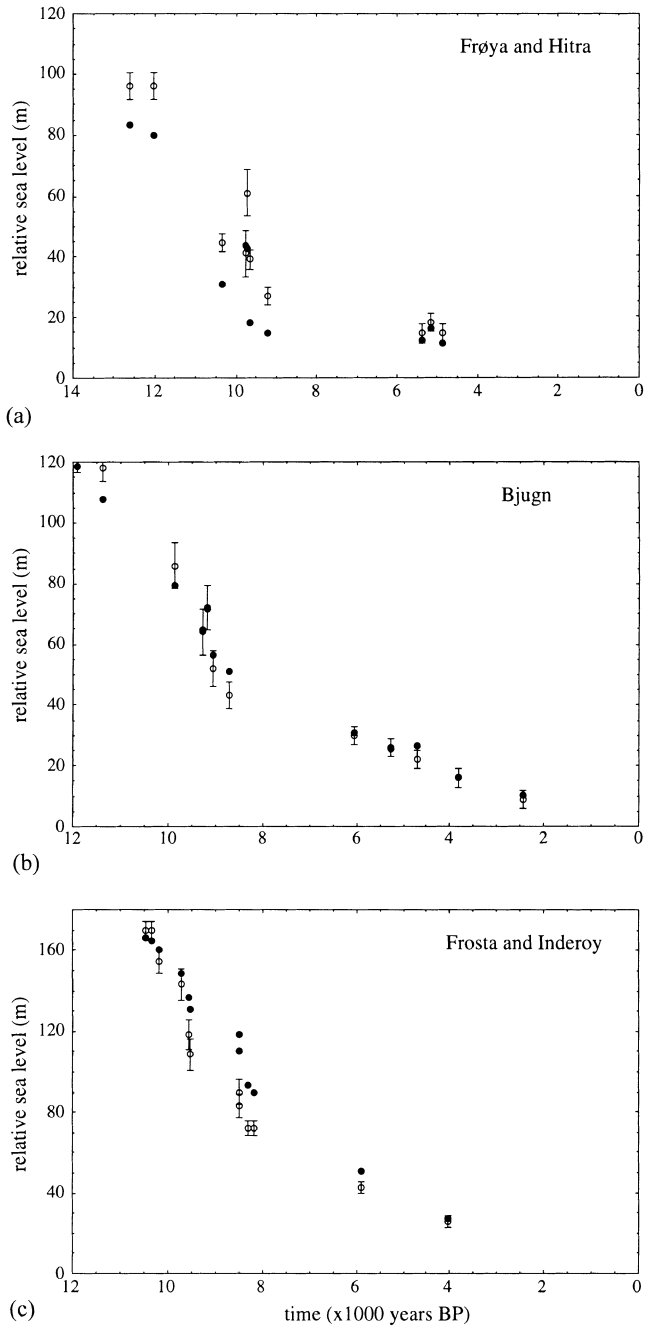

Figure 30. Comparison of observations (with error bars) and predictions for three localities in the Trondheimsfjorden area: (a) Frøya and Hitra, close to the coast, (b) Bjugn, about 60 km inland, and (c) Frosta and Inderoy, about 90 km inland.

to greater than 0.8 for western Norway and the Oslofjord region. In addition, some of the regional solutions point to variation of β within a zone (e.g. Fig. 22). Table 4 summarizes the β estimates for the individual zones based on both the optimum solution for each zone and for the solutions based on the laterally homogeneous earth-model parameters (13) (the second column of β-values). An important aspect of these solutions is that, for each zone, β generally varies only slowly over the acceptable model space (e.g. Fig. 21) such that the estimates are not strongly dependent on the choice of earth-model parameters. Also, for many of the zones the individual solutions do not differ greatly from those for the laterally uniform earth model such that the β are largely earth-model independent within the range of acceptable models. The exceptions occur for the western Norway zones, where the local earth models also depart substantially from the average model and where the representation of the ice-model limitations by a single β parameter is unsatisfactory if the location of the ice limit is not well defined.

Greater resolution of the spatial variability in the β factor results if the averaged earth-model parameters (13) are adopted and smaller subsets of the observational data are used to estimate local values for this parameter. Fig. 31 illustrates such results, which confirm the previous conclusion that the ice-scaling parameter varies substantially across the region, with the ice profiles in the east and south being distinctly different from the characteristic form described by (2). The original Denton & Hughes based ice model scaled by these spatially variable β-values constitutes the first iteration of the revised ice model.

One limitation of the method used to estimate the ice-scaling parameters necessitates further iterations. This arises from the assumption of a simple relation between local rebound and local ice heights, which becomes of limited value when β varies significantly over the region. The rebound in Finland, for example, can be considered as the sum of two parts: a local ice load over the eastern region and a more distant but adjacent ice load over the western region. The latter is sufficiently far from the Finland sites for its contribution to be of opposite sign to that of the local contribution. Predictions for these sites, on the assumption of a reduced β for the entire ice model, therefore lead to an underestimation of β. Likewise, the analysis of the western zone data would lead to an overestimation of β for this region. Thus, in the second-iteration solution, the first-iteration ice model is used to estimate new earth- and ice-model parameters. Also, the solutions are now carried out only for the two principal tectonic provinces, the Baltic Shield (comprising zones 1–3, 5a, 6) and Norway (zones 4, 8–10). Table 5 summarizes the second-iteration results for the two earth-model parameters corresponding to the two principal tectonic provinces. Some trade-off between earth-model and ice-model parameters now seems to have been introduced, with the new solutions favouring models with a thicker lithosphere (80–100 km) and reduced values for the lower-mantle viscosity of about $(5–20)\times 10^{21}$ Pa s. The new β-values for further scaling of the first-iteration ice model now tend to be greater than unity in the east and south and less than unity in the west, confirming that the previous iteration overestimated the corrections to the original ice model.

To ensure convergence, the above procedures have been repeated once more, with the solutions for both the Baltic Shield and the Norway regions giving comparable results. The corrective scale parameters are, with the exception of the Limfjord zone, now all unity to within a few per cent and no further iteration appears to be required.

6 DISCUSSION

The analysis of the glacial rebound data for Scandinavia has yielded two first-order results: (1) a model for the mantle rheology and (2) a model for the Scandinavian ice sheet that represents a significant departure from models that are characterized by quasi-parabolic cross-sections with symmetry about

Table 5. Solution for earth-model parameters for groups of zones and for the entire region in which the β parameter is included as an unknown for each zone.

	H_2 (km)	η_{um} ($\times 10^{20}$ Pa s)	η_{lm} ($\times 10^{22}$ Pa s)
First iteration			
Baltic Shield (zones 1–3, 5a, 6)	56 ± 12	3.2 ± 0.8	5 ± 2
Norway (zones 4, 8–10)	65 ± 11	2.0 ± 0.7	$2.5 \pm {}^{4.0}_{1.5}$
All zones	61 ± 7	2.6 ± 0.6	4
Second iteration			
Baltic Shield	90 ± 10	3 ± 0.5	0.5
Norway	80 ± 10	3 ± 0.5	2.0
All zones	85 ± 8	3 ± 0.4	$1.0 \pm {}^{1.0}_{0.5}$
Third iteration			
Baltic Shield	75	3	0.7
Norway	75	3	0.5
Combined solution all Scandinavia, British Isles and North Sea	75 ± 10	3.6	$0.8 \pm {}^{0.5}_{0.2}$

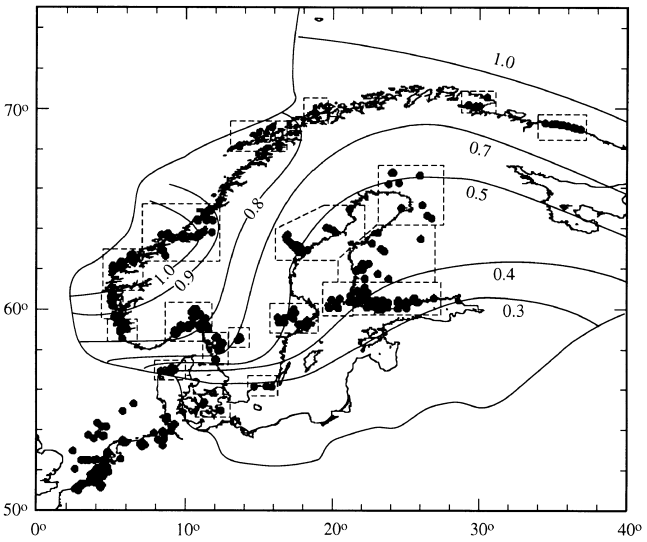

Figure 31. Subdivision of the relative sea-level data into subzones used to estimate the ice–height scale factor across the region (boxed areas outlined by broken lines) and contours of the resulting β parameter.

the centre. This model has been based on the regional analyses from the Scandinavian data, and the North Sea evidence has not been included for a reason that relates to the nature of these observations. However, these observations can be used to test the model developed so far. In particular, they may provide a useful test for lateral variation in the mantle response.

6.1 Comparison of the rebound model with the North Sea evidence of sea-level change

An important data set for testing the rebound model is provided by the evidence from the North Sea locations and from the coastal zones of Germany, the Netherlands and Belgium, sites that lie well beyond the ice margin at the time of the maximum glaciation (Fig. 4). At these localities, the major contribution to the departure of sea level from its eustatic value is the water-load term for the totality of the ice sheets (*cf.* Figs 11 and 12). As this load is of long wavelength, of the dimensions of the Atlantic Ocean, the ability to separate upper- and lower-mantle viscosities should be enhanced by the inclusion of these data (see Fig. 12). However, the observations for this region are mainly in the form of upper limits to sea level, rather than estimates of the position of mean sea level, and the method of data analysis used for the other regions is now not appropriate: the least-squares approach results in parameters that place the predictions near the middle of the age–height points illustrated in Fig. 5 rather than below the points as is dictated by the nature of the observations. Instead, a search through the earth-model space is conducted for parameters that meet the requirement

$$(\Delta\zeta_o - \Delta\zeta_p) > (0 - \sigma) \tag{14}$$

for the maximum number of these upper-limit observations, where σ is the standard deviation of the observation. Because the contributions to sea level from the Scandinavian ice sheet are relatively small for these sites (Fig. 11), any residual uncertainties in this ice model are unlikely to be significant for the predicted values $\Delta\zeta_p$. Hence only earth-model parameters will be sought in the parameter search. Also, previous studies have indicated that for $t \lesssim 6$ ka the eustatic sea-level change $\Delta\zeta_e$ may be non-zero and could amount to as much as -3 or -4 m at 6 ka, larger than the observational uncertainty of the data within this age range (Nakada & Lambeck 1988; Lambeck 1997). Neglect of this term therefore could invalidate the above requirement that predictions, without such a term, must lie below the observed values. For the earlier times the magnitude of the correction to the eustatic function is not well established but is generally of the order of, or less than, the accuracy of the data (e.g. Lambeck *et al.* 1996) and the neglect of this term is relatively less important. Thus in the first instance the comparison of observations with model predictions is carried out only for data points older than 6500 years. Fig. 32 illustrates the fraction of points that meet the criterion (14) for a model with a lithospheric thickness of 50 km. Low upper-mantle viscosity solutions are excluded, and acceptable lower-mantle viscosity estimates exceed about 5×10^{21} Pa s. Results for other values of H_1 give similar results and resolution for lithospheric thickness is not high, with values in the range 50–120 km yielding similar viscosity solutions for which all data points meet the above criterion.

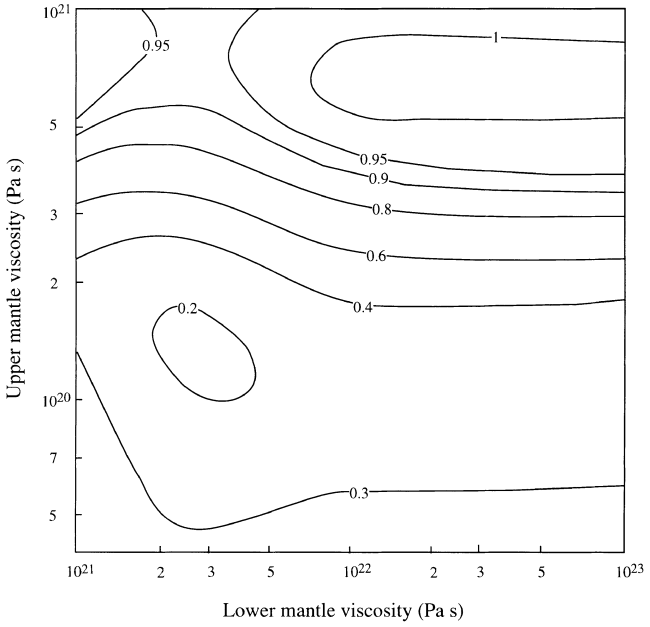

Figure 32. Fraction of North Sea data points (with times greater than 6500 BP) satisfying the criterion (14), as a function of upper- and lower-mantle viscosity for $H_1 = 50$ km.

6.2 Earth-model parameters

A satisfactory description of the rheological response to surface loading is obtained with a three-layer model defined by an effective elastic lithosphere of thickness about 75 km, a uniform upper-mantle viscosity from the base of the lithosphere to 670 km depth of about 3×10^{20} Pa s, and a lower-mantle viscosity greater than 5×10^{21} Pa s (Table 5, third-iteration solutions), with the upper limit to the last parameter being poorly constrained. One reason for the lack of constraint on this parameter is that the Scandinavian solution contains no sea-level information from sites that lie well beyond the ice limit where the isostatic contribution from the long-wavelength water load becomes relatively important. In contrast, the British Isles solution (Lambeck *et al.* 1996) yielded a better constrained value for η_{lm} because this database contained significant observations from outside the area of former glaciation. The inferred viscosity for Scandinavia is comparable to, but slightly higher than, values obtained in the earlier work for the British Isles. However, a direct comparison may not be valid since the British Isles solution assumed an ice model for Scandinavia that, on the basis of the present analysis, overestimates the ice load, and this may affect the solution for the earth-model parameters from the British solution. Hence a further iteration of the British solution, based on the modified Scandinavian ice model, would appear to be appropriate. For the present, however, the inference for earth-model parameters only is made in which the ice sheets are held fixed according to the optimum models derived here for Scandinavia and in Lambeck *et al.* (1996) for the British Isles. The sea-level observations now comprise the present Scandinavian database, the data for the British Isles summarized in Lambeck (1993), North Sea data points that correspond to estimates of mean sea level rather than to limiting values, and the data for the French Atlantic and English Channel coasts discussed in Lambeck (1997), to give a total of 1053 time–height estimates of mean sea level. The data for Scandinavia have been binned according to eq. (11), whereas for the British Isles the time-interpolated observations are used. Typical results for the variance function Ψ_k^2 (defined by eq. 9) are illustrated in Fig. 33, and the optimum parameters according to the statistic $\Phi_k^2 \leq 1$ are (see also Table 5):

$$H_1 = 75 \pm 10 \text{ km}$$
$$\eta_{um} = (3.6 \pm 1) 10^{20} \text{ Pa s} \qquad (15)$$
$$\eta_{lm} = 8 \left(^{-4}_{+22}\right) \times 10^{21} \text{ Pa s}.$$

The solution (15) is not statistically different from the Scandinavian solution only, although the lower-mantle viscosity now appears to be better constrained for the reason discussed above. This model is accepted as the representative solution for the mantle of northwestern Europe. This solution is also consistent with that obtained by Lambeck *et al.* (1990) and Mitrovica (1996) based on analyses of only small subsets of the observational database.

As for the British Isles solution, this solution exhibits some trade-off between the earth-model parameters if the parameter search is conducted through only a subset of the parameters. Thus if the thickness of the lithosphere is arbitrarily set to 100 km and the search is conducted in viscosity space only, the solution yields a higher upper-mantle viscosity η_{um} and a decreased value for lower-mantle viscosity η_{lm} (Fig. 33c). Or, if the lithospheric thickness is set at a relatively low value, say 50 km, then the solution yields a lower value for η_{um} and a higher value for η_{lm}. Neither of these solutions, however, give the overall least variance within the confines of the three-parameter earth models. This only occurs when $H_1 \simeq 75$ km.

Other than the assumption of lateral uniformity of the mantle response, the solutions rest on two other rheological assumptions: that the three-layer models provide an adequate description of the viscosity depth zonation, and that appropriate boundary conditions for the mineralogical phase transition zones have been adopted. Concerning the first assumption, the earlier work for the British Isles showed that some improvement in the solution is obtained when greater depth variation in viscosity is introduced, but that for all predictive purposes of sea-level change and shoreline evolution, three-layer or five-layer models are essentially equivalent. Whether or not this is also the case for the larger areal extent of the Scandinavian ice sheet remains to be tested. Concerning the second assumption, the boundary conditions imposed at the 670 and 400 km depth phase transitions are based on the hypothesis that the kinetics of the transition are slow, such that density contrasts across the boundary are advected with the deformation. An alternative limiting set of conditions is that the kinetics of the phase transition are rapid such that the pressure at the boundary remains unchanged through time (Johnston *et al.* 1997). Comparisons for the British Isles data set showed that the two assumptions gave very similar earth-parameter estimates but that there may be a trade-off between the choice of boundary condition and the ice-scaling parameter. Whether this also holds for the larger Scandinavian load remains to be tested.

Within the uncertainty of the mantle parameters, there appears to be little evidence for lateral variation in the effective parameters describing the mantle response for the Scandinavian region, although the uncertainties in the ice models across the Norwegian shelf makes rigorous tests for

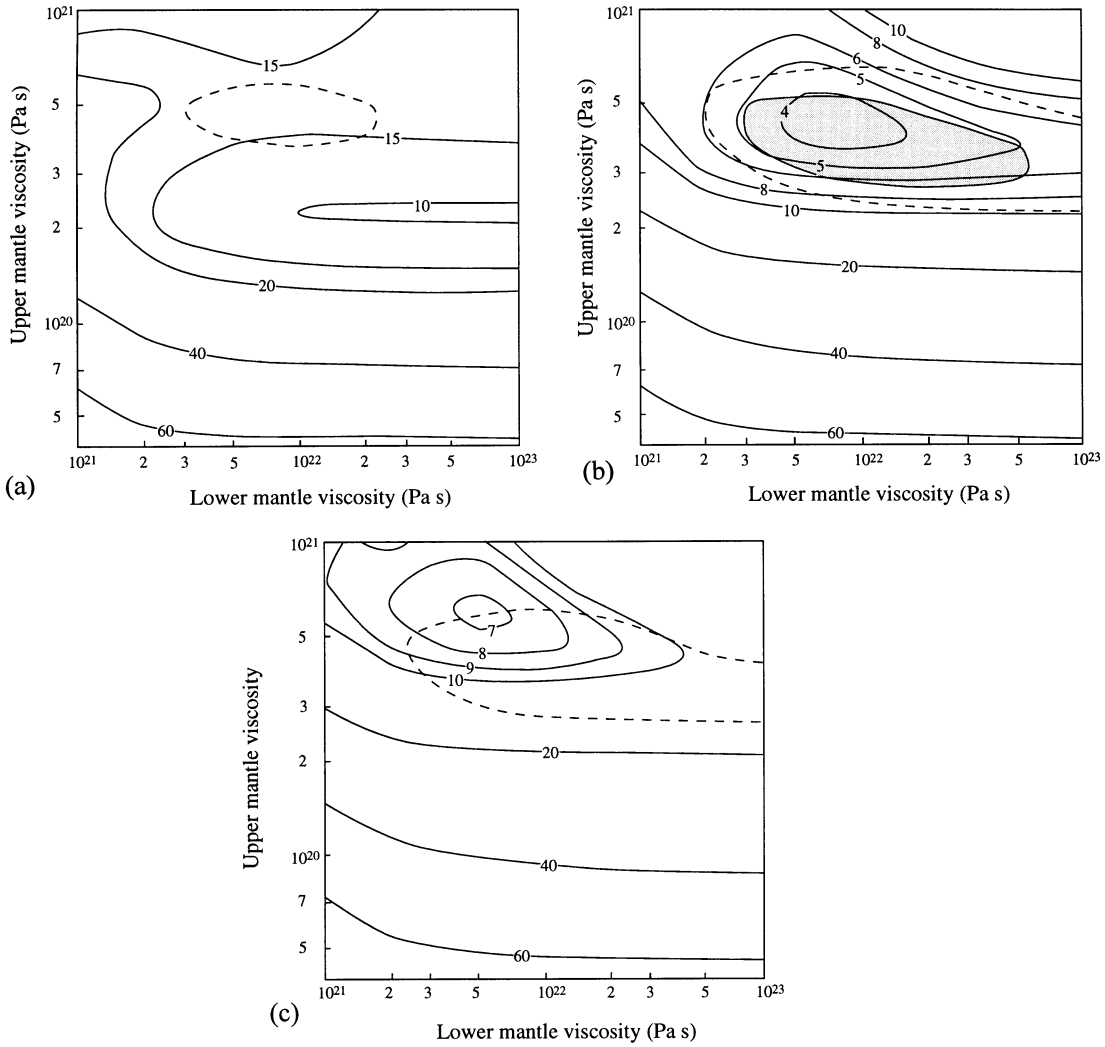

Figure 33. Variance function Ψ_k^2 as a function of upper-mantle and lower-mantle viscosity, based on observational data from Scandinavia, the North Sea, the British Isles, and French Atlantic and English Channel sites, for (a) $H_1=50$, (b) $H_1=80$ and (c) $H_1=100$ km. The $\Phi^2=1$ statistic is shown in (b) where the shaded area of the solution space shows the range of models that agree with the best-fit model to within the observational uncertainties. For $H_1=50$ and 100 km the $\Phi^2=1$ contour does not intersect the η_{um}–η_{lm} planes, and the dashed lines show the $\Phi^2=2$ contour.

such variation difficult. The limiting North Sea values rule out significant lateral variation between this region and the Scandinavian region itself. Lateral variations in upper-mantle and lithospheric seismic velocities have been noted across the region, particularly across the major tectonic boundary between Archaean northern Europe (e.g. Zielhuis & Nolet 1994) and between the North Sea and the bounding land areas. However, these variations at seismic frequencies do not appear to be reflected to the same degree in the loading response at the much lower frequencies, and the relationship between the physical properties of the mantle at difference frequencies needs to be re-examined.

6.3 Ice sheet parameters

One of the important results that has emerged from the analysis of the sea-level data for Scandinavia is that the thick, parabolic profile, symmetric ice models of the type proposed by Denton & Hughes (1981) are not appropriate for a large part of the Scandinavian ice cover during Late Weichselian time. Aspects of the new model will undoubtedly require further modification when evidence for the location of the offshore ice margins is reappraised, but essential features that are likely to be retained are the significant reduction in the ice-sheet thickness and an asymmetry in the ice profiles between the western and eastern sections of the ice sheet, with proportionally thinner cover in the east and south than in the western sectors of the ice sheet.

The new ice-sheet profiles are compared with the initial profiles in Fig. 34 along two sections, one latitudinal section through the northern part of the Gulf of Bothnia and a longitudinal section through Finland. The two profiles intersect in the northern part of the Gulf of Bothnia, where the Denton & Hughes models reach their maximum ice thickness of 3400 m. Such models, however, depress the underlying crust by a much greater amount than is indicated not only by the relative sea-level data for northern Finland and northern Sweden but also by the absence of evidence of a flooding of the Baltic from the north the moment the region became ice-free. The modified ice sheet, in contrast, attains only about

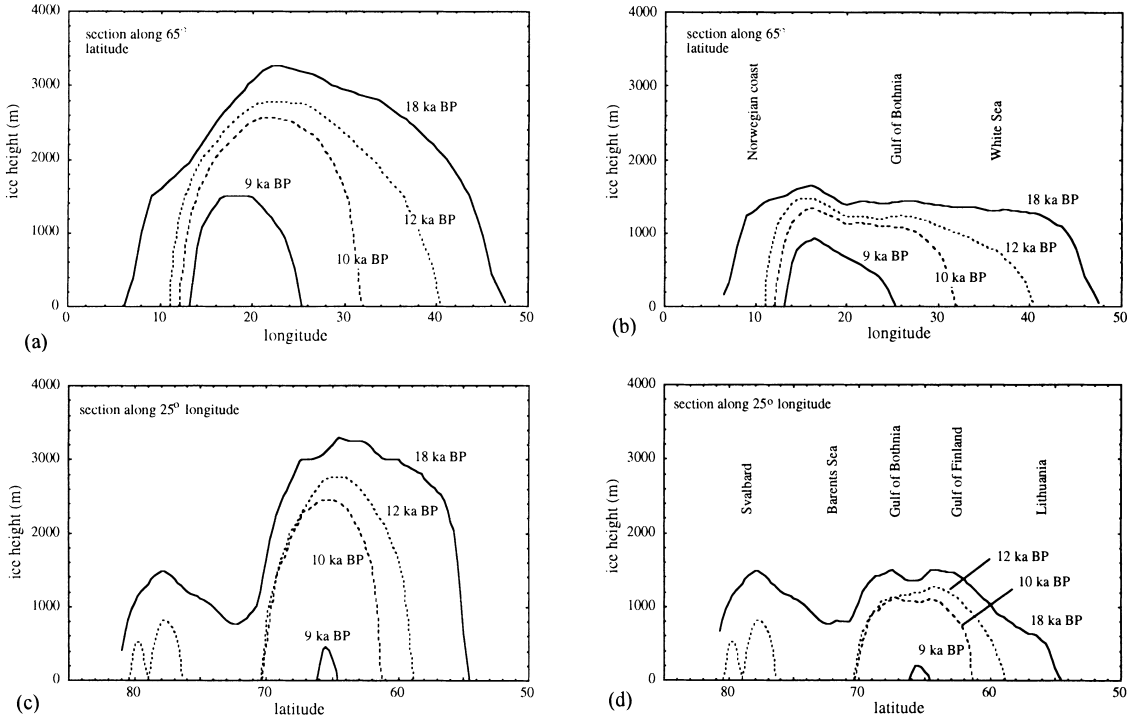

Figure 34. The original (a, c) and modified (b, d) ice thickness profiles across the ice sheet at 65° north latitude (a, b) and 25° east longitude (c, d).

1500 m maximum thickness over this area, with the maximum ice thickness of about 2000 m occurring further to the west. The need to reduce the maximum ice thickness over Scandinavia proposed by models such as that of Denton & Hughes (1981) has been previously noted (e.g. Lambeck *et al.* 1990; Tushingham & Peltier 1991). Tushingham & Peltier, for example, in their model ICE-3G inferred a maximum ice thickness of about 2200 m for the region, essentially consistent with the present result. In the subsequent ICE-4G model this estimate appears to have been substantially increased (Peltier 1994). Now the maximum ice thickness appears to be in excess of 3000 m, with the 2000 m ice thickness contour covering much of Sweden, Norway and northern Finland (Fig. 4 of Peltier 1994), areas where the current model predicts values of not much greater than about 1500 m. In a more recent paper this thickness appears to have been increased further, stated to be '… very modest over most of the region, reaching a maximum of 800 m in a localized region centred over the head of the Gulf of Bothnia' (Peltier 1996; page 1362).

The other feature that appears to be required by the sea-level data is ice profiles over the eastern part of Scandinavia, as well as over the western part of the Baltic and Denmark, that are characterized by a less rapid increase in ice height with distance inwards from the ice margin than is the case for the quasi-parabolic profiles adopted in the initial model. Both features of the modified ice sheet appear to be robust requirements but with the actual amplitudes of the ice heights and ice-height gradients being to some extent earth-model dependent. Other areas where modifications of the ice sheet appear warranted include the western Norwegian margin and southern and central Denmark. In the former case the comparisons between observed and predicted sea-level change suggest that the grounded ice cover may have extended as much as 40 km beyond the assumed margin but that the ice thickness over the shelf may have been less than that adopted in the starting model. Improved and independent information on the ice-margin limit and on the ice retreat across the Norwegian shelf is clearly desirable.

Many theoretical reconstructions of ice sheets, such as that by Denton & Hughes (1981), tend to generate symmetrical ice domes in which the ice thickness increases rapidly over short distances behind the ice margin. This is largely a consequence of assumptions made about the conditions at the base of the ice sheet and about whether or not the ice sheet reached steady-state conditions: steady-state models in which there is strong coupling between ice and bedrock lead to parabolic-type ice profiles (e.g. Paterson 1969). However, models in which the ice rests on a deformable surface have the effect of reducing the ice thickness and significantly modifying the ice profiles (e.g. Fisher *et al.* 1985; Boulton *et al.* 1985). Thus the proposed ice sheet supports models that exhibit regional variability in the basal conditions, with the western part tending to be cold-based where strong coupling between ice and bedrock occurs, and the eastern and southwestern parts resting on deformable beds, wholly consistent with the morphological features of much of Finland and with the recognition that many of the till beds in Finland predate the last ice advance over the region (e.g. Kleman *et al.* 1997). Hence, in further analysis of the glacial rebound problem of Scandinavia, it will be necessary to re-examine the starting ice model and construct ice profiles using spatially variable and realistic basal conditions.

6.4 The eustatic sea-level function in Late Holocene time

One of the by-products of the solution is the corrective term to the eustatic sea-level function, the $\delta\zeta_e(t)$ term in eq. (8), that was introduced because earlier solutions indicated that melting

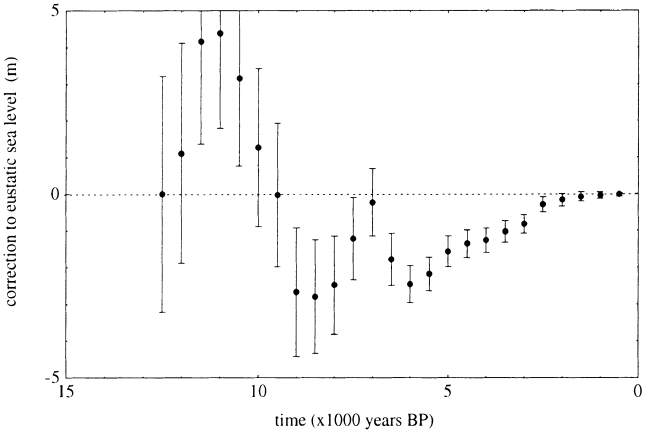

Figure 35. The corrective term $\delta\zeta_e(t)$ to the eustatic sea-level function (eq. 8).

of the ice sheets may not have ceased 6000 years ago (Nakada & Lambeck 1988; Lambeck & Nakada 1990). The present analysis gives a similar corrective term to that previously established in which the eustatic sea level over the past 6000 years increased at an average rate of about 0.5 mm yr^{-1}, for a total of about 3 m (Fig. 35). The corrective term for the earlier period is less well determined and the estimates are statistically insignificant.

6.5 A comparison of the model predictions with observations

Fig. 36 compares the observations with predictions for the entire data set as (a) a plot of observations versus predictions, (b) a plot of the observed-less-predicted as a function of time, and (c) as a histogram of these differences normalized by the standard deviations of the observations. In the first case the relationship is linear, with a slope of near unity and a correlation coefficient of 0.984. While some substantial discrepancies do occur, overall agreement between observations and predictions is satisfactory. The plot of residuals as a function of time indicates considerable scatter, with most of the major differences occurring for data points that have already been identified as anomalous in the regional Scandinavian solutions, or as being a consequence of the inadequacy of the ice sheet along the western Norwegian margin. The histogram of the residuals normalized by the observational standard deviations also indicates a range of values that is greater than expected in the absence of model errors and for realistic observational accuracy estimates. Some of these discrepancies are more evident when the time series for specific localities are examined as in Fig. 37. In these comparisons the predictions are for the actual coordinates of the observation sites and no attempt has been made to reduce the data to a common locality. Hence some of the scatter observed in these figures is a consequence of the spatial variability of the sea-level change within the chosen locality.

For sites near the interior of the former ice sheet, the model predicts well the amplitudes of the sea-level change for most of the data points, as for the Ångermanälven and Västerbotten region, the Stockholm–Uppsala region, and southwestern and northern Finland. Some discrepancies occur for the older Ångermanälven data points that may relate to residual problems remaining between the radiocarbon and varve timescales

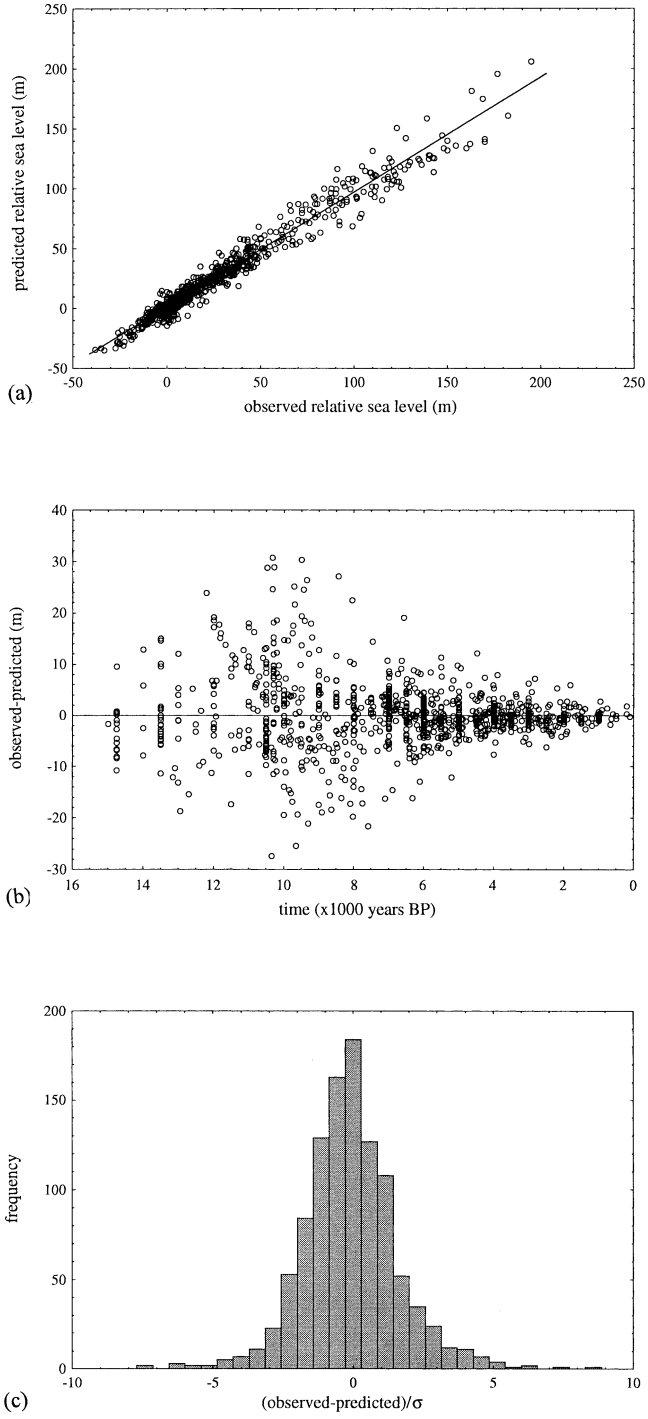

Figure 36. Comparisons of observations with predictions for all observational data points. (a) Predicted versus observed relative sea-level estimates. The regression coefficient is 0.96 and the correlation is 0.984. (b) Observed–predicted sea level as a function of time. (c) Histogram of the observed–predicted, normalized by observational standard deviations.

(Wohlfarth *et al.* 1993). Some inconsistencies also occur in northern Finland, where the observed data points are few in number and not always consistent with each other so that new information from this region is highly desirable. At some localities in the Oslofjord region, such as Kragerø, the model fails to predict well the rapid changes observed at the time of

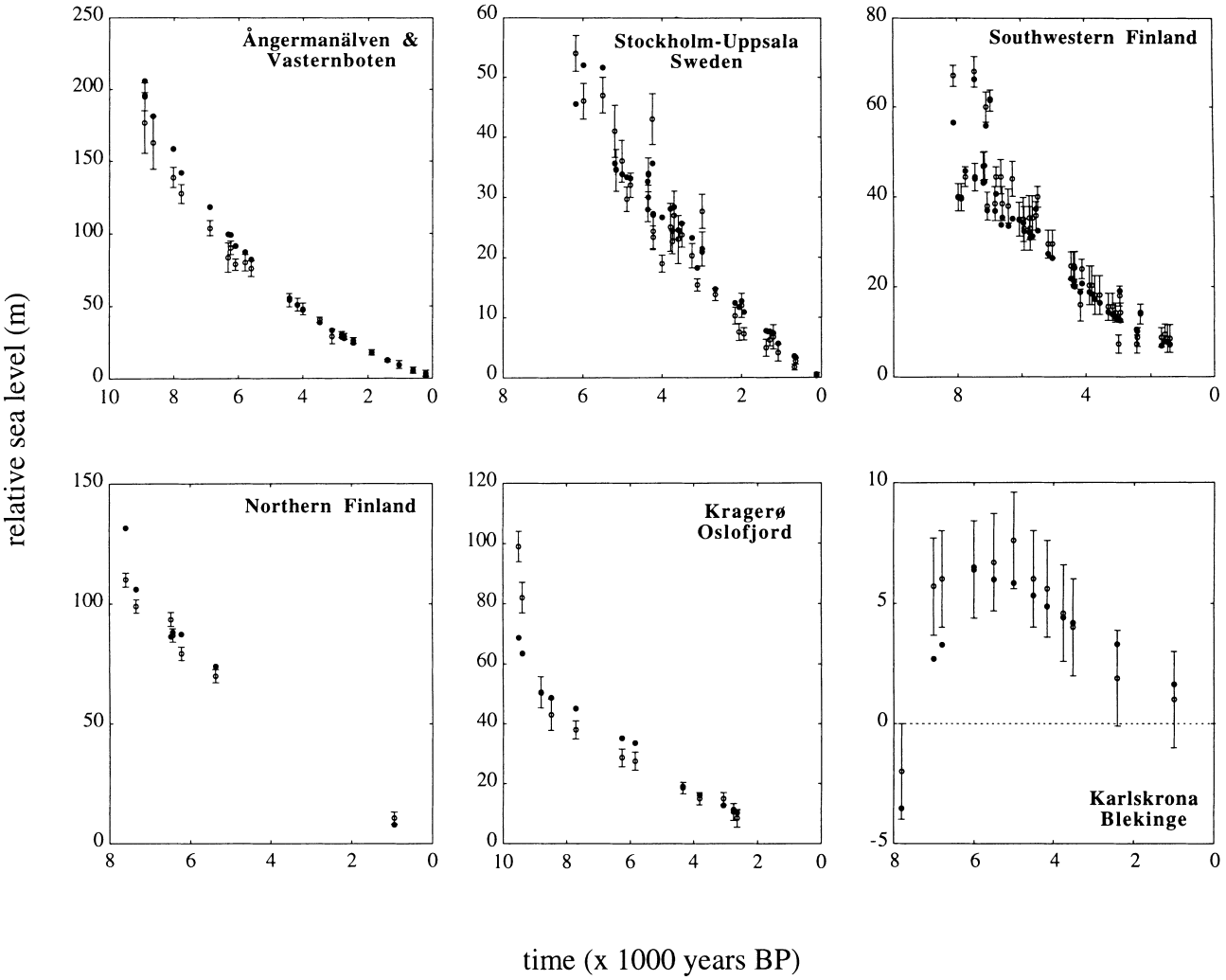

Figure 37. Time series of observed (with error bars) and corresponding predicted sea levels for selected localities. (Within any one region the observations may not be from exactly the same locality, resulting in the apparent irregularity in some of the height–age plots).

the Younger Dryas stadial, possibly a consequence of the failure of the model to represent well the local ice movements at this time, possibly a consequence of inadequate age control on some of the older data points where discrepancies between the radiocarbon and pollen ages are not uncommon (e.g. Björck *et al.* 1996). In southern Sweden, at Karlskrona for example, agreement between observations and predictions is satisfactory but the discrepancies become larger at the Danish localities of Præstø and Limfjord, reflecting the inadequate model representation of the local ice movements over this area in late glacial times (*cf.* Houmark-Nielsen 1989).

Along the Atlantic coast of Norway, the nature of the agreement is also variable. At Brusand, Jæren, several large discrepancies occur between 8000 and 10 000 BP but the corresponding data are some of the least reliable used (see Fig. 7 of Bird & Klemsdal 1986). Nevertheless, these data are important because they extend further back in time than do many of the other records from southwestern Norway, and because the low amplitude levels for Lateglacial time support ice models in which there was no thick ice sheet over the North Sea at the time of the maximum glaciation. An improved data set from this region would also be most desirable and useful for constraining the ice model over southwestern Norway.

The model predicts well the observed pattern of change at sites to the north, such as Bømlo, and within the Trondheimsfjorden (Bjugn and Frosta). In particular, the predictions for Bømlo model well the oscillations recorded there for the past 10 000 years, although in some instances, such as at Frosta, the model underestimates the levels in Younger Dryas time, suggesting that locally the ice may have been somewhat thicker than inferred from the inversions. Further north again, at Andøya, agreement for the glacial stage is unsatisfactory, with the model apparently containing insufficient ice at the time of maximum glaciation. The importance of this data set is that the record goes back to the time of the Last Glacial Maximum, meaning that the region, at least locally, was ice-free at that time and that the ice margin here did not extend out onto the shelf. However, the relatively high shorelines observed at this time do point to there having been more ice in the neighbourhood of the site than was assumed in the model in which the ice was allowed onto the shelf at maximum glaciation. Increasing the ice load to the east and south of the site does not lead to an improved

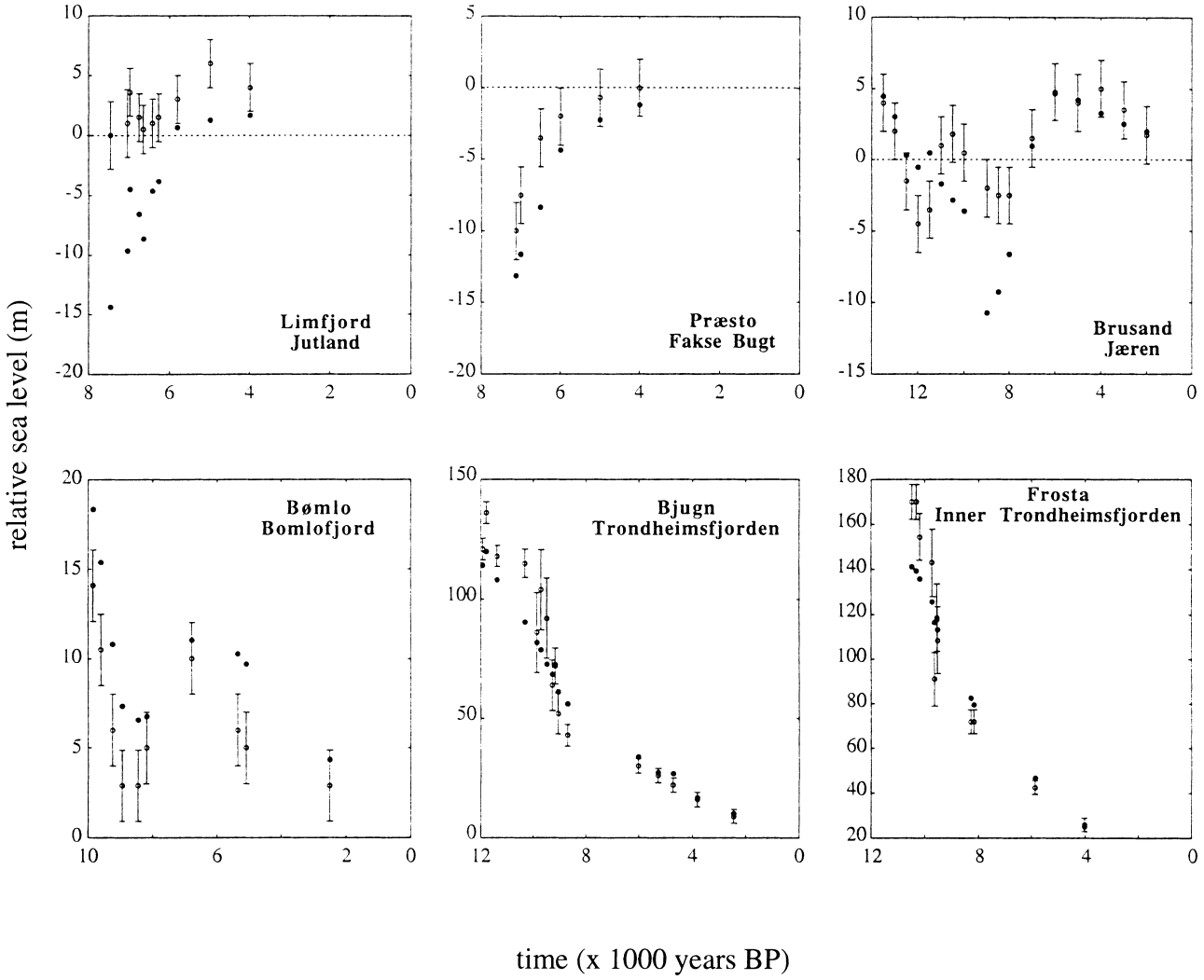

Figure 37. (*Continued.*)

comparison since this would actually lower the predicted levels for localities beyond the ice margin. This intriguing discrepancy also warrants new information, particularly as further north, at Tromsø, a similar discrepancy occurs for the two oldest data points.

Beyond the immediate Scandinavian ice limits, in the Netherlands, Scotland, and southern England (Bridgewater and Dungeness), the model predictions are generally in good agreement with the observational evidence. However, a further iteration of the modelling may be warranted here because of the separate treatments given to the British and Scandinavian ice sheets: in the earlier analyses of the British sea-level information, a model of the Scandinavian ice sheet was used that overestimated the ice load and this may feed back into the inferred parameters for the former ice sheet, as can be seen if the predictions for these sites illustrated in Fig. 37 are compared with similar predictions in Fig. 12 of Lambeck *et al.* (1996).

The above comparisons between observations and predictions indicates that there is scope for further improvements in the modelling as well as for a re-assessment of some of the observational data. Further iterations of the modelling for new ice-sheet parameters are not attempted here at this stage because any improvements in the internal consistency of the model would only lead to a greater correlation between earth- and ice-model parameters. The next iteration should therefore involve a new analysis of the observational evidence for the ice movements across the region and the construction of a new ice model that is largely free from assumptions about the rheological parameters of the Earth but which takes into consideration the principal features identified in this paper. Other improvements in the modelling that should be examined include the introduction of a greater depth dependence of viscosity than permitted by the three-layer model used here; the examination of the consequence of the assumed kinetics of the phase transformations at the 400 and 670 km boundaries; and an examination of the consequences of introducing a degree of lateral variability into the mantle response. Also, any subsequent iteration would require a re-evaluation of the observational evidence. This would include the conversion of all data to a consistent and linear timescale, the examination of some of the apparently anomalous data points identified here, an incorporation of the Baltic Lake level data together with models for the evolution of the Baltic, and a search for additional data from some of the more critical areas where currently the database is sparse. Complementary data types

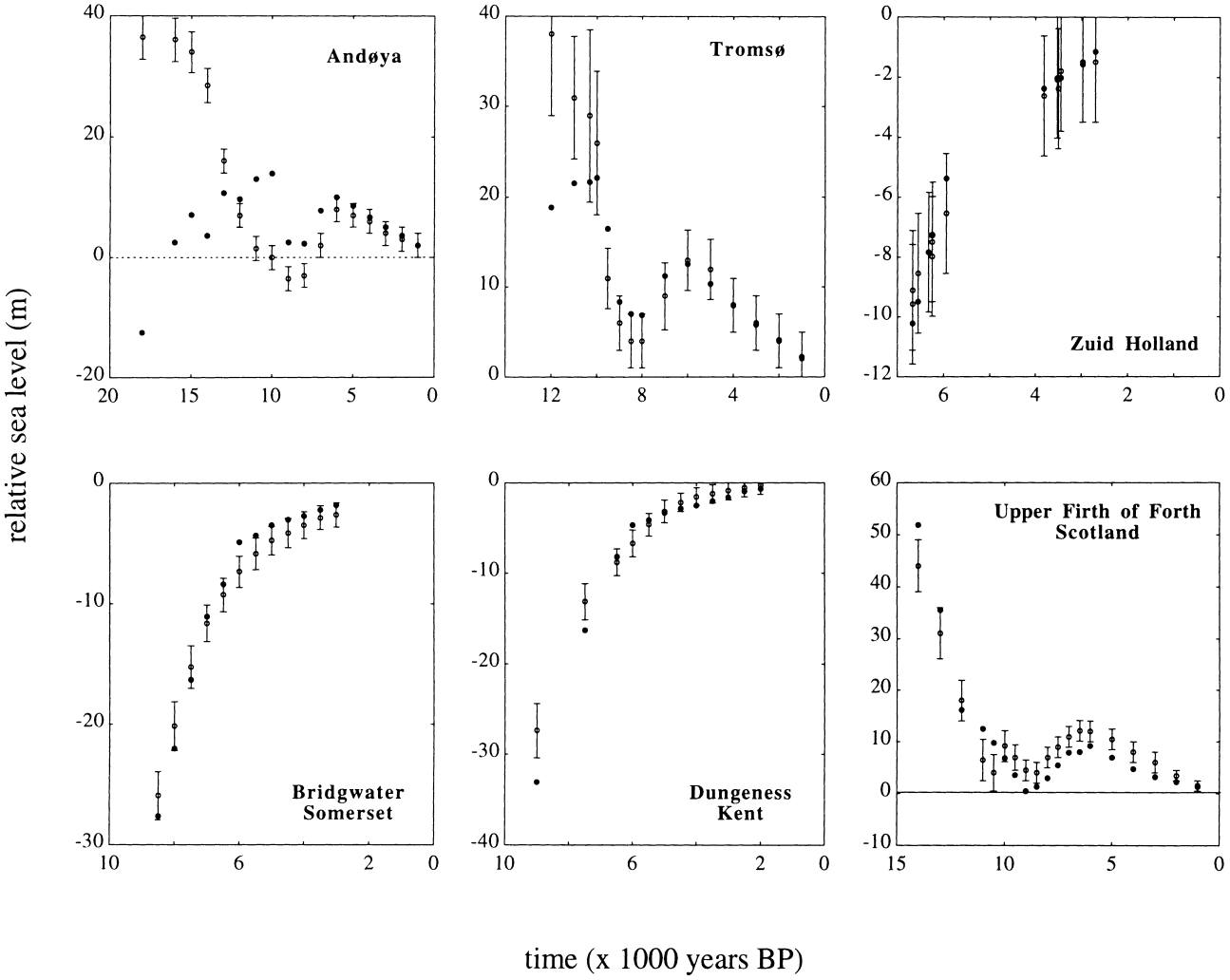

Figure 37. (*Continued.*)

would also be incorporated, such as the shoreline elevations for the Baltic Lake stages (Lambeck 1998b) and the recent epoch information from mareograph and geodetic levelling observations (Lambeck, Smither & Ekman 1998).

ACKNOWLEDGMENTS

Numerous people have assisted in this work. From the University of Bergen, Professor E. Husebye was a gracious host and he and Professors Y. Mangerud and the late K. Anundsen acted as sources of information and guides through a vast scientific literature. Professor S. Björck, formerly at the University of Lund, likewise assisted greatly with the interpretation of some of the Swedish data, as did Dr K. S. Petersen of the Geological Survey of Denmark for the Danish counterparts. Professors M. Eronen, then at Oulu University, H. Hyvärinen at the University of Helsinki, and G. Glückert at Turku University assisted with the Finnish data and showed me some of the evidence in the field. Dr P. Kiden and colleagues of the Netherlands Geological Survey helped with the interpretation of the North Sea data. Constructive comments on the manuscript were received from Drs P. Wu and G. Kaufmann. The research was partly funded by the Meetkundige Dienst of the Directoraat-Generaal Rijkswaterstaat of the Netherlands.

REFERENCES

Andersen, B.G., 1981. Late Weichselian ice sheets in Eurasia and Greenland, in *The Last Great Ice Sheets,* pp. 1–65, eds Denton, G.H. & Hughes, T.J., Wiley, New York, NY.

Anundsen, K., 1978. Marine transgression in Younger Dryas in Norway, *Boreas,* **7,** 49–60.

Anundsen, K., 1985. Changes in shore-level and ice-front position in Late Weichsel and Holocene, southern Norway, *Norsk. Geogr. Tidsskr.,* **39,** 205–225.

Baeteman, C., 1981. De Holocene ontwikkeling van de westelijke kustvlakte (België), *PhD thesis,* Vrije University of Brussel, Brussels.

Beets, D.J., Roep, T.B. & de Jong, J., 1981. Sedimentary sequences of the sub-recent North Sea coast of the western Netherlands near Alkmaar, *Spec. Publ. Int. Ass. Sediment.,* **5,** 133–145.

Berglund, B.E., 1964. The Post-glacial shore displacement in eastern Blekinge, southeastern Sweden, *Sver. Geol. Unders,* **C599**.

Berglund, B.E., 1971. Littorina transgressions in Blekinge, South Sweden. A preliminary survey, *Geol. Fören. Stockholm Förh.,* **93,** 625–652.

Bird, E.C.F. & Klemsdal, T., 1986. Shore displacement and the origin of the lagoon at Brusand, southwestern Norway, *Norsk geogr. Tidsskr.,* **40,** 27–35.

Björck, S., 1979. Late Weichselian stratigraphy of Blekinge, SE Sweden and water level changes in the Baltic Ice Lake, *Report LUNBBS/NBGK-1007,* University of Lund, Department of Quaternary Geology.

Björck, S., 1995. A review of the history of the Baltic Sea, 13 000–8 000 bp, *Quat. Int.,* **27,** 19–40.

Björck, S. & Digerfeldt, G., 1982. Late Weichselian shore displacement at Hunneberg, southern Sweden, indicating complex uplift, *Geologiska Föreningens i Stockholm Förhandlingar,* **104,** 132–155.

Björck, S. & Digerfeldt, G., 1986. Late Weichselian–Early Holocene shore displacement west of Mt. Billingen, within the Middle Swedish end-moraine zone, *Boreas,* **15,** 1–18.

Björck, S. & Digerfeldt, G., 1991. Allerød-Younger Dryas sea level changes in southwestern Sweden and their relation to the Baltic Ice Lake development, *Boreas,* **20,** 115–133.

Björck, S., Kromer, B., Johnsen, S., Bennike, O., Hammarlund, D., Lemdahl, G., Possnert, G., Rasmussen, T.-L., Wohlfarth, B., Hammer, C.-U. & Spurk, M., 1996. Synchronized terrestrial atmospheric deglacial records around the North Atlantic, *Science,* **274,** 1155–1160.

Boulton, G.S., Smith, G.D., Jones, A.S. & Newsome, J., 1985. Glacial geology and glaciology of the last mid-latitide ice sheets, *J. geol. Soc., Lond.*, **142,** 447–474.

Broadbent, N., 1978. Arkeologi och landhojning i nossa Västerbotten—en kritisk undersökning, in *Studier i norrländsk forntid,* pp. 19–30, Västerbottens Museum, Umeä.

Cato, I., 1992. Shore displacement data based on lake isolations confirm the postglacial part of the Swedish Geochronological Time Scale, *Sveriges Geologiska Undersökning Ser. Ca,* **81,** 75–80.

Danielsen, A., 1970. Pollen-analytical Late Quaternary studies in the Ra District of Østfold, southeast Norway, in *Mat. Natur. Serie no. 14,* pp. 127–129, Norwegian Universities Press, Oslo.

Denton, G.H. & Hughes, T.J. (eds), 1981. *The Last Great Ice Sheets,* Wiley, New York, NY.

Denys, L., 1993. Paleoecologisch diatomeeënonderzoek van de holocene afzettingen in de westelijke Belgische kustvlakte, *PhD thesis,* University of Instellingen Antwerpen, Antwerp.

Denys, L. & Baeteman, C., 1995. Holocene evolution of relative sea level and local mean high water spring tides in Belgium—a first assessment, *Mar. Geol,* **124,** 1–19.

Donner, J., Eronen, M. & Jugner, H., 1977. The dating of the Holocene relative sea-level changes in Finnmark, North Norway, *Norsk geografisk Tidsskrift,* **31,** 103–128.

Dziewonski, A.M. & Anderson, D.L., 1981. Preliminary reference Earth model, *Phys. Earth planet. Inter.,* **25,** 297–356.

Eronen, M., 1974. The history of the Litorina Sea and associated Holocene events, *Commentationes Physico-Mathematicae,* **44,** 79–191.

Eronen, M., van, Glückert, G., de Plassche, O., van der Plicht, J. & Rantala, P., 1995. *Land Uplift in the Olkilvoto-Pyhsa_ tJ sa_ tRvi Area, Southwestern Finland, During the Last 8000 Years,* Nuclear Waste Commission of Finnish Power Companies, Helsinki.

Farrell, W.E. & Clark, J.A., 1976. On postglacial sea level, *Geophys. J.*, **46,** 79–116.

Fisher, D.A., Reeh, N. & Langley, K., 1985. Objective reconstruction of the Late Wisconsin Ice Sheet and the significance of the deformable beds, *Géographie physique et Quaternaire,* **39,** 229–238.

Fjeldskaar, W., 1994. Viscosity and thickness of the asthenosphere detected from the Fennoscandian uplift, *Earth planet. Sci. Lett.,* **126,** 399–410.

Glückert, G., 1976. Post-Glacial shore-level displacement of the Baltic in SW Finland, *Geologica-Geographica,* A. III. 118, 1–92.

Glückert, G., 1978. Østersjöns postglaciala strandf örskjutning och skogens historia på Åland, *Department Quaternary Geol, University Turku,* **34.**

Gutenberg, B., 1941. Changes in sea level, postglacial uplift, and mobility of the Earth's interior, *Bull. geol. Soc. Am.,* **52,** 721–772.

Hafsten, U., 1956. Pollen-analytic investigations on the late Quaternary development in the inner Oslofjord area, in *Universitetet I Bergen Arbok,* 1956, pp. 139–151, Naturvitenskapelig rekke Nr. 8.

Hafsten, U., 1983. Biostratigraphical evidence for Late Weichselian and Holocene sea-level changes in southern Norway, in *Shorelines and Isostasy,* pp. 161–181, eds Smith, D.E. & Dawson, A.G., Academic Press, London.

Hald, M. & Vorren, T.O., 1983. A shore displacement curve from the Tromsø district, North Norway, *Norsk Geologisk Tidsskrift,* **63,** 103–110.

Haskell, N.A., 1935. The motion of a viscous fluid under a surface load, *Physics,* **61,** 265–269.

Haskell, N.A., 1937. The viscosity of the asthenosphere, *Am. J. Sci.,* **233,** 22–28.

Henningsmoen, K.E., 1979. En karbon-datest strandforskyvings curve fra søndre Vesfold, in *Fortiden i Søkelyset,* pp. 239–247, eds Hydal, R., Westin, S., Hafsten, U. & Gulliksen, S., Laboratoiriet for Radiologisk Datering, Oslo.

Houmark-Nielsen, M., 1989. The last interglacial–glacial cycle in Denmark, *Quat. Int.,* **3,** 31–39.

Hyvärinen, H., 1980. Relative sea-level changes near Helsinki, southern Finland, during early Litorina times., *Bull. geol. Soc. Finland,* **52–2,** 207–219.

Hyvärinen, H., 1987. Models of fluctuating eustatic sea-level in the Holocene falsified by a Baltic sea-level record, in *XII INQUA Congress, Ottawa,* Abstracts p. 191.

Jelgersma, S., 1961. Holocene sea-level changes in the Netherlands, *Meded. Geol. Stichting,* **C.IV (7),** 1–100.

Johansen, O.-I., Henningsmoen, K. & Sollid, J.L., 1985. Deglaciation of Tingvollhalvøya and adjacent areas, Nordvestlandet, in light of the vegetation development, *Norsk geogr. Tidsskr,* **39,** 155–174.

Johnston, P., 1993. The effect of spatially non-uniform water loads on the prediction of sea-level change, *Geophys. J. Int.,* **114,** 615–634.

Johnston, P., Lambeck, K. & Wolf, D., 1997. Material versus isobaric internal boundaries in the Earth and their influence on glacial rebound, *Geophys. J. Int.,* **129,** 252–268.

Kaland, P.E., 1984. Holocene shore displacement and shorelines in Hordaland, western Norway, *Boreas,* **13,** 203–242.

Kaland, P.E., Krzywinski, K. & Stabell, B., 1984. Radiocarbon-dating of transitions between marine and lacustrine sediments and their relation to the development of lakes, *Boreas,* **13,** 243–258.

Kiden, P., 1989. Holocene water level movements in the lower Scheldt perimarine area, in *Quaternary Sea-Level Investigations from Belgium. A Contribution to IGCP Project, 200,* **241** (1989/6), Geol. Dienst België, Ministerie van Economische Zaken.

Kjemperud, A., 1981. A shoreline displacement investigation from Frosta in Trondheimsfjorden, Nord-Trøndelag, Norway, *Norsk Geologisk Tidsskrift,* **61,** 1–15.

Kjemperud, A., 1982. *Late Weichselian and Holocene Shoreline Displacement in Parts of Trondelag, Central Norway,* Department of Geology, Oslo.

Kjemperud, A., 1986. Late Weichselian and Holocene shoreline displacement in the Trondheimsfjord area, central Norway, *Boreas,* **15,** 61–82.

Kleman, J., Hättestrand, C., Borgström, I. & Stroeven, A., 1997. Fennoscandian palaeoglaciology reconstructed using a glacial geological inversion model, *J. Glaciol.*, **43,** 283–299.

Krog, H., 1979. Late Pleistocene and Holocene shorelines in Western Denmark, in *The Quaternary History of the North Sea,* vol. 2, pp. 75–83, eds Oele, E., Schuttenhelm, R.T.E. & Wiggers, A.J., Acta University of Ups. Symp. University of Ups. Annum Quingentesimum Celebrantis.

Krzywinski, K. & Stabell, B., 1984. Late Weichselian sea level changes at Sotra, Hordaland, western Norway, *Boreas,* **13,** 159–202.

Lambeck, K., 1993. Glacial Rebound of the British Isles. II: a high resolution, high-precision model, *Geophys. J. Int.*, **115,** 960–990.

Lambeck, K., 1995a. Late Devensian and Holocene shorelines of the British Isles and North Sea from models of glacio-hydro-isostatic rebound, *J. geol. Soc. Lond,* **152,** 437–448.

Lambeck, K., 1995b. Late Pleistocene and Holocene sea-level change in Greece and southwestern Turkey: a separation of eustatic, isostatic and tectonic contributions, *Geophys. J. Int*., **122,** 1022–1044.

Lambeck, K., 1995c. Constraints on the Late Weichselian ice sheet over the Barents Sea from observations of raised shorelines, *Quat. Sci. Rev*., **14,** 1–16.

Lambeck, K., 1996. Limits on the areal extent of the Barents Sea ice sheet in Late Weischelian time, *Palaeogeogr. Palaeoclimatol. Palaeoecol*., **12,** 41–51.

Lambeck, K., 1997. Sea-level change along the French Atlantic and Channel Coasts since the time of the Last Glacial Maximum, *Palaeogeogr. Palaeoclimatol. Palaeoecol*., **129,** 1–22.

Lambeck, K., 1998a. On the choice of time scale in glacial rebound modelling; mantle viscosity estimates and the radiocarbon time scale, *Geophys. J. Int.,* in press.

Lambeck, K., 1998b. Shoreline displacements in southern-central Sweden and the evolution of the Baltic Sea, *J. geol. Soc. Lond.,* submitted.

Lambeck, K. & Nakada, M., 1990. Late Pleistocene and Holocene Sea-Level Change along the Australian Coast, *Palaeogeogr. Palaeoclimatol. Palaeoecol. (Global Planetary Change Section),* **89,** 143–176.

Lambeck, K., Johnston, P. & Nakada, M., 1990. Holocene glacial rebound and sea-level change in NW Europe, *Geophys. J. Int*., **103,** 451–468.

Lambeck, K., Johnston, P., Smither, C. & Nakada, M., 1996. Glacial rebound of the British Isles–III. Constraints on mantle viscosity, *Geophys. J. Int*., **125,** 340–354.

Lambeck, K., Smither, C. & Ekman, M., 1998. Tests of glacial rebound models for Fennoscandinavia based on instrumented sea- and lake-level records, *Geophys. J. Int.,* submitted.

Larsen, E. & Sejrup, H.P., 1990. Weichselian land–sea interactions: western Norway—Norwegian Sea, *Quat. Sci. Rev*., **9,** 85–97.

Lidén, R., 1938. Den senkvartara strandförskjutningens forlopp och kronologi i Angermanland, *Geol. Fören. Furhandl.,* **Bd. 60,** H3, 397–404.

Lie, S.E., Stabell, B. & Mangerud, J., 1983. Diatom stratigraphy related to Late Weichselian sea-level changes in Sunnmøre, Western Norway, *Norges geologiske undersøkelse,* **380,** 203–219.

Linke, G., 1979. Ergebnisse geologischer Untersuchungen im Küsternbereich südlisch Cuxhaven—Ein Betrag zur Diskussion holozäner Fragen, *Probl. d. Küstenforsch. im südl. Nordseegebiet,* **13,** 39–83.

Linke, G., 1982. Der Ablauf der Holozänen Transgression der Nordsee Aufgrund von Ergebnissen aus dem Gebiet Neuwork/Scharhörn, *Probl. d. Küstenforsch. im südl. Nordseegebiet,* **14,** 123–157.

Lliboutry, L.A., 1971. Properties of the asthenosphere from Fennoscandian data, *J. geophys. Res.,* **76,** 1433–1446.

Ludwig, G., Müller, H. & Streif, H., 1979. Neuere Daten zum holozänen Meeresspiegelanstieg im Bereich der Deutschen Bucht, *Geol. Jb,* **D32,** 3–22.

Mitrovica, J.X., 1996. Haskell [1935] revisited, *J. geophys. Res*., **101,** 555–569.

Mitrovica, J.X. & Peltier, W.R., 1991. On postglacial geoid subsidence over the equatorial oceans, *J. geophys. Res.,* **96,** 20 053–20 071.

Mitrovica, J.X. & Peltier, W.R., 1993. The inference of mantle viscosity from an inversion of the Fennoscandian relaxation spectrum, *Geophys. J. Int*., **114,** 45–62.

Møller, J.J., 1984. Holocene shore displacement at Nappstraumen, Lofoten, North Norway, *Norsk Geologisk Tiddskrift,* **64,** 1–5.

Møller, J.J., 1986. Holocene transgression maximum about 6000 years BP at Ramså, Vesterålen, North Norway, *Norsk geografisk Tidsskrift,* **40,** 77–84.

Nakada, M. & Lambeck, K., 1987. Glacial rebound and relative sealevel variations: A new appraisal, *Geophys. J. R. astr. Soc.,* **90,** 171–224.

Nakada, M. & Lambeck, K., 1988. The melting history of the Late Pleistocene Antarctic ice sheet, *Nature,* **333,** 36–40.

Niskanen, E., 1939. On the upheaval of land in Fennoscandia, *Ann. Acad. Sci. Fennicae,* **53,** Ser. A, 1–30.

Niskanen, E., 1948. On the viscosity of the Earth's interior and crust, *Ann. Acad. Sci. Fennicae,* **15,** Ser. A, 1–28.

Påsse, T., 1987. Shore displacement during the Late Weichselian and Holocene in the Sandsjöbacka area, SW Sweden, *Geologiska Föreningens i Stockholm Förhandlingar,* **109,** 197–210.

Paterson, W.S.B., 1969. *The Physics of Glaciers,* Pergamon, New York, NY.

Pedersen, S.S., 1995. Israndslinier i Norden, Danm. Geol. Unders., Copenhagen.

Peltier, W.R., 1994. Ice age paleotopography, *Science,* **265,** 195–201.

Peltier, W.R., 1996. Mantle viscosity and ice-age ice sheet topography, *Science,* **273,** 1359–1364.

Petersen, K.S., 1975. Om Limfjordens postglaciale marine udvikling og niveauforhold, belyst ved mollusk-faunaen og C-14 dateringer, *Danm. geol. Unders*., **1–2,** 75–103.

Petersen, K.S., 1977. Den postglaciale transgression og molluskfaunaen i Tude Å-området, Store Bælt, Danmark, *Danm. geol, Unders*., **23,** 39–52.

Petersen, K.S., 1994. Limfjordstangerne–Holocæne marine miljøudvikling, *Danm. geol, Unders*., Copenhagen, **85**.

Ramfjord, H., 1982. On the Late Weichselian and Flandrian shoreline displace in Nærøy, Nord-Trøndelag, Norway, *Norsk Geologisk Tidsskrift,* **62,** 191–205.

Renberg, I. & Segerström, U., 1981. The initial points on a shoreline displacement curve for Southern Västerbotten, dated by Varve-counts of lake sediments, *Striae,* **14,** 174–176.

Saarnisto, M., 1981. Holocene emergence history and stratigraphy in the area north of the Gulf of Bothnia, *Ann. Acad. Sci. Fennicae,* **AIII, 130**.

Salomaa, R., 1982. Post-glacial shoreline displacement in the Lauhanvuori area, western Finland, *Ann. Acad. Sci. Fennicae,* Ser. **I, III 134,** 81–97.

Shackleton, N.J., 1987. Oxygen isotopes, ice volume and sea level, *Quat. Sci. Rev.,* **6,** 183–190.

Snyder, J.A., Korsun, S.A. & Forman, S.L., 1996. Postglacial emergence and the Tapes transgression, north-central Kola Peninsula, Russia, *Boreas,* **25,** 47–56.

Sørensen, R., 1979. Late Weichselian deglaciation in the Oslofjord area, south Norway, *Boreas,* **8,** 241–246.

Stabell, B., 1980. Holocene shorelevel displacement in Telemark, southern Norway, *Norsk Geologisk Tiddskrift,* **60,** 71–81.

Stone, J.O., Lambeck, K., Fifield, L.K., Evans, J.M. & Cresswell, R.G., 1996. A Lateglacial age for the Main Rock Platform, western Scotland, *Geology,* **24,** 707–710.

Svedhage, K., 1985. Shore displacement during Late Weichselian and early Holocene in the Risveden area, SW Sweden, *Geol. Inst. Publ.,* **51A,** Göteborgs Universitet.

Svendsen, J.I. & Mangerud, J., 1987. Late Weichselian and Holocene sea-level history for a cross-section of western Norway, *J. Quat. Sci.,* **2,** 113–132.

Svensson, N.-O., 1989. Late Wiechselian and early Holocene shore displacement in the central Baltic based on stratigraphical and morphological records from eastern Småland and Gotland, Sweden, *Lundqua thesis,* **25,** Dept Quaternary Geology, Lund University.

Svensson, N.-O., 1991. Late Weichselian and Early Holocene shore displacement in the central Baltic Sea, *Quat. Int*., **9,** 7–26.

Thomsen, H., 1982. Late Weichselian shore-level displacement on Nord-Jaeren, south-west Norway, *Geologiska Föreningens i Stockholm Förhandlingar,* **103,** 447–468.

Tushingham, A.M. & Peltier, W.R., 1991. Ice 36: A new global model of Late Pleistocene deglaciation based upon geophysical predictions of post-glacial relative sea-level change, *J. geophys. Res.,* **96,** 4497–4523.

van Bemmelen, R.W. & Berlage, H.P., 1935. Versuch einer mathematischen behandling geotektonischer probleme unter besonderer berücksichtigung der undationstheorie, *Gerlands Beiträge Geophys,* **43,** 19–55.

van de Plassche, O., 1982. Sea-level change and water-level movements in the Netherlands during the Holocene, *Med. Rijks Geologische Dienst,* **36,** 1–93.

Vening Meinesz, F.A., 1937. The determination of the Earth's plasticity from the postglacial uplift of Scandinavia: isostatic adjustment, *Kon. Akad. Wettensch,* **40,** 654–662.

Vorren, K.-D. & Moe, D., 1986. The early Holocene climate and sea-level changes in Lofoten and VesterŒlen, North Norway, *Norsk Geologisk Tiddskrift,* **66,** 135–143.

Vorren, T.O., Vorren, K.-D., Alm, T., Gullimsen, S. & Løvlie, R., 1988. The last delgaciation (20,000–11,000 B.P.) on Andøya, northern Norway, *Boreas,* **17,** 41–77.

Wallin, J.-E., 1993. Den fasta jordbruksnäringens utveckling i Ångermanälvens nedre dalgång under järnåldern och medeltiden, *Studier i Österbottens förhistoria,* **3,** 12–16.

Wohlfarth, B., Björck, S., Possnert, G., Lemdahl, G., Brunnberg, L., Ising, L., Olsson, S. & Svensson, N.-O., 1993. AMS dating Swedish varved clays of the last glacial/interglacial transition and the potential/difficulties of calibrating Late Weichselian 'absolute' chronologies, *Boreas,* **22,** 113–128.

Zielhuis, A. & Nolet, G., 1994. Deep seismic expression of an ancient plate boundary in Europe, *Science,* **265,** 79–81.